

**Biophysical and Biochemical Studies of
Alpha II Spectrin and Its Break-Down Products by Caspase-3**

BY

MARTA A. WITEK
B.S. with Honors, University of Illinois at Chicago, 2007

THESIS

Submitted as a partial fulfillment of the requirements
for the degree of Doctor of Philosophy in Chemistry
in the Graduate College of the
University of Illinois at Chicago, 2013

Chicago, Illinois

Defense Committee:

Leslie W.-M. Fung, Chair and Advisor, Chemistry
Richard Kassner, Chemistry
Lawrence W. Miller, Chemistry
Jung-Hyun Min, Chemistry
Luisa DiPietro, UIC, College of Dentistry

ACKNOWLEDGMENTS

I would like to express my deep gratitude to my advisor, Professor Leslie W.-M. Fung for her continuous support, from the early stages of my graduate studies and through ongoing advice and encouragement to this day. I feel fortunate to have received the training that not only taught me how to be an independent thinker but also help me to understand that the unexpected requires knowledge, time and an open mind.

Deep gratitude to Professor Richard Burns who opened the “science research door” for me and who was always there, waiting to hear “good news”. I would like to thank Professor Luisa DiPietro for her continuous support for the caspase/spectrin project and the UIC College of Dentistry for awarding me the MOST (Multidisciplinary Oral Science Training)-T32 training grant for the time period 2009-2011 and as my committee member. To my other committee members, Drs. Richard Kassner, Lawrence Miller, and Jung-Hyun Min for their valuable and constructive suggestions for my research projects and also advice on post-doctoral positions.

Many thanks to Drs. Michael Johnson, Shahila Mehboob, Bernie Santarsiero, Akin Sevinc, and Yuanli Song for their fruitful collaborations. Especially, Shahila and Bernie for teaching me protein crystallography. I will never forget those long nights at Argonne collecting data.

I would also like to thank all the current and former lab members from Professor Fung’s lab for their support in day to day lab activities. Special thanks go to Nina Wolf, Mike Tuntland, Pauline Kabre, and Anna Kim, for their valuable insights and for being there for me, in big and small ways. And to all my friends in the Chemistry Department for helping me to develop a tolerance for frustration.

I would like to extend my thanks to the Chemistry Department not only for their financial support, but also giving me the opportunity to teach several chemistry classes. The interactions with students have been an enormous rewarding experience.

Finally, my biggest and most heartfelt thanks go to my family, my parents Lucyna and Fryderyk, my brother Rafal, his wife Rachel, and their daughter Rebecca, for their love, support, motivation, and a great source of strength to me over the past years.

TABLE OF CONTENTS

<u>CHAPTER</u>		<u>PAGE</u>
1	INTRODUCTION..	1
2	BACKGROUND	
	2.1 Non-Erythroid α -Spectrin	
	2.1.1 Distribution and Localization	3
	2.1.2 Structure - Dimers and Tetramers	3
	2.1.3 Non-Erythroid vs. Erythroid Spectrin	8
	2.1.4 Spectrin Mutations at the Tetramerization Site.	9
	2.1.5 Spectrin Tryptophans: Intrinsic Reporters of Spectrin Structure and Function	11
	2.2 Caspase-3	
	2.2.1 Distribution and Localization	11
	2.2.2 Structural Organization	11
	2.2.3 Apoptotic Functions of Caspase-3	12
	2.2.4 Non-apoptotic Functions of Caspase-3	14
	2.2.5 Caspase-3 Substrate Specificity	14
	2.3 Spectrin α & Caspase-3	
	2.3.1 Spectrin α - Prominent Target of Caspase-3	17
	2.3.2 Sjögren's Syndrome (SS).....	18
	2.3.3 Biological Significance	18
	2.4 Biophysical Methods Used	
	2.4.1 Circular Dichroism (CD)	19
	2.4.2 Fluorescence	20
	2.4.3 Isothermal Titration Calorimetry (ITC)	22
	2.4.4 ITC vs. Yeast Two Hybrid (Y2H) Method	25
	2.4.5 X-ray Crystallography	
	2.4.5.1 Protein Crystallization.	26
	2.4.5.2 Data Collection	27
	2.4.5.3 Phasing	29
	2.4.5.4 Model Building & Structure Refinement	30
3	CRYSTAL STRUCTURE OF THE NONERYTHROID α -SPECTRIN TETRAMERIZATION SITE REVEALS DIFFERENCES BETWEEN ERYTHROID AND NONERYTHROID SPECTRIN TETRAMER FORMATION	
	3.1 Experimental Procedures	
	3.1.1 Recombinant Proteins.	32
	3.1.1.1 CD of Spectrin Model Proteins.....	33
	3.1.1.2 Crystallization of α -N1.....	33
	3.1.2 Structural Analysis.....	33

TABLE OF CONTENTS (continued)

	3.1.3 Protein Thermal Stability	34
	3.1.4 ITC of Spectrin Association.....	34
3.2	Results	
	3.2.1 Protein Characterization	35
	3.2.2 II-N1 Crystals.	35
	3.2.3 Thermal Stability and Inter-Helix Interactions.	35
	3.2.4 Association Affinity at the Tetramerization Site.	40
3.3	Discussion	42
4	YEAST TWO-HYBRID AND ITC STUDIES OF ALPHA AND BETA SPECTRIN INTERACTION AT THE TETRAMERIZATION SITE	
	4.1 Experimental Procedures	
	4.1.1 ITC.	45
4.2	Results	
	4.2.1 Recombinant Protein Analysis.....	46
	4.2.2 ITC Results.....	46
4.3	Discussion.....	48
5	QUANTITATIVE STUDIES OF CASPASE-3 CATALYZED II-SPECTRIN BREAK-DOWN WITH ELECTROPHORESIS AND FLUORESCENCE METHODS	
5.1	Introduction	50
5.2	Experimental Procedures	
	5.2.1 DNA Plasmid Preparation.....	52
	5.2.2 Protein Design, Expression, Purification and Characterization	
	5.2.2.1 Spectrin Model Proteins.....	53
	5.2.2.2 Caspase-3.	53
	5.2.2.3 Caspase-3 Activity Assay.....	55
	5.2.3 Cleavage of Spectrin Fragments by Caspase-3	
	5.2.3.1 SDS-PAGE Detection	55
	5.2.3.2 Fluorescence Detection.	56
	5.2.3.3 Structure Prediction.....	57
5.3	Results	
	5.3.1 Protein Characterization	
	5.3.1.1 Spectrin	57
	5.3.1.2 Caspase-3	63
	5.3.2 Cleavage of Spectrin Proteins by Caspase-3	
	5.3.2.1 Gel Electrophoresis Studies	63
	5.3.2.2 Fluorescence Studies	72
5.4	Discussion.	81

TABLE OF CONTENTS (continued)

6	CRYSTALLIZATION OF SPECTRIN MODEL PROTEINS CONTAINING CASPASE-3 RECOGNITION SITE	
6.1	Introduction	86
6.2	Experimental Procedures	
6.2.1	DNA Plasmid Preparation	87
6.2.2	Crystallization of Spectrin Model Proteins	88
6.2.2.1	D8-D11	
6.2.2.2	D10-D11	
6.2.2.2	D10-D13	
6.2.2.3	D13	
6.2.3	X-ray Data Collection & Analysis.	90
6.3	Results.	90
6.4	Discussion.	96
	REFERENCES	98
	CURRICULUM VITAE.	109
	APPENDICES	
	A. Crystal Structure of the Nonerythroid α -Spectrin Tetramerization Site Reveals Differences between Erythroid and Nonerythroid Spectrin Tetramer Formation. Shahila Mehboob, Yuanli Song, Marta Witek, Fei Long, Bernard D. Santarsiero, Michael E. Johnson, and Leslie W.-M. Fung. <i>J. Biol. Chem.</i> 2010, 285: 14572-14584.	115
	B. Yeast Two-Hybrid and ITC Studies of Alpha and Beta Spectrin interaction at the Tetramerization Site. Akin Sevinc, Marta A. Witek, and Leslie W.-M. Fung. <i>Cell. Mol. Biol. Lett.</i> 2011, 16: 452-461.	160
	C. Copyright permissions.	179

LIST OF TABLES

<u>TABLE</u>		<u>PAGE</u>
Table 5-1	The mass predicted from sequence, gel electrophoresis, and from mass spectrometry methods for II-spectrin proteins.	59
Table 5-2	Equilibrium and kinetic results of caspase-3 cleavage at a specific site in spectrin model proteins	79
Table 5-3	Caspase/caspase-3 cleavage site predictions on II-spectrin.....	80
Table 6-1	Data collection and refinement statistics for II-D13	91

LIST OF FIGURES

<u>FIGURE</u>	<u>PAGE</u>
Fig 2.1	The cell body of the neuron.4
Fig 2.2	A model for the cortical cytoskeleton in axons5
Fig 2.3	Spectrin structural organization.7
Fig 2.4	I-N1 vs II-N1 structure10
Fig 2.5	Caspase-3 structural organization.....13
Fig 2.6	Intrinsic and extrinsic caspase-3 activation pathways15
Fig 2.7	Amino acid substrate sequence specificity of caspase-316
Fig 2.8	CD spectra of proteins with representative secondary structures.21
Fig 2.9	Configuration of an ITC sample cell & data integration.23
Fig 2.10	Crystal packing and the Bragg's law28
Fig 3.1	Crystal structure of II-N137
Fig 3.2	Thermal denaturation of I-N1 and II-N1/ II-N1-SelMet.38
Fig 3.3	CD spectra of I-N1, II-N1, and II-N1-R37P39
Fig 3.4	ITC for II-N1, II-N1-R37P, and I-N1 all with I-C1.....41
Fig 4.1	ITC - V22 mutants with I-C1.....47
Fig 5.1	Sequence alignment of D10, D10' and D13 all with D160
Fig 5.2	D10-D11 and D8-D11 in the presence of caspase-3/SDS-PAGE66
Fig 5.3	D13 and D12-D13 in the presence of caspase-3/SDS-PAGE68
Fig 5.4	D10-D13 and D10-D13(D1185E) in the presence of caspase-3 / SDS-PAGE....70
Fig 5.5	D10-D11 w, D10-D11 w-1, D10-D11 w-2 in the presence of caspase-3 / fluorescence74
Fig 5.6	D10-D11 w in the presence of caspase-3 / fluorescence75
Fig 5.7	D13 w in the presence of caspase-3 / fluorescence.....77
Fig 6.1	II-D13 crystal structure.92
Fig 6.2	B-factors for D1393
Fig 6.3	Crystals for D10-D13 spectrin model protein94
Fig 6.4	D5 with D13 sequence alignment95

LIST OF ABBREVIATIONS

$A_1B_1C_1$	the first II structural domain consisting of Helices A_1 , B_1 , and C_1
$A_{13}B_{13}C_{13}$	the thirteenth II structural domain consisting of Helices A_{13} , B_{13} , and C_{13}
A'B'C'	helical bundle of Helices A', B', and C'
I-N1	a recombinant protein of I-spectrin segment with residues 1-156
II	a non-erythroid alpha spectrin
II-N1	a recombinant protein of II-spectrin segment with residues 1-147
II-N	a recombinant protein of II-spectrin segment with residues 1-359
II-N-V22Δ	a recombinant protein with a single residue replacement at position 22 of II-N
II-N1-R37P (II-R37P)	a recombinant protein with a mutation at residue Arg 37 of II-N1
I	an erythroid beta spectrin
I-C1	a recombinant protein of I-spectrin segment with residues 1898-2083
II	a non-erythroid beta spectrin
III	spectrin isoform found in Golgi and vesicular membrane skeletons, plasma membrane in neurons and epithelial cells
IV	spectrin isoform found in neurons (axon, initial segment, nodes of Ranvier) and pancreatic islets, nucleus
II-C1	a recombinant protein of II-spectrin segment with residues 1906-2093
CD	circular dichroism
[casp-3]	the concentration of recombinant caspase-3
caspase activity buffer	20 mM piperazine-N,N'-bis-(2-ethanesulfonic acid) with 100 mM NaCl, 10 mM DTT, 1 mM EDTA, 0.1% CHAPS, and 10% sucrose at pH 7.2
CHAPS	3[(3-cholamidopropyl)dimethylammonio] -propane sulfonic acid
CSF	cerebrospinal fluid
D1	first structural domain consisting of residues 1-147 of II-spectrin
D5	fifth structural domain of II-spectrin

D8-D11	a recombinant protein consisting of residues 780-1344 of II-spectrin plus GS as the first two residues
D10-D11	a recombinant protein consisting of residues 1087-1344 of II-spectrin plus GS as the first two residues
D10-D11 Δ_w -1	D10-D11 with all its tryptophan residues except W1192 replaced with phenylalanine residues
D10-D11 Δ_w -2	D10-D11 with all its tryptophan residues except W1215 and W1192 replaced with phenylalanine residues
D10-D11 Δ_w	D10-D11 with all its tryptophan residues except W1192 and W1106 replaced with phenylalanine residues
D10-D13	a recombinant protein consisting of residues 1087-1556 of II-spectrin plus GS as the first two residues
D12-D13	a recombinant protein consisting of residues 1335-1556 of II-spectrin plus GS as the first two residues
D13	a recombinant protein consisting of residues 1441-1556 of II-spectrin plus GS as the first two residues
D13 Δ_w	D13 with W1533F mutation
EPR	electron paramagnetic resonance
ITC	isothermal titration calorimetry
K_d	equilibrium dissociation constant
M1	monomer 1
M2	monomer 2
MAD	multi-wavelength anomalous dispersion
mass _{ele}	electrophoretic mass
mass _{ms}	molecular mass determined by mass spectrometry
mass _{seq}	mass calculated from amino acid sequence
NBC	non-bonded contacts
NMR	nuclear magnetic resonance
PEG	polyethylene glycol
PBS 7.4	5 mM phosphate buffer with 150 mM NaCl at pH 7.4
P1-P1'	cleavage is catalyzed between P1 and P1' (scissile bond)
PPIs	protein-protein interactions

RRC	Research Resources Center at the University of Illinois at Chicago
SBDP	spectrin break-down product
SBDP37	the 37 kDa N-terminal SBDP of SBDP150
SBDP120	the 120 kDa C-terminal fragment of SBDP
SBDP150	the 150 kDa C-terminal fragment of SBDP
SDS-PAGE	sodium dodecyl sulphate polyacrylamide gel electrophoresis
SS	Sjögren's Syndrome
TBI	traumatic brain injury
WT	wild type
Y2H	yeast two-hybrid

CHAPTER 1

INTRODUCTION

This thesis is divided into six chapters. I have two publications that resulted from the first part of my studies at UIC. Recently, I have submitted my first author paper for publication and the details of this work are described in Chapter 5.

In chapter 2, I introduce the background information on the biological systems and biophysical methods used in my research projects. I also provide an up-to-date picture of what is known on spectrin II and caspase systems.

Chapter 3 describes the work that was done in collaboration with Shahila Mehboob, Yuanli Song, Fei Long, Bernard D. Santarsiero and Michael E. Johnson on characterization of the tetramer formation of the brain spectrin isoforms. The atomic structure of the brain II-spectrin N-terminal segment was obtained using X-ray crystallography and molecular dynamic simulations methods. We also characterized the structure of the first 147 residues of II (II-N1) in terms of stability and binding affinity towards its binding partners with circular dichroism (CD) and isothermal titration calorimetry (ITC), respectively. I was involved in the purification of spectrin II-N1 and its seleno-Met variant and their characterization using CD. I prepared some crystals with previously determined growth conditions. I purified a mutant II-R37P protein and used ITC for its binding studies with I-spectrin. Moreover, I did ITC experiments for spectrin association using erythroid I with I and non-erythroid II with I protein titration pairs (data not shown in the paper). I performed thermal unfolding of all three proteins used in the studies, erythrocyte I-segment with residues 1-156 (I-N1), non-erythrocyte II-segment with residues 1-147 (II-N1), and its seleno-Met-labeled variant needed for X-ray studies. In addition, I was involved in the final stages of the structure refinement using Coot and its analysis with PDBsum. I helped in initial model building for

complex used in the molecular dynamics (MD) simulation studies performed by Yuanli Song, a former laboratory member.

Chapter 4 describes the effect of point mutation on a single residue at position 22 on spectrin dimer association. Yeast two-hybrid (Y2H) and ITC methods were used to study interactions. I expressed and purified six proteins used for ITC experiments. All proteins were characterized with CD. I performed all ITC measurements. The Y2H studies were done by Akin Sevinc, a former laboratory member.

The work described in chapter 5 was supported from an NIH training grant (MOST-T32) for the time period 2009-2011 awarded by UIC College of Dentistry. We have followed the break-down of α -spectrin model proteins by caspase-3 in detail with fluorescence and gel electrophoresis methods. This work resulted in a manuscript with me as the first author and has been submitted recently.

Chapter 6 describes experiments done recently toward the characterization of the caspase recognition sites using recombinant spectrin model protein. The atomic structure of domain thirteen (D13) of brain α -spectrin consisting of residues 1441-1556 residues was obtained. D13 consists of the D1478 caspase-3 cleavage site. Using the structural information from x-ray diffraction data, together with studies of spectrin model proteins involved in caspase-3 catalysis discussed in chapter 5, we examined structure - sequence correlation and its effect on the cleavage efficiency. In addition, I was able to get diffractable crystals for spectrin model proteins containing the D1185 site. However, the structure is not yet solved at this time. This work will be continued by other members in the laboratory.

CHAPTER 2

BACKGROUND

2.1 Non-Erythroid α -Spectrin

2.1.1 Distribution and Localization

Spectrin originally discovered for its key role in red cell flexibility, serves as a linking element between the cell membrane and the cytoskeleton. More recently, spectrin has been shown to be involved in a variety of membrane-cytoskeletal interactions, signal pathways, and motor protein functions in non-erythroid (brain) cells (Fig 2.1). Spectrin consists of 3% of the total membrane protein in the brain (Yan and Jeromin, 2012). The major brain spectrin variants are the α II, α II, α III, and α IV subunits. Spectrins can be found in neuronal cell bodies, dendrites, and postsynaptic terminals. Furthermore, spectrin expression has been also identified in glial cells in the central and peripheral nervous systems, including astrocytes and Schwann cells (Susuki *et al.*, 2011). Both α II- and α II-spectrins are required during nervous system development. They are found in axon initial and terminal segments (Fig 2.2) and nodes of Ranvier, and they are recognized for their crucial role in stabilization of synapses in neurons (Xu *et al.*, 2013). Moreover, other studies showed importance of α II in the DNA intrastrand cross-links repair (Machnicka *et al.*, 2011).

2.1.2 Spectrin Structure

The primary structure of both spectrin subunits (α and β) was found to consist of many in tandem homologous sequence motifs (Speicher *et al.*, 1983). Each motif is about 106 amino acids in length, with 21 such sequence motifs in α -spectrin and 16 in β -spectrin. These homologous sequence motifs fold into similar structural domains, consisting mostly of coiled-coils of triple α -helices (Speicher *et al.*, 1984).

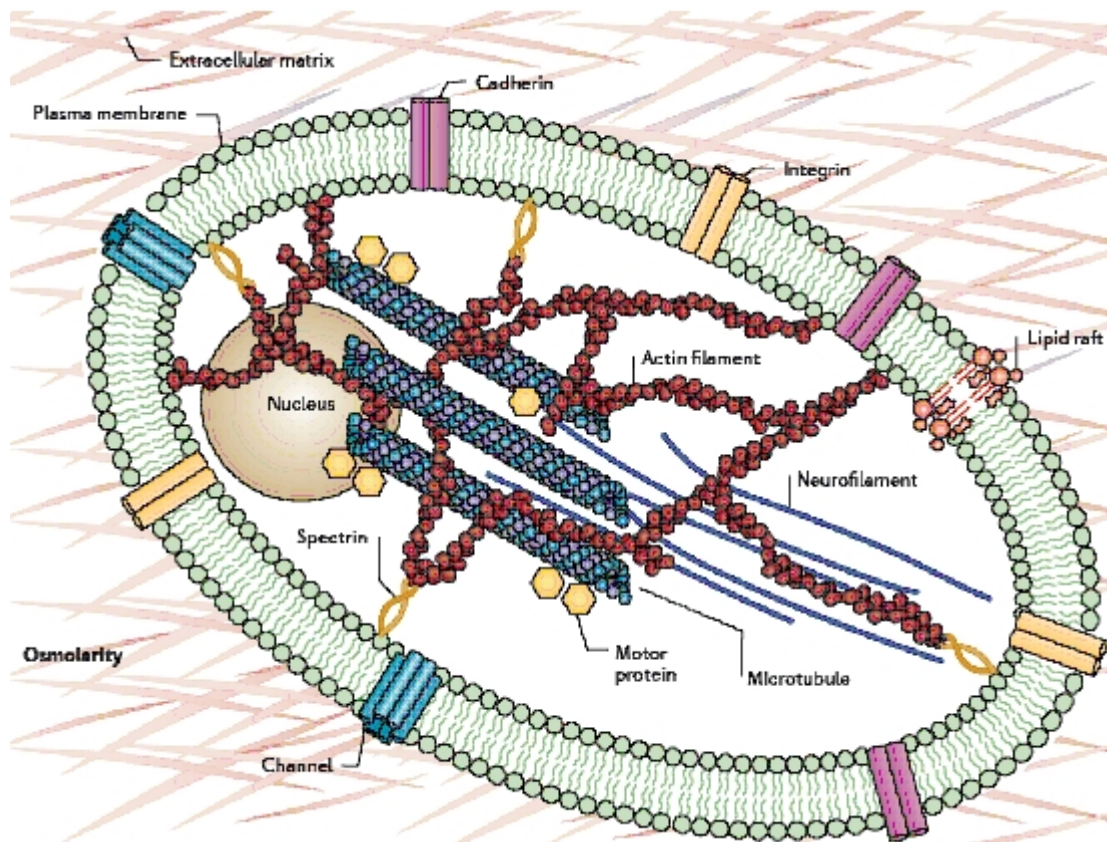


Fig 2.1 The cell body of a neuron. The components illustrated, such as the plasma membrane, ion channels, actin filaments, microtubules, neurofilaments, motor proteins, spectrins, integrins, extracellular matrix, lipid rafts and osmolarity, have key roles in neuronal and glial function. Reprinted by permission from Macmillan Publishers Ltd: Nature Reviews, Tyler, W. J. The mechanobiology of brain function. 13, 867-878, copyright (2012).

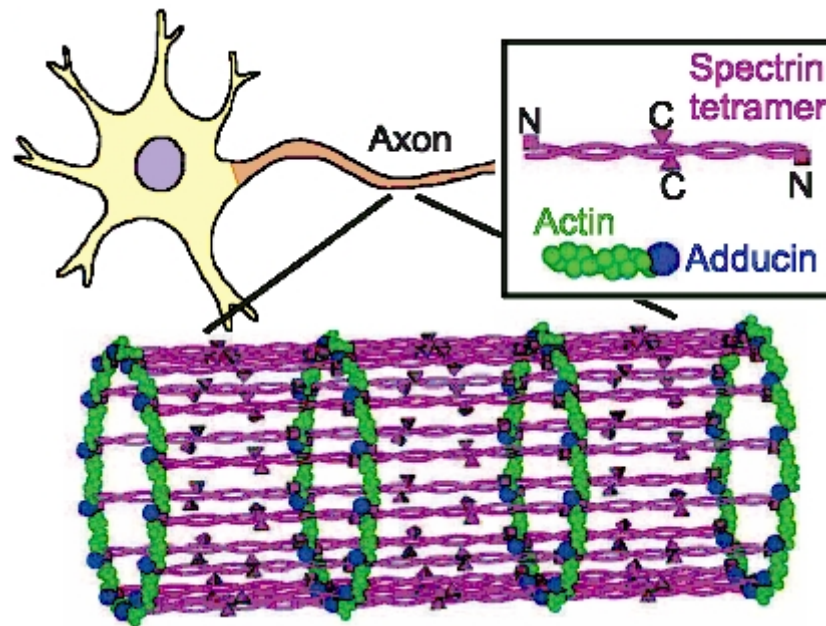


Fig 2.2 A model for the cortical cytoskeleton in axons. Short actin filaments (green), capped by adducin (blue) at one end, form ringlike structures wrapping around the circumference of the axon. Spectrin tetramers (magenta) connect the adjacent actin/adducin rings along the axon with a periodicity of ~180 to 190 nm. The letters “C” and “N” denote the C terminus (magenta triangles) and N terminus (magenta squares) of α -II-spectrin, respectively. Reprinted by permission from The American Association for the Advancement of Science: Science, Xu, K., Zhou, G., and Zhuang, X. Actin, Spectrin, and Associated Proteins Form a Periodic Cytoskeletal Structure in Axons. 339, 452-456, copyright (2013).

In such helices, the amino acid residues display a periodic heptad pattern where amino acid residue positions are designated as *a-g*. The *a* and *d* positions are occupied by non-polar residues that are involved in hydrophobic interactions. The *e* and *g* positions often contain charged residues that can form interhelical salt-bridges with oppositely charged residues (Parry *et al.*, 1992). However, naturally occurring coiled coils do not necessarily follow the ideal pattern.

The spectrin - based skeleton is composed of α , β -spectrin heterodimers that associate head-to-head into tetramers. Tetramer formation involves association of the N-terminal region of the β -subunit (C' helix) with the C-terminal region (A₁, B₁ helices) of the α -subunit forming a composite 3-helix bundle (Fig 2.3 A, B) (Mehboob *et al.*, 2010).

Spectrin domains have often been referred to as spectrin repeat, implying that all spectrin structural domains are identical. However, experimental data shows that this is far oversimplified statement. The atomic structures of 12 different spectrin domains have been published. These domains include D14 of Drosophila spectrin (Yan *et al.*, 1993; PDB code: 2SPC), human erythroid I-D1 (Park *et al.*, 2003; 1OWA), I-D8-D9 (Kusunoki *et al.*, 2004; 1S35) and I-D14-D15 (Stabach *et al.*, 2009; 3EDU and 43; 3F57), non-erythroid II-D14-D16 (Davis *et al.*, 2009; 3EDV), and chicken brain II-D15-D17 (Kusunoki *et al.*, 2004; 1U5P & 1U4Q, 2; 1CUN and Pascual *et al.*, 1997; 1AJ3). All published X-ray structures show extensive structural variation between spectrin domains. Like the domain 15 of I-spectrin with the BC loop, which is a unique ankyrin binding site (Davis *et al.*, 2009). Also, the different conformations in the junction regions of N-terminal I- and II-spectrin which affect tetramerization affinity (Li and Fung, 2009).

In addition, a systematic study of the thermal unfolding of erythroid and non-erythroid spectrin domains have show different thermal stabilities and unfolding patterns going from one domain to another (Lusitani *et al.*, 1994; An *et al.*, 2006).

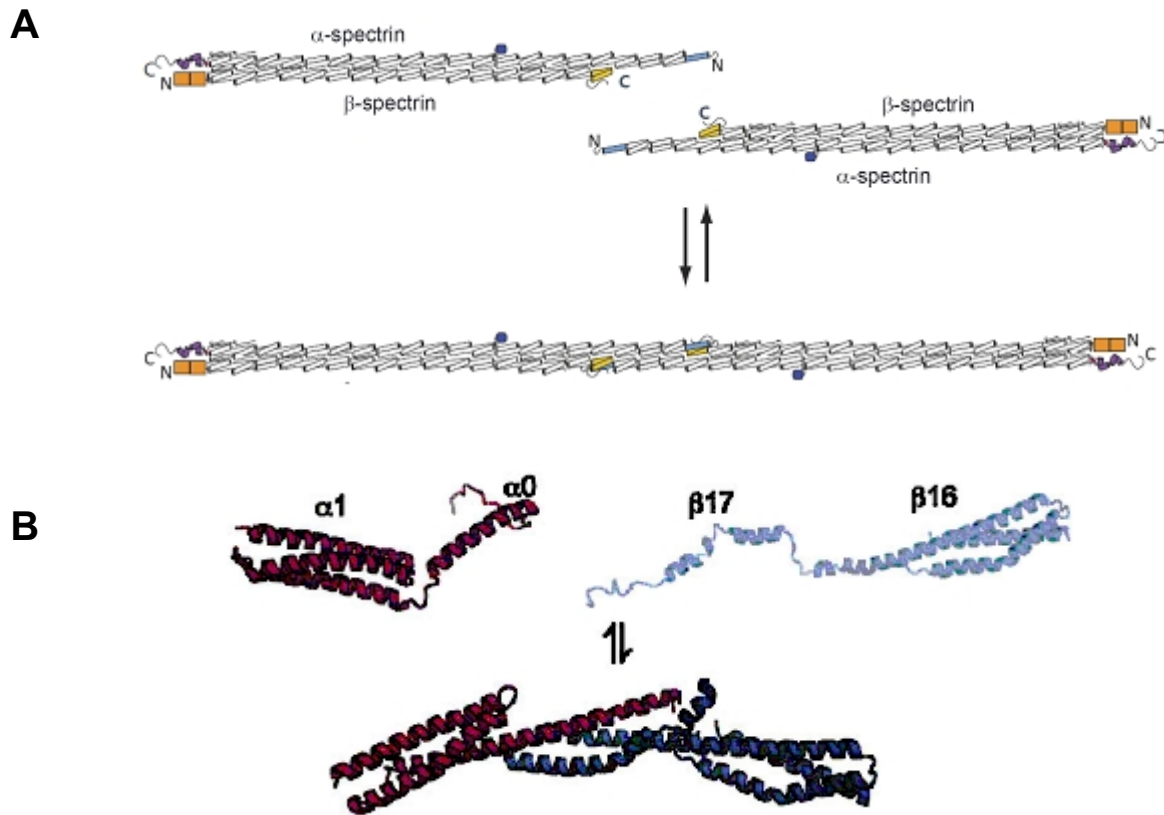


Fig 2.3 (A) spectrin assembly by formation of dimers first by specialized dimerization domains. Subsequent tetramer formation occurs through head-to-head association of spectrin heterodimers. Tetramer formation involves association of the N-terminal region of the subunit (blue) with the C-terminal region (α_1 , β_1 helices) of the subunit (yellow). (B) Association of I-N1 (pink) and 16 17 (blue) at the tetramerization site. Cartoon of unbound I-N1 is based on an NMR structure (pdb 1OWA) Park *et al.*, 2003. The cartoon of the final bound complex is based on a crystal structure (pdb 3LBX) Ipsaro *et al.*, 2010. Adapted from: Shammass *et al.*, 2012 and Ipsaro *et al.*, 2010.

Those unique structural features in each domain may lead to different contributions to the overall functional properties of spectrin, such as spectrin's rigidity/flexibility in the cytoskeletal network of different cells.

2.1.3 Non-Erythroid vs. Erythroid Spectrin

Non-erythroid, or brain, spectrin (spectrin II) exhibits high sequence homology with erythroid spectrin (spectrin I), despite their different cellular physiological functions (Bennett and Healy, 2008). Non-erythroid α -spectrin (II-spectrin) associates with non-erythroid β -spectrin (II-spectrin) to form tetramers in a manner similar to that of erythroid spectrin, except with higher affinity (Li, *et al.*, 2009).

The N-terminal partial domain region in II shares over 60% sequence similarity and more than 50% identity with the corresponding region in I (Mehboob *et al.*, 2003; Li and Fung, 2009), and the C-terminal partial domain region in II (residues 2010-2087) shares over 80% sequence similarity and over 70% identity with I (residues 2002-2079). Yet, spectrin II exhibits about 15-fold higher affinity than spectrin I in its $\alpha\beta$ association at the tetramerization site (Begg *et al.*, 1997).

In previous work, we have provided indirect evidence that the conformation of the region connecting the first structural domain and the partial domain region of α -spectrin plays an important role in the interactions between α - and β -spectrin leading to the formation of spectrin tetramers (Mehboob *et al.*, 2003; Long *et al.*, 2007; Song *et al.*, 2009). Specifically, our NMR (Park *et al.*, 2003), small angle X-ray scattering (Mehboob *et al.*, 2003) and spin label EPR (Antoniou *et al.*, 2008) studies of I have shown that the junction region in I is unstructured, and that mutations in Helix C' produce decreased association that correlates with the severity of hereditary spherocytosis (Park *et al.*, 2002). More recently, our small angle X-ray scattering (Mehboob *et al.*, 2003) and spin label EPR (Li and Fung, 2009) studies of II suggest that the junction region in II is helical, while our spin label EPR studies show that the N-terminal end of Helix C' is frayed (Fig

2.4) (Li and Fung, 2009).

In addition, apparent stiffness or rigidity of spectrin molecules is correlated with its structural domain stability (An *et al.*, 2006), and the brain spectrin with higher rigidity indeed shows greater structural stability in many structural domains compared to those in erythrocyte spectrin despite the similarity in their primary structures.

Another important characteristic of α II that distinguishes it from α I, is the presence of 34 amino acids insert in the middle part of the protein (domain 10) near SH3 domain. This region bears several cleavage sites for different proteases, including calpains and caspase-3.

It has been shown recently that the periodic organization of the cytoskeleton in axons is distinct from pentagonal or hexagonal structure observed for the erythrocyte membrane cytoskeleton. In axons spectrin tetramers are aligned longitudinally along the axonal shaft and connect the adjacent actin/adducin rings along the axon with a periodicity of ~180 to 190 nm representing the length of single spectrin tetramer (Fig 2.2) (Xu *et al.*, 2013).

2.1.4 Spectrin Mutations at the Tetramerization Site

Hereditary elliptocytosis (HE), hereditary pyropoikilocytosis (HPP), and hereditary spherocytosis (HS) diseases involve mutations in erythroid spectrin that destabilize its tetramers, resulting in low levels of spectrin tetramers and high levels of dimers (Delaunay and Dhermy, 1993; Delaunay, 2007). It has been found that affected patients' red blood cells are osmotically fragile and lose their membrane spontaneously (Baines, 2009). The majority of HE/HPP mutations in this region eliminate or modify a positively charged residues (R45[S/T], K48R). These mutations extensively perturb binding affinity (Lam *et al.*, 2009). In addition, G46V and L49F have been shown to affect the binding interface or α -spectrin itself, respectively (Kang *et al.*, 2010; Song *et al.*, 2009). No mutations at the tetramerization site of α II have been reported previously.

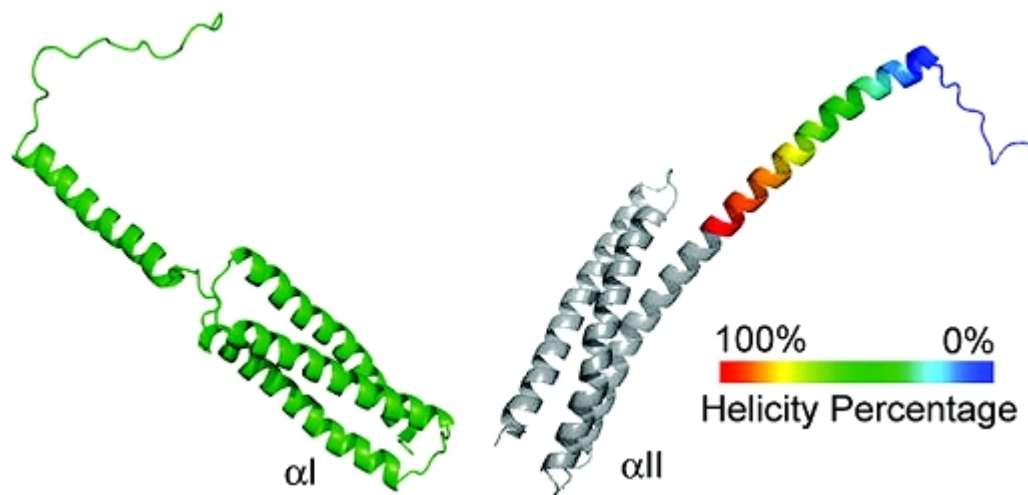


Fig 2.4 I-N1 vs II-N1. NMR structure of I-N1 shows junction region to be unstructured (Park *et al.*, 2003). EPR structure of II-N1 shows junction region to be helical (Li and Fung, 2009). Figure from Li and Fung, 2009.

However, the high sequence homology among α I, α II, β I, and β II-spectrin at the tetramerization site suggests similar coiled coil helical bundling for spectrin I and spectrin II to form tetramers (Li *et al.*, 2009). Therefore, it is possible in theory to use most of the molecular information obtained from the well studied spectrin I (both α I and β I subunits) and apply to the less studied spectrin II (α II and β II).

2.1.5 Spectrin Tryptophans: Intrinsic Reporters of Spectrin Structure and Function

There are 42 tryptophans in each of the α and β subunits in the spectrin dimer (Winkelman *et al.*, 1990). These tryptophans are distributed over the entire spectrin molecule. The typical 106 amino acid long domain in spectrin have 2 tryptophans located at the 16th and 88th residue (Mehboob *et al.*, 2010). Some of these tryptophans have been shown to promote folding of spectrin domains (MacDonald *et al.*, 1994) and contribute to their thermodynamic stability (Pantazatos and MacDonald, 1997). The fact that tryptophans are distributed over the entire molecule and yet are localized in the same position in each domain makes them convenient intrinsic fluorescence reporter groups for monitoring environmental changes upon caspase-3 cleavage.

2.2 Caspase-3

2.2.1 Distribution and Localization

Pro-caspases are known to be present in most, if not all cells (Chan and Mattson, 1999). Caspase-3 is the most abundant caspase in cells, around 200 nM (Denault and Salvesen, 2001). Caspase-3 expression is regulated spatially and temporally depending on cell type and developmental stage (Chan and Mattson, 1999). Caspase-3 mRNA is decreased during brain development (Kumar *et al.*, 1994). Mice lacking caspase-3 have severe defects in nervous system development.

2.2.2 Structural Organization

Fourteen caspases have been identified that can be divided into three functional groups

associated with the inflammation or apoptosis. First group associated with inflammation contains caspases-1, -4, and -5. The other two groups associated with apoptosis include initiator caspases (-2, -8, -9, and -10) and the effector caspases (-3, -6, and -7). According to the position in the signaling pathway, caspases are divided into two groups. Caspase-2, 8, 9, and 10 are initiator caspases because they are located on the upstream of the signaling cascade. Caspase-3, 6, and 7 are executioner caspases which are located on the bottom of the cascade.

Caspase-3 is synthesized in the cytosol as immature zymogen requiring specific proteolysis for activation. Caspase-3 zymogen (procaspase-3) is a homodimer of heterodimers, with each heterodimer containing a small subunit of approximately 10 kDa and a large subunit of approximately 20 kDa. Subsequent cleavage by either caspase-8 or -9 within the catalytic domain is essential for the activation process. Caspase-3 in its active form is a dimer with two small and two large subunits and two identical active sites (Fig 2.5 A). Each caspase-3 active site consists of the conserved catalytic histidine-cysteine motif and a large pocket capable of accommodating its substrate.

The subunits of each catalytic domain are sandwiches, folded into a compact cylinder with six-stranded β -sheets in the center surrounded by five helices. The catalytic dimer contains monomers arranged by two-fold symmetry, with two active sites found at opposite ends of the dimer.

2.2.3 Apoptotic Functions of Caspase-3

The programmed cell death, also named apoptosis, is a critical event in the cell life cycle. Apoptosis is a highly regulated process that is crucial for normal development and homeostasis of multicellular organisms. Normal healthy individual produces between 10^{11} to 10^{12} cells per day (Denault and Salvesen, 2001). This proliferation is balanced by programmed cell death to maintain a constant cell number.



Fig 2.5 (A) Caspase-3 structural organization. 277 a.a homodimer of heterodimers. Each heterodimer contains a small subunit (yellow) ~10 kDa, and a large subunit (orange) ~20 kDa. Intrachain cleavage (initiator caspases) is needed for activation. Upon activation the N-terminal domain (28 a.a) is removed C-terminal end of the large subunit becomes the L2 loop (contains the catalytic cysteine) N-terminal end of the small subunit becomes the L2' loop. Substrate-binding groove is composed of 4 loops (L1-red, L2-blue, L3-magenta, and L4-black) from one monomer (pointing arrow). PDB ID: 1CP3 (Mittle *et al.*, 1997) (B) Schematic representation of caspase substrate binding site with a scissile bond. Reprinted by permission from Annual Reviews: Annu. Rev. Biochem., Crawford, E. D., and Wells, J. A. Caspase substrates and cellular remodeling. 80, 1055-1087, copyright (2011).

Too much apoptosis results in degenerative disorders, ischemic injury and too little results in oncogenesis, autoimmune diseases etc.

Caspases are recognized as essential mediators of apoptotic cell death. In both the intrinsic and extrinsic apoptotic pathways, initiator caspases act as signal transducers, directing the cell toward death by activating executioner caspases (Fig 2.6). Apoptosis is characterized by a series of highly ordered cell morphological and biochemical changes, including blebbing, loss of membrane asymmetry and attachment, cell shrinkage, nuclear fragmentation, chromatin condensation, and chromosomal DNA fragmentation (Fischer *et al.*, 2003). In the end, the cell will be lysed and debris will be degraded. In general, apoptosis occurs when a cell is injured beyond repair, infected by virus, or under stressful conditions such as heat or radiation.

2.2.4 Non-apoptotic Functions of Caspase-3

Recent studies showed that more than one-third of proteolytic fragments generated by caspase-3 cleavage are stable and they may be involved in totally new functions (Dix *et al.*, 2008). This is in contrast to the notion that cleaved caspase substrates are rapidly degraded. Caspases are involved in cytokine processing during inflammation, cell cycle progression, differentiation of progenitor cells during erythropoiesis and of muscle cells, lens fiber development, and proliferation of T lymphocytes (Gulyaeva, 2003). Different expression of caspase-3 in a rat brain during development and aging suggests that caspases not only contribute to the regulation of neuronal death, but also to synaptic plasticity (D'Amelio *et al.*, 2010).

2.2.5 Caspase-3 Substrate Specificity

A peptide containing sequence P4-P3-P2-P1-P1', with P1-P1' as scissile bond (Fig 2.5 B), is a caspase substrate when (1) the P1 residue is Asp, (2) the P1' residue is small and uncharged (Gly, Ser, Ala) (Fig 2.7), (3) P4-P3-P2 residues are complementary for interactions with the catalytic groove, and (4) the substrate cleavage site (P4-P1') is exposed to the aqueous environment (Pop and Salvesen, 2009).

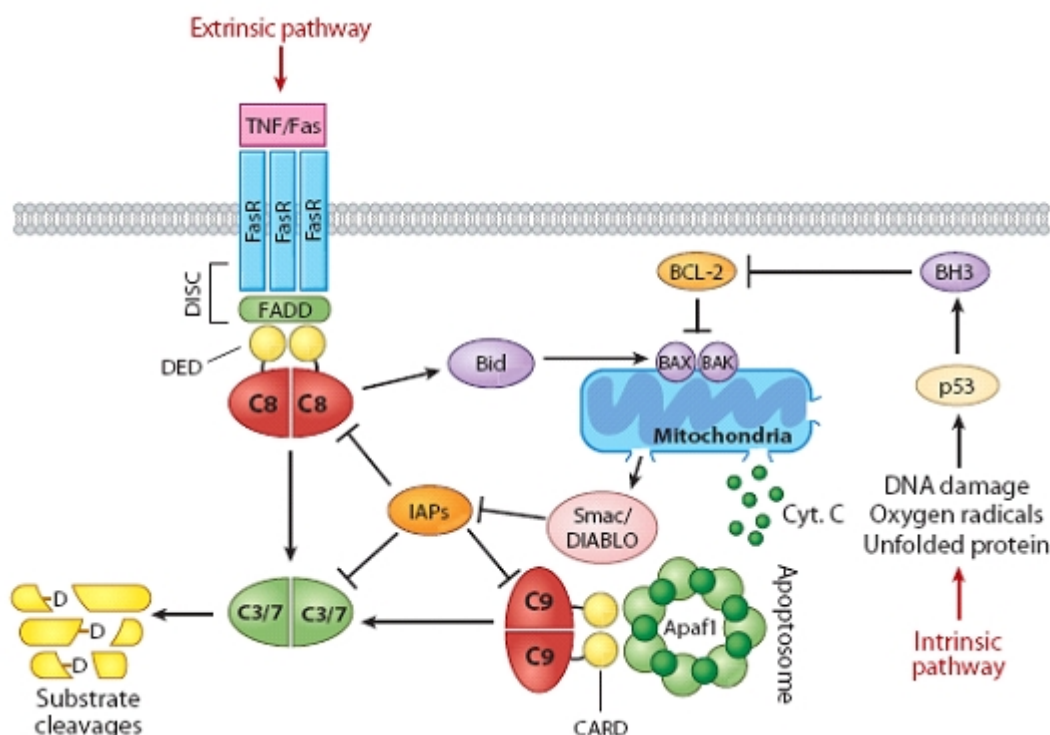


Fig 2.6 Intrinsic and Extrinsic Caspase-3 Activation Pathways. The extrinsic pathway is initiated by an extracellular stimulus that is transmitted to the cytosol by transmembrane death receptors that belong to the family of tumor necrosis factor (TNF) receptors. Recruitment of procaspases-8 and -10 as well as other ligands at this receptor leads to the formation of a death-inducing signaling complex (DISC). The intrinsic pathway responds to apoptotic stimuli such as mitochondrial/DNA damage, cytotoxic stress, or UV radiation. Release of cytochrome c from the mitochondria stimulates the formation of an apoptosome which contains the apoptotic protease activating factor 1 (Apaf-1) as its central element. Apaf-1 then associates procaspase-9 via its CARD domain resulting in the casp-9 activation. In a second step, the effector procaspases-3, -6, and -7 are processed by their upstream initiators. Reprinted by permission from Annual Reviews: Annu. Rev. Biochem., Crawford, E. D., and Wells, J. A. Caspase substrates and cellular remodeling. 80, 1055-1087, copyright (2011).

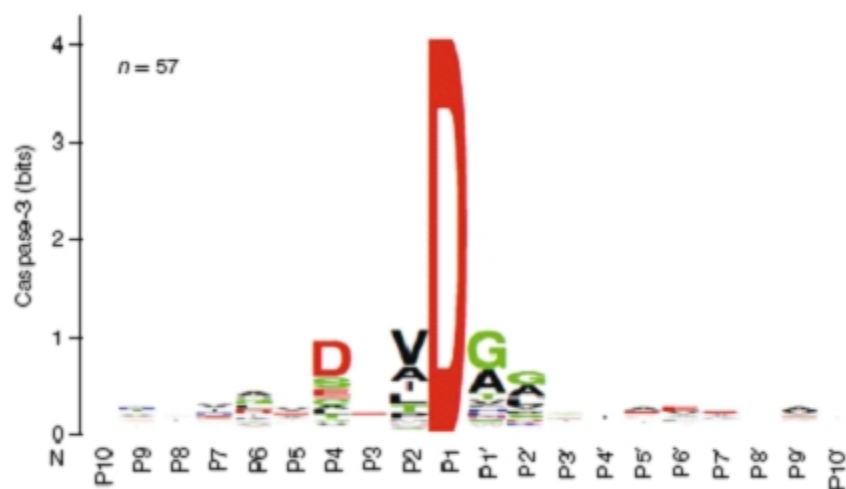


Fig 2.7 Amino acid substrate sequence specificity of caspase-3. Reprinted by permission from Nature Publishing Group: Nat. Struct. Mol. Biol., Timmer, J. C., Zhu, W., Pop, C, Regan, T., Snipas, S. J., Eroshkin A. M., Riedl, S. J., and Salvesen, G. S. Structural and kinetic determinants of protease substrates. 16, 1101-1109, copyright (2009).

However, the presence of the preferred cleavage site sequence is not sufficient for a protein substrate to be cut. Several natural caspase substrates containing non-canonical cleavage recognition sequences were found (Timmer and Salvesen, 2007). Thus, the preferred cleavage site sequence on a protein is neither sufficient nor necessary to be a real cleavage site *in vivo*.

Primary structure is only one aspect of caspase substrate recognition; secondary, tertiary, and quaternary structure effects, as well as localization, are also important. Our current understanding of caspase-3 cleavage site preferences is still limited and could not be reliably used to predict the sites without experimentation.

2.3 Spectrin & Caspase-3

2.3.1 Spectrin II - Prominent target of Caspase-3

While many proteins are cleaved during apoptosis, a prominent target of caspase-3 action is II-spectrin. II-spectrin has long been recognized to be a significant substrate for caspase-3 during apoptosis in lymphocytes, hematopoietic cells, and neurons (Wang et al., 1998). Numerous studies report that the spectrin breakdown products (SBDP), of molecular mass 150 kDa (SBDP150) and 120 kDa (SBDP120) are detected in several brain related injuries, such as traumatic brain injury (Hyman and Yuan, 2012), mechanical stretch injury (Pike *et al.*, 2000), ischemia, and degenerative diseases. SBDPs are found in postsynaptic densities. Spectrin regulates the surface morphology of cells and thus its partial degradation would be expected to produce persistent modifications in synapses (Lynch and Baudry, 1984).

Furthermore, SBDP120 has been shown in the salivary gland, and plays a crucial role as an auto-antigen in the development of primary Sjögren's Syndrome (Haneji *et al.*, 1997). There is also increased evidence for nonapoptotic roles of caspase-3 in the brain, including the regulation of synaptic plasticity (Crawford and Wells, 2011) and of neuronal morphology via local remodeling of the spectrin cytoskeleton (Westphal, 2010).

2.3.2 Sjogren's Syndrome (SS)

Sjögren's Syndrome, also known as "Sicca Syndrome", is a systemic autoimmune disease in which immune cells attack and destroy the exocrine glands that produce tears and saliva, resulting in xerophthalmia (dry eye) and xerostomia (dry mouth) (Moody *et al.*, 2001). It has been suggested by various studies that the autoimmune aspect of the disease comes from apoptotic cell death which is caused by the degradation of cellular proteins. Spectrin II has been identified as one of these proteins, and elevated levels of anti-spectrin antibodies have been identified in SS patients (Jin *et al.*, 2011). These antibodies are not reactive to intact spectrin, but are reactive to spectrin fragments (SBDP120) generated by caspase-3 cleavage. It has also been shown that mucosal administration of spectrin II in mice effectively inhibits the progression of SS autoimmunity (He *et al.*, 2008), further emphasizing the significance of spectrin in SS.

2.3.3 Biological Significance

In the event of neuronal stress, traumatic brain injury (TBI), mechanical stretch injury, ischemia and under acute and chronic degenerative conditions, enhanced spectrin-break down catalyzed by caspase-3 occurs. It has been reported that SBDP accumulating in cerebral spinal fluid (CSF) after TBI are associated with injury magnitude and predict lesion size (Pike *et al.*, 2000). Elevation of spectrin break-down products in different areas of the body leads to their potential application as biomarkers for neurodegenerative disorders (Yan and Jeromin, 2012).

Furthermore, recent studies show that the vast majority of proteolyzed proteins yielded persistent fragments that correspond to discrete protein domains, suggesting that the generation of active effector proteins may be a principal function of apoptotic proteolytic cascades (Dix *et al.*, 2008).

2.4 Biophysical Methods Used

2.4.1 Circular Dichroism

Circular dichroism (CD) is defined as the unequal absorption of left-handed and right-handed circularly polarized light (Greenfield, 2006). After circular polarized light passes through a medium of optically active molecules, the light remains circular polarized, but the intensity changes, and the absorbance depends on whether it is left- or right-circularly polarized light.

A molecule is optically active if it interacts differently with left- (L) and right- (R) circularly polarized light. The optical activity of small molecules arises from their lack of symmetry - particularly from the presence of asymmetric carbon atoms and from the effect of these atoms have on any nearby chromophores. Optical activity is detected as the differential absorption (dichroism) of L and R ($\epsilon_L \neq \epsilon_R$). This is so called circular dichroism.

CD can be measured by exposing a sample alternately to L and R and detecting just the differential absorptions. When the resulting two circularly polarized lights, with different amplitudes, combine, we have elliptically polarized light. The detected signal can then be processed to give a plot of $\Delta A(A_L - A_R)$ versus λ . CD data are presented in terms of either ellipticity $[\theta]$ (degrees) or differential absorbance (ΔA). The data are normalized by scaling to molar concentrations of the protein.

An advantage of the CD technique in studies of proteins is that complementary structural information can be obtained from number of spectral regions. In proteins, chromophores of interest include the peptide bond (absorption below 240 nm), aromatic amino acid side chains (absorption in the range 260 to 320 nm) and disulfide bonds (weak broad absorption bands centered around 260 nm) (Kelly *et al.*, 2005). CD of an α -helical protein, a negative band near 222 nm ($n \rightarrow \pi^*$) is observed due to strong hydrogen-bonding environment of this conformation. This transition is relatively independent of the length of the helix. A second transition at 190 nm ($\pi \rightarrow \pi^*$) is split into

a negative band near 208 nm and a positive band near 192 nm (Fig 2.8, black square). Both bands are reduced in intensity in short helices. The CD spectra of β -sheets display a negative band near 216 nm, a positive band between 195 and 200 nm, and a negative band near 175 nm (Fig 2.8, red circle). However, the position and magnitude of these bands is variable, resulting in less accurate predictions for β -structure than for α -helices by CD (Pelton and McLean, 2000).

The “low resolution” structures resulting from CD clearly do not provide the detailed structural information. Nevertheless, it can help to bridge the gap between amino acid sequence and function by providing clues to the structure a protein may adopt (Pelton and McLean, 2000).

2.4.2 Fluorescence

Fluorescence is a light emission, as opposed to light absorption, spectroscopy. There are several advantages of using fluorescence over other techniques: (1) fluorescence signals are very sensitive to the immediate environment of the probe, (2) the technique provides a very high signal-to-noise ratio using relatively small amount of material (10^{-8} M), about two orders of magnitude lower than those used for absorption spectroscopy, and (3) the time scale of emission is in the nanosecond range.

Fluorescence intensity depends on the lifetime of molecule in the excited state, which depends on competition between radiative emission and non-radiative processes (transfer of excitation energy to the surrounding - internal conversion, inter-system crossing, and quenching of various types). It is now well established that changes in intensity and emission maxima (λ_{max}) of intrinsic fluorescence can be used to monitor conformational changes of proteins (Beechem and Brand, 1985). In most proteins, the fluorescence is dominated by tryptophan.

Tryptophan, due to its aromatic character, is often found fully or partially buried in the hydrophobic core of protein, at the interface between two protein domains or subdomains, or at the subunit interface in oligomeric protein systems (Royer, 2006).

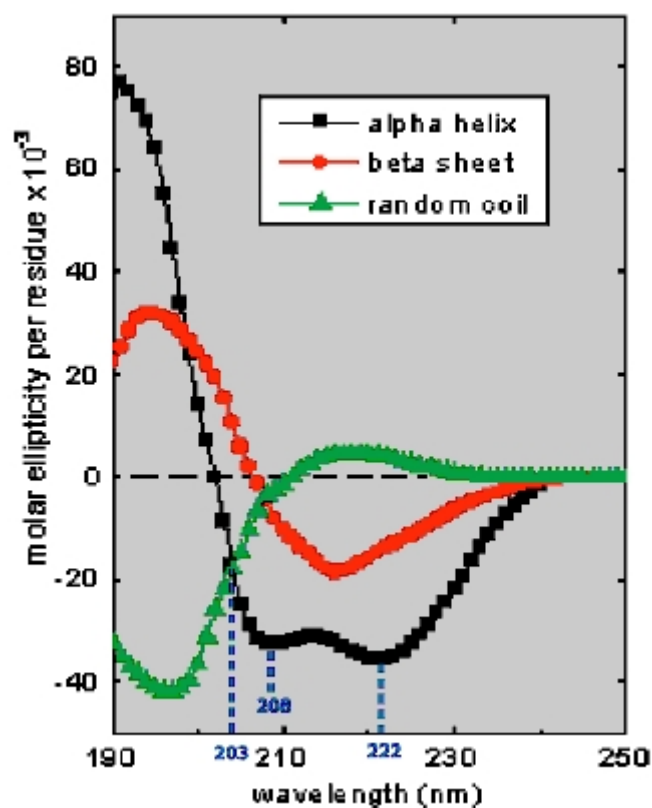


Fig 2.8 Typical CD spectra of proteins with representative secondary structures. Characteristic negative band near 208, 222 nm, and a positive band near 192 nm for α -helix (black square). The CD spectra of β -sheets display a negative band near 216 nm, and positive band between 195 and 200 nm (reg circle). Green triangle represents random coil.

The typical spectra of tryptophan in the solvent exposed environment has λ_{max} of about 355 nm.

However, it is difficult to predict the effect of the solvent on the overall maximum fluorescence intensity. This is due to the fact that several amino acid side chains, as well as the peptide bond, are efficient quenchers of tryptophan fluorescence. Generally speaking, if no major quenching occurs in the folded state, then one can predict that the solvent exposure will lead to an overall decrease in the intensity. However, in cases where strong quenching occurs in the folded state, exposure to solvent may actually result in an increase in overall fluorescence intensity (Royer, 2006).

2.4.3 Isothermal Titration Calorimetry (ITC)

Isothermal titration calorimetry is a quantitative, biophysical method used to measure the binding equilibrium directly, by determining the heat absorbed or released on association of a ligand with its binding partner.

A VP-ITC calorimeter (MicroCal, Piscataway, NJ) is composed of two identical cells made of a highly efficient thermal conducting material such as gold, surrounded by an adiabatic jacket. A protein is placed in a sample cell that is temperature controlled and coupled to a reference cell, filled with buffer or water, via a thermocouple circuit. Prior to addition of a ligand, a constant power (<1 mW) is applied to the reference cell. This directs a feedback circuit, activating a heater located on the sample cell (VP-ITC user's manual).

A ligand is then injected in small aliquots into the sample cell of the precisely known volume (Fig 2.9 A). The heat released or absorbed (depending on the nature of reaction, exothermic or endothermic, respectively) is in direct proportion to the amount of binding that occurs. Measurements consist of the time-dependent input of power required to re-establish thermal equilibrium between the sample and the reference cell.

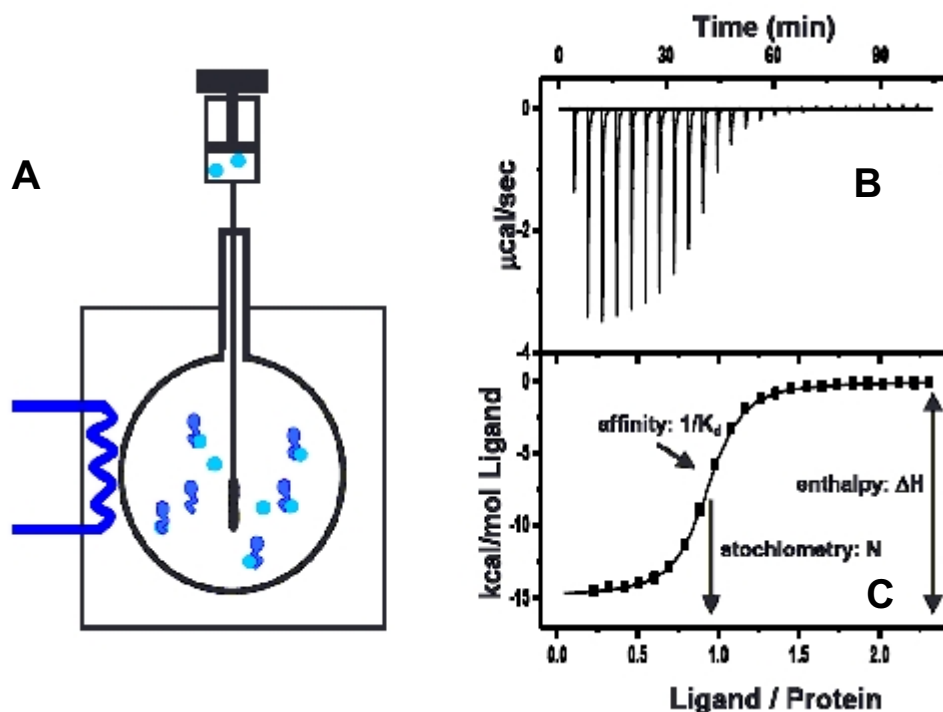


Fig 2.9 Configuration of an ITC sample cell. The cell volume is 1.4 ml and initially is filled with the macromolecule solution (dark blue). (A) The injection syringe is filled with the ligand solution (light blue). (B) At specified time intervals, a small volume of the ligand solution is injected into the sample cell triggering the binding reaction. (C) After integration of the area under each peak the individual heats are plotted against the molar ratio from which, through nonlinear regression, it is possible to estimate the thermodynamic parameters, n , K_d , and ΔH .

The obtained raw data consist of a series of spikes, each spike representing the power in cal/sec needed to maintain the reference and the sample cell at an identical temperature for every injection of a ligand (Fig 2.9 B). When the protein in the cell becomes saturated with added ligand, the differential power signal diminishes and only the background heat of dilution is observed.

To extract different thermodynamic parameters, the heat formation is plotted against the molar ratio of ligand/protein (Fig 2.9 C). By using data fitting for the suitable binding model, the change in enthalpy ΔH , the stoichiometry n , and the association constant K_a can be determined directly. The change in enthalpy corresponds to the intercept of the two asymptotic lines corresponding to the minimal and maximal heat of formation, n controls the position of the inflection point, and the slope at the inflection point reflects the association constant ($K_a = 1/K_d$). The terms ΔS and ΔG are subsequently derived from these data.

K_d values are obtained from fitting the amounts of heat evolved as various mole fractions of ligand are added to the protein, and can be obtained relatively accurately.

ΔH can also be obtained relatively accurately in well designed experiments such that, at the start of the titration, most all of the titrating ligand forms a complex with its partner, giving a relatively flat plateau. With the heat determined from the initial titration and an accurate determination of protein concentration, an accurate value (k_{cal}/mol) for ΔH can be obtained.

The K_d and ΔH values are obtained directly from regression of the ITC data.

ΔS accuracy may be lower, since ΔS is a secondary parameter calculated from K_d and ΔH , and includes the uncertainties of both. ΔG values obtained from summing the experimental values of ΔH and $-T\Delta S$ are not necessarily equal to the value calculated directly from K_d values ($\Delta G - K_d$).

Several features of ITC have facilitated its preferential use compared to other techniques which estimate binding affinity. It is a sensitive, rapid and direct method with no requirement for chemical modification or immobilization.

2.4.4 ITC vs. Yeast Two Hybrid (Y2H) Method

There are many methods available to study protein-protein interactions (PPIs) that extend from very qualitative approaches to highly quantitative measurements. Yeast two-hybrid assay (Y2H) has proven to be a powerful method to detect PPIs, however it is a poor method for quantitative characterization of the strength of an association. Isothermal titration calorimetry (ITC) is the method of choice where a quantitative understanding of the association affinity of the well-established interacting protein pairs is needed (Falconer, 2010). The method does not require that the target protein be labeled or bound to a surface, allowing the proteins to be studied in solution in a native state (Doig, 2007). In contrast to Y2H system ITC gives the direct measurement of the affinity that is not affected by the cell environment, location or the concentration of other proteins within the cell (Doig, 2007).

ITC method provides detailed information on binding thermodynamics well as interaction affinities from a single experiment. The measured values are directly determined from the resulting heat uptake or release upon binding, as opposed to the use of non-calorimetric methods relying on estimating these values (Falconer, 2010).

The affinity range that can be measured accurately by ITC is generally limited to between $\sim 1 \text{ nM} < K_d < \sim \text{several hundred micromolar}$ (Falconer, 2010). The low affinity limitation arises because at very high K_d (low binding) the concentration of sample in the cell must be very high this may lead to precipitation of proteins at high concentration.

Numerous articles have been written describing in detail the practical, theoretical aspects of ITC and its applications (Freire, 2009; Pierce, 1999; Freyer, 2008).

In chapter four, we have demonstrated ITC as a method of choice to accurately determine and discriminate the order of binding affinities of several spectrin mutants as the well-established protein-protein binding model. ITC allowed us to discriminate the effect of the mutation on the dissociation affinity that could not be established using Y2H method.

2.4.5 X-ray Crystallography

Two methods are currently widely used for determining protein structures, X-ray protein crystallography and nuclear magnetic resonance (NMR). Compared with NMR, crystallography has no limitation on the size of macromolecules. The entire process of protein crystallography includes the following steps: crystallization, data collection, phasing, model building, and structure refinement.

2.4.5.1 Protein Crystallization

Crystallization techniques fall into several categories such as, vapor diffusion, batch, and dialysis. The most commonly used technique found under the category of vapor diffusion is the hanging drop. Hanging drop is a popular method used for setting up initial crystal screening because it is easy to perform, requires a small amount of sample, allows a large amount of flexibility during screening and optimization, and easy access to the drop.

A small (0.1 to 20 μ l) droplet of the sample mixed with crystallization reagent is placed on a siliconized glass cover slide inverted over the reservoir in vapor equilibration with the reagent. The initial reagent concentration in the droplet is less than the reservoir. Over time the reservoir will pull the water from the droplet in a vapor phase such that an equilibrium will exist between the drop and the reservoir. During this equilibration process, the sample is also concentrated, increasing the relative supersaturation of the sample in the drop.

Crystals can appear as needles, blades, spherulites, plates, and various geometric shapes within few hours after set up. Crystals vary in size anywhere from a barely observable 20 microns to 1 or more mm but most seem to fall in the range of 0.05 to 0.5 mm (Hampton Research; Aliso Viejo, CA). Crystals useful for x-ray diffraction analysis are typically single, 0.05 mm or larger, and free of cracks and defects.

2.4.5.2 Data Collection

A crystal is a three-dimensional periodic array that consists of a unit cell replicated in space. Crystal is formed by highly ordered repeats of unit cells, Fig 2.10 A. The principle of protein X-ray crystallography is shown in figure 2.10 B and it is described by the Bragg's law, $n\lambda = 2d \sin \theta$.

In this equation, λ is the wavelength of the radiation used, n is an integer, d is the perpendicular spacing between the lattice planes in the crystal, and θ is the complement ($90^\circ - \theta$) of the angle of incidence of the X-ray beam (and thus also the complement of the angle of scattering or "reflection"). In Fig 2.10 B, 1 and 1' correspond to two equivalent atoms in two repeated unit cells. Two reflections (diffracted beams), a and b from planes m and m' respectively are generated when X-ray beam hits these two atoms. Since X-rays are a type of electromagnetic wave, the amplitudes of a and b will be amplified if they are in the same phase when they reach the detector. On the other hand, their amplitudes will be cancelled out if they are in opposite phases. According to Bragg's law, if the difference between the pathlengths of a and b equals $n\lambda$ then a and b will have the same phase when they reach the detector. This means we can find the θ by simply rotating the crystal because λ and d are constants for a particular experiment. Since every equivalent atom in each unit cell will generate a reflection, once the X-rays strike the crystal from the right angle θ , the amplitudes of all these reflections will be summed up on the detector and thus form one bright spot. In contrast, reflections generated by nonequivalent atoms will not generate any data because their amplitudes will be canceled out due to different phases. The intensity of the spot is proportional to the square of the amplitude of the diffracted wave. With the phase and intensity information, a directly Fourier transform operation would produce electron density information, and thus structural information.

Since low temperature can increase the stability of molecules and thus enhance diffraction quality, X-ray diffraction data are currently collected under a stream of liquid nitrogen.

Following the Bragg's law, an X-ray beam will be diffracted into many particular directions after striking the crystal and thus form a spot on the detector. The detector will record the diffraction pattern as one diffraction frame. The crystal is rotating during the data collection. In order to determine the protein structure, a large number of frames must be taken at different angles. Data collection should be completed in the shortest time as possible in order to prevent the X-ray radiation damage to overall alignment of unit cells in the crystal.

2.4.5.3 Phasing

The electron density at a point x, y, z in a unit cell of volume V_c is

$$\rho(xyz) = 1 / V_c \sum_{\text{all } hkl} \sum_{\text{all } hkl} |F(hkl)| \cos[2\pi(hx + ky + lz) - \phi(hkl)]$$

Therefore, if we knew $|F(hkl)|$ (structure factor amplitude) and $\phi(hkl)$ (structure factor phase; relative phase angles) we could compute $\rho(xyz)$ (structure factor) for all values of x, y , and z and plot the values obtained to give a three-dimensional electron-density map. However, we can obtain only structure factor amplitudes and not relative phase angles directly from experimental measurements. The phase angle can have any value between 0 and 2π . There are at least 2^n possible choices of phase for a set of n diffraction spots.

Multiple isomorphous replacement is one of the methods to overcome the phase problem. In principle, isomorphous heavy-atom derivatives are obtained by attaching covalently a heavy atom metal to the protein, and then to subject it to crystallization conditions. However, replacing or adding atoms can disturb structure of the protein so that a formed crystal is no longer isomorphous. Often, one uses multiple wavelength anomalous dispersion (MAD) method where only one crystal is studied. The crystal contains atoms called anomalous scatterers, such as selenium. The scattered intensities of the parent and the derivatives are compared. A difference Patterson map calculated directly from the intensities mostly shows just heavy atom vectors. This allows a preliminary estimate of the heavy-atoms positions. Using these positions and the

differences between scattered intensities of the parent crystal and the derivatives, it is possible to estimate the phase of the scattered radiation. Finally, phases are available accurate enough to use in conjugation with the measured intensities to compute an image of the structure.

2.4.5.4 Model Building & Structure Refinement

Based on the electron density map, a protein structural model can be built. Usually the main chain atoms of the protein are fitted first into the density map. Side chain atoms are then added one by one according to the protein sequence. High resolution data can provide more detailed information. Generally speaking, the overall shape of a protein can be seen with the data of 5.5 Å and a position of single atoms can be determined with the resolution of 1.5 Å and better. The last step is refinement. In this step, the conformation of each individual residue needs to be examined. If the model structure does not fit the electron density perfectly, then the new electron density map is generated. The agreement of the individual observed structure factor amplitude with those calculated for the refined model is shown with the discrepancy index, R value. The discrepancy index is a useful but by no means definitive index of reliability of a structure analysis. Any anomalies in the molecular geometry, like abnormal bond distances etc. should be evaluated with the greatest care.

CHAPTER 3

CRYSTAL STRUCTURE OF THE NONERYTHROID α -SPECTRIN TETRAMERIZATION SITE REVEALS DIFFERENCES BETWEEN ERYTHROID AND NONERYTHROID SPECTRIN TETRAMER FORMATION

*The published work is attached as Appendix A.

*The procedures and results obtained by myself and not appeared in the publication are given in 3.1.

3.1 Experimental Procedures

3.1.1 Recombinant Proteins

An N-terminal segment of brain II-spectrin consisting of the first 147 residues (II-N1), similar to a well-studied erythroid I-spectrin segment consisting of the first 156 residues (I-N1) (Park *et al.*, 2003), was prepared from a similar recombinant protein with 149 residues (Mehboob *et al.*, 2003), following standard procedures (Li and Fung, 2009, Song *et al.*, 2009). This segment is predicted to include a partial domain that is responsible for associating with -spectrin to form tetramers, followed by the first full structural domain of brain -spectrin (Mehboob *et al.*, 2003; Li and Fung, 2009).

The procedures for preparing L-seleno-methionine (seleno-Met)-labeled II-N1 samples were similar to those used for NMR samples (Long *et al.*, 2007) except with methionine-auxotroph and protease-deficient competent cells B834(DE3) (Novagen - EMD Chemicals, Gibbstown, NJ). There are four methionine residues in II-1-147 spectrin model protein. Cells were grown in the M9 medium supplemented with seleno-Met (60 mg/L, ACROS Organics, Thermo Fisher Scientific Inc., USA) until the culture reached OD value of 0.7. Protein expression was induced by addition of 0.5 mM IPTG followed by six hours incubation at 37 °C with shaking. 9 g of cells were obtained from 4.5 L of media.

Three other recombinant model proteins, I-N1, a C-terminal segment of erythroid I consisting of residues 1898-2083 (I-C1), and a non-erythroid II segment consisting of residues 1906-2093 (II-C1), were also prepared. The plasmid of II-N1 with R37P mutation was prepared using site-directed mutagenesis methods with mutated primers to prepare the DNA construct and transformed into *E. coli* cells for protein expression and purification.

3.1.1.1 CD of Spectrin Model Proteins

Circular dichroism (CD) spectra at 20 °C for all proteins were obtained using a CD spectrometer (J-810, JASCO, Japan) with a 0.1-cm path length sample cell. Mean residue molar ellipticity values at 222 nm were used to calculate the helical content of the proteins using a value of -36,000 deg cm² dmol⁻¹ for a 100% helical conformation (Greenfield *et al.*, 1969).

3.1.1.2 Crystallization of II-N1

II-N1 and the seleno-Met-labeled II-N1 in 10 mM Tris buffer at pH 7.4 were concentrated to 7.5 mg/mL (500 M) and used for crystallization with hanging-drop vapor-diffusion methods at 20 °C. Each protein solution was mixed with an equal volume of reservoir solution to give a 2 L droplet. The reservoir solution contained a mixture of PEG8000 (Hampton Research, Aliso Viejo, CA) and PEG1000 (1:2 molar ratio) for II-N1, or of a PEG4000 and PEG1000 mixture (1:2 molar ratio) for seleno-Met labeled II-N1, both with 4% (final concentration) butane-1,4-diol (Hampton Research). Crystals from solutions without butane-1,4-diol diffracted poorly. To reduce radiation damage, all crystals used for diffraction experiments were frozen at 100 K, with 20% (v/v) Paratone-N (Hampton Research) added as a cryo-protectant.

3.1.2 Structural Analysis

The secondary structural elements (Kabsch and Sander, 1983), protein-protein interface areas and molecular interactions were analyzed with PDBsum (Laskowski, 2009). For molecular interactions, PDBsum identifies non-bonded contacts (NBC), and within NBC, specific interactions were identified as hydrogen bonds using strict geometric criteria (Xu *et al.*, 1997; Wallace *et al.*, 1995). In addition, salt bridges (Kumar and Nussinov, 1999) were identified separately.

Since PDBsum identifies protein-protein interactions as chain-chain interactions, we modified our pdb file and labeled each helix in our structure as a chain, including half of the loops connecting to the adjacent helices, in each PDB file to give inter-helical interactions. From these

inter-helical interactions, we examined clusters of atoms involved in NBC between helices, which consisted of hydrogen bonds, and salt-bridges. We also identified hydrophobic clusters from the NBC atom pairs, considering F, I, L, M, V, W and Y residues as hydrophobic cluster members (Silva, 2008).

3.1.3 Protein Thermal Stability

Protein samples (10-15 μ M) of II-N1, seleno-Met labeled II-N1 and I-N1 in PBS 7.4 were used for thermal stability studies. CD signal intensities at 222 nm of a sample were monitored as a function of temperature with a thermostated cell, from 20 to 100 $^{\circ}$ C at an interval of 1 $^{\circ}$ C. Fractions of thermal unfolding as a function of temperature were obtained from curve fitting of mean residue molar ellipticity values as before (Lusitani *et al.*, 1998) to give T_m . T_m was also obtained using the maximum of the first derivative of the CD signal as a function of temperature in order to minimize errors due to corrections for pre and post transitions used in curve fitting.

3.1.4 ITC of Spectrin Association

ITC measurements were performed at 25 $^{\circ}$ C with an isothermal titration calorimeter (VP ITC, MicroCal, LLC, Northampton, MA). Protein titration pairs (I-N1 and I-C1, I-N1 and II-C1, II-N1 and I-C1, II-N1 and II-C1, and II-N1-R37P and I-C1) were dialyzed together in 5 mM phosphate buffer with 150 mM sodium chloride at pH 7.4 to ensure identical solution conditions of the titration pairs to avoid introducing heat of dilution in the titration experiments. Each α -spectrin protein (about 400 μ M I-N1 or 60 μ M II-N1) was titrated into the sample cell containing one of the β -spectrin proteins (about 40 μ M in I or 6 μ M in II titration). The titration isotherm was analyzed by a single binding site model, provided by MicroCal software, to obtain an association constant (K_a), which was converted to a dissociation constant (K_d).

3.2 Results

3.2.1 Protein Characterization

The expected mass for II-N1 is 17,662.9 Da, and the experimental mass from the high resolution mass spectrometry is 17,662.2 Da. The expected mass for seleno-Met-labeled II-N1, with all four methionine residues labeled, is 17,850.6 Da, and the experimental mass is 17,850.3 Da. The II mutant R37P mass is 17,604.1 Da, with an expected mass of 17,603.9 Da. The helical content from CD measurements is about 70% for II-N1, 62% for the seleno-Met-labeled II-N1, 48% for II-N1-R37P and 52% for I-N1. The values for II WT and I-N1 are similar to our published values (Mehboob *et al.*, 2001). Dynamic light scattering experiments indicate that II-N1, at 2 mg/mL, is monomeric in solution, with a hydrodynamic radius (R_h) of about 30 Å (Long *et al.*, 2009).

3.2.2 II-N1 crystals

The native II-N1 crystals appeared 3 days after 20 °C incubation. The size of the crystal was 0.2 mm (Fig 3.1). Full description of X-ray diffraction data is given in the paper at the beginning of this chapter.

3.2.3 Thermal Stability and Inter-Helix Interactions

We observed similar thermal unfolding profiles for II-N1 and seleno-Met- II-N1. The T_m values are 73.1 °C and 74.6 °C. Determined T_m values from the direct fit and from the 1st derivative were very similar. The unfolding profile of the corresponding I protein (residues 1-156; I-N1) showed a similar unfolding pattern, except at lower temperatures, with a T_m value of 56.0 °C (Fig 3.2).

With an atomic resolution structure of D1- II, interaction analysis of inter-helical interactions shows multiple hydrogen bonds in M1 and M2. These hydrogen bonds satisfy the published, strict geometric criteria (Xu *et al.*, 1997; Wallace *et al.*, 1995) (see Experimental Procedures). Hydrogen

bonds are spread throughout the interfaces of the three helices to form hydrogen bond networks that stabilize the triple helical structural domain D1- II. No additional salt bridges are evident. Similar interaction analysis of D1- I of four randomly selected NMR structures (PDB code: 1OWA) shows only 1-2 inter-helix hydrogen bonds, and no hydrogen bond networks.

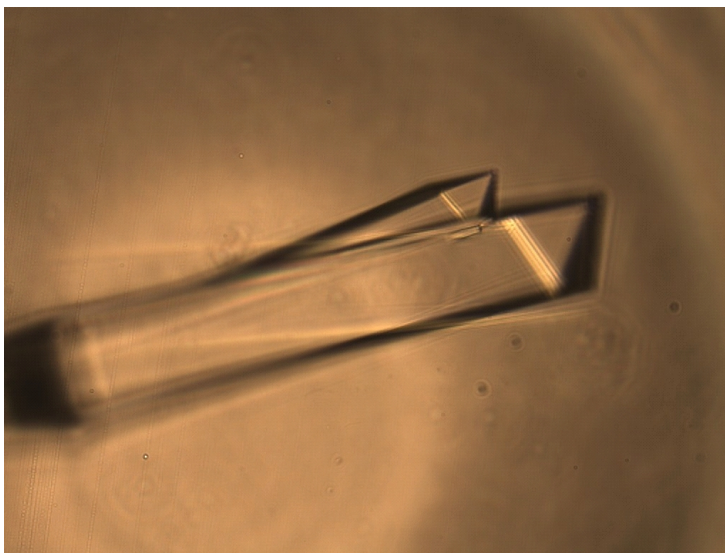


Fig 3.1 Crystal of II-N1. II-N1 was concentrated to 7.5 mg/ml (~ 500 M) and used for crystallization with hanging-drop vapor-diffusion method. Reservoir solution contained a mixture of PEG8000 and PEG1000 with 4% butane-1,4-diol. Crystals appeared after 3 days of incubation at 20 °C (70x magnification).

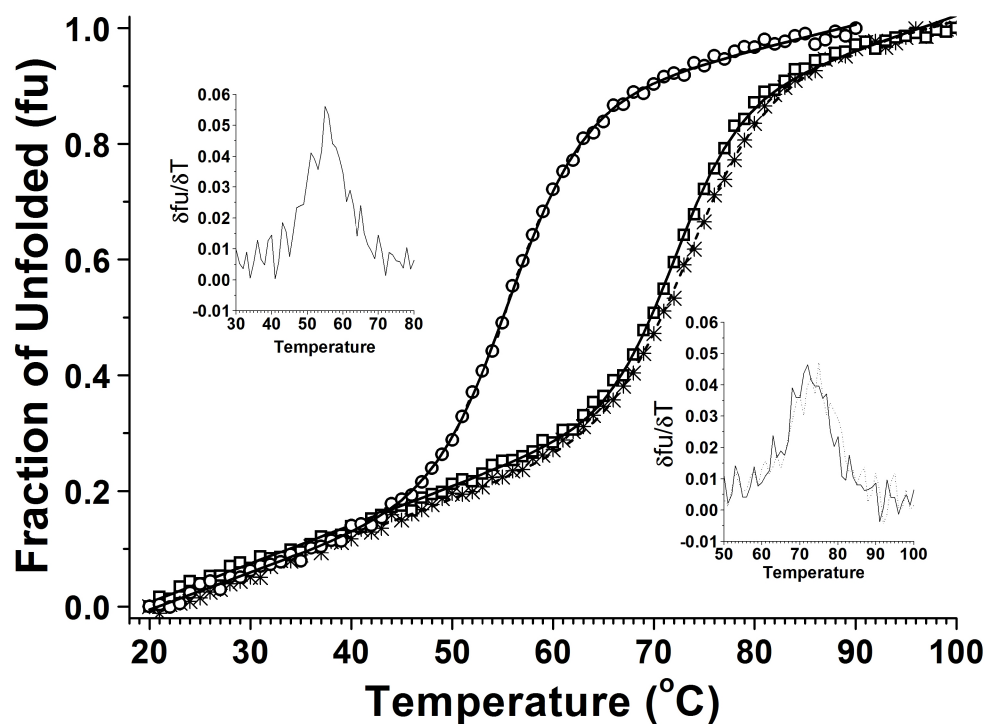


Fig 3.2 Thermal denaturation of I-N1 and II-N1. Fractions of thermal unfolding as a function of temperature and values T_m in PBS7.4 (~10-15 M) were obtained from curve fitting of mean residue ellipticity values, calculated from CD signals at 222 nm, at different temperatures. The T_m values are 56 °C for I-N1, 73.1 °C for II-N1 and 74.6 °C for seleno-Met-labeled II-N1. The maximum of the first derivative of the fractions of thermal unfolding as a function of temperature was also used to obtain T_m values (inset graphs).

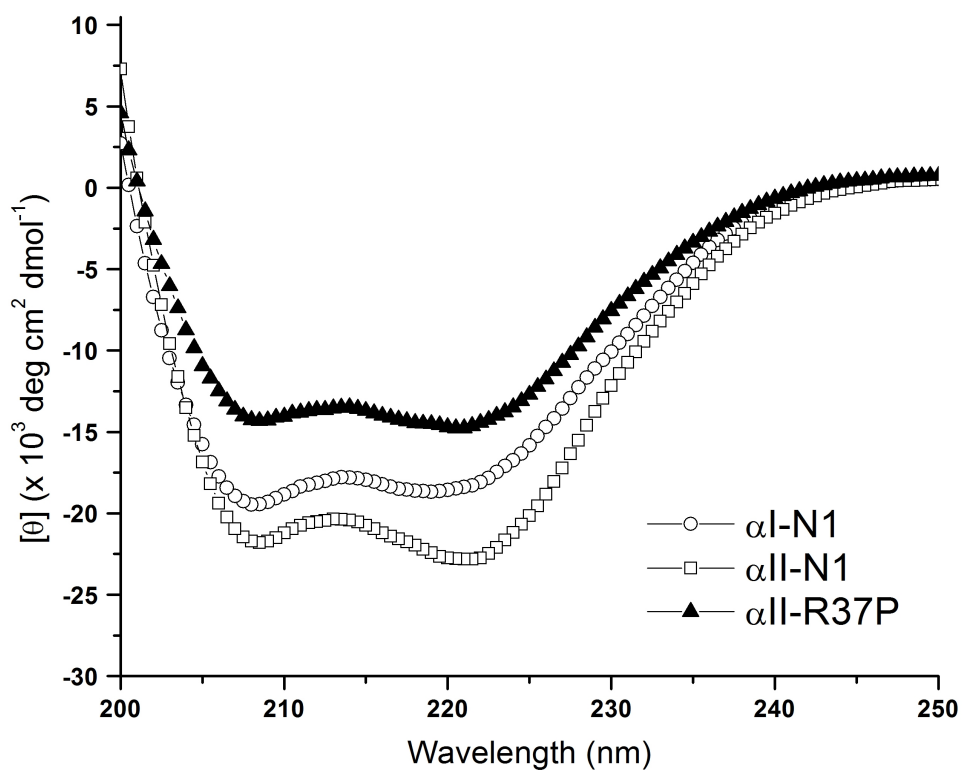


Fig 3.3 CD spectra of I-N1 (10 M), II-N1 (10 M), and II-R37P (10 M) in PBS7.4.

Ellipticity (θ , mdeg) values from raw CD spectra were converted to mean residue ellipticity ($[\theta]$, deg \cdot cm² \cdot dmol⁻¹) values. R37P has low helical content (43%) comparing to II-147 (65%) and I-156 (52%).

Also, no additional salt bridges were identified by the PDBsum program.

3.2.4 Association Affinity at the Tetramerization Site

Typical ITC results for the titration of I-N1 or II-N1 with I-C1 or II-C1 show that α -spectrin I and II do not contribute to the observed differences in dimer association to form tetramers; the differences are mostly due to differences in α -spectrin I and II. In fact, sequence alignment shows 54% sequence identity for I-N1 and II-N2 and 70% for I-C1 and II-C1. Our previously published K_d values are about 1 μ M for the association of I-N1 with I-C1 (Mehboob *et al.*, 2003; Long *et al.*, 2007; Lam *et al.*, 2009), and about 10 nM (Li and Fung, 2009; Long *et al.*, 2009) for II-N1 with I-C1.

Our lab has previously shown that the mutant R37P in II has an impaired ability to form tetramers with II (Sumandea and Fung, 2005). A proline residue mutation is, of course, likely to disrupt the helical conformation that we observed in the II WT junction region. Thus, we prepared an II-N1-R37P model protein. The CD measurements show that the helical content value is 43% for R37P, a value not only lower than that of II-N1 (65%), but also lower than that of I-N1 (52%). (Fig 3.3). The ITC results show a K_d value of about 10 μ M (Fig 3.4), a value much higher than that for WT, and even an order of magnitude higher than that for I.

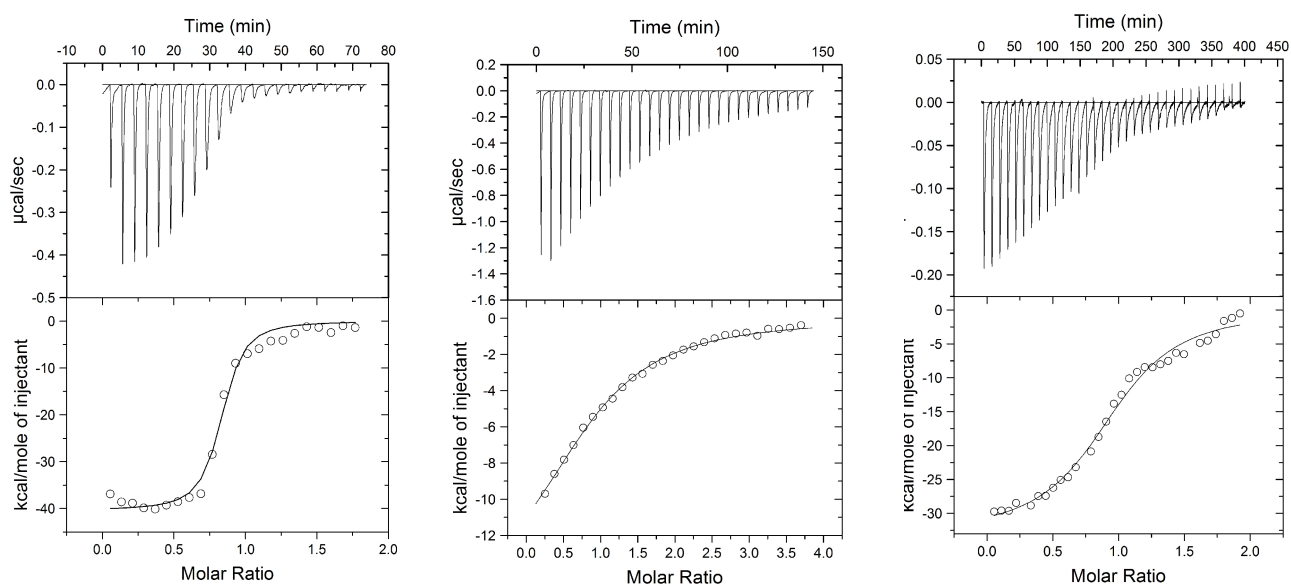


Fig 3.4 ITC data at 25 °C for II-N1/ I-C1 (WT) (left), II-N1-R37P/ I-C1 (center), and I-N1/ I-C1 (right). All protein samples were dialyzed together in 5 mM phosphate buffer with 150 mM sodium chloride at pH 7.4 to ensure identical solution conditions of the titration pairs to avoid introducing heat of dilution in the titration experiments. The K_d value is around 10 nM for WT with I-C1 (left), about 10 μ M for II-N1-R37P with I-C1 (center), and around 1 μ M for I-N1 with I-C1 (right).

3.3 Discussion

Functional properties from ITC measurements and structural information from X-ray and MD simulations provide mechanistic understanding of α association. The canonical triple helical bundle conformation does not reveal specific functions associated with either different domains, or different isoforms. The unique structural features in each domain, and even each partial domain, lead to different contributions toward the overall functional properties of spectrin, such as spectrin's rigidity/flexibility and the ability of dimers to associate to form tetramers, in the cytoskeletal network of different cells.

In this study, we found that the N-terminal regions of α I and α II are generally similar, but with each exhibiting specific unique features. One important common feature is the structural flexibility in the first helix, Helix C', to allow association with the helices in β -spectrin to form spectrin tetramers. An important feature unique to each is the conformation of the junction region connecting the first lone helix to the triple helical structural domain, with an unstructured conformation in α I and a helical conformation in α II. These differences modulate the association affinity of α spectrin.

Atomic level information on the structure allowed us to understand the stability of the first structural domain in α II, a domain that exhibited a T_m value about 20 °C higher than that of domain 1 in α I spectrin. Various spectrin segments have been reported to have different T_m values (An *et al.*, 2006). Examination of specific stabilizing interactions for D1- α I and for D1- α II shows more specific hydrogen bonds in D1- α II than D1- α I, but with similar hydrophobic internal packing and provides an atomic level of understanding of the different stabilities in these two structural domains.

By using isothermal titration calorimetry, we were able to show that the conformation of the junction region contributes to the difference in association affinity of spectrin tetramerization. Mutations affecting C' structural flexibility and the junction region conformation in α spectrin, as well

as inter-helix electrostatic interactions, will alter the equilibrium between spectrin dimers and spectrin tetramers and may lead to neurological disorders.

CHAPTER 4

YEAST TWO-HYBRID AND ITC STUDIES OF ALPHA AND BETA SPECTRIN INTERACTION AT THE TETRAMERIZATION SITE

*The published work is attached as Appendix B.

*The procedures and results obtained by myself and not appeared in the publication are given in 4.1.

4.1 Experimental Procedures

4.1.1 Isothermal Titration Calorimetry

Recombinant proteins II-N, II-N-V22 (V22D, V22F, V22M and V22W) and I-C were prepared, following standard laboratory techniques (Mehboob *et al.*, 2010). Briefly, protein expression vector pGEX-2T was used to express glutathione S-transferase fusion protein, and purified with affinity column chromatography, with thrombin cleavage of fusion protein. DNA sequence analysis and protein mass spectrometry analysis results were obtained (Research Resources Center, University of Illinois at Chicago). Protein purity was checked with gel electrophoresis, using 16% polyacrylamide gel with 0.1% SDS. Helical contents of the proteins were determined using circular dichroism spectra (Mehboob *et al.*, 2005). All proteins used for ITC are checked with DLS for optimal buffer selection, salt concentration, and protein concentration. We have found that I-C and II-C proteins exhibit similar affinities for II-N (Mehboob *et al.*, 2010). However, II-C recombinant protein is more difficult to prepare than I-C protein due to its low expression level. Thus, I-C was used for ITC experiments.

ITC measurements were performed at 25 °C using an isothermal titration calorimeter (VP ITC, MicroCal, LLC, Northampton, MA) (Mehboob *et al.*, 2010). Protein pairs (I-C with II-N, or II-N-V22 Δ) were dialyzed overnight in 5 mM phosphate buffer with 150 mM sodium chloride at pH 7.4 (PBS) to ensure identical solution conditions in titrating protein pairs. In addition, all samples were thoroughly degassed prior to calorimetry titration. Each II-N or II-N-V22 sample (30 μ M) was titrated into the sample cell containing I-C protein (3 μ M). Titrations of I-C (30 - 100 μ M) into II-N or II-N-V22 (3 μ M) were also performed. Titration isotherms were analyzed with a single binding site assumption, as before (Mehboob *et al.*, 2010), to obtain dissociation constants, K_d .

4.2 Results

4.2.1 Recombinant Protein Analysis

The SDS gel electrophoresis data showed that all II-N (wild type and mutants) and I-C proteins were ~90% pure. Electrophoretic masses were ~42 kDa for II-N proteins and ~22 kDa for I-C. Mass spectrometric results showed 42,241.0 Da for II-N (expected mass is 42,242.5 Da), 42,258.6 Da for II-N-V22D (expected mass is 42,258.5 Da), 42,289.0 Da for II-N-V22F (expected mass is 42,290.6 Da), 42,274.8 Da for II-N-V22M (expected mass is 42,274.6 Da), 42,329.8 Da for II-N-V22W (expected mass is 42,329.6 Da) and 22,036.9 Da for I-C (expected mass is 22,036.9 Da). The CD spectra of II-N, II-N-V22 and I-C exhibited characteristic features of similar spectrin recombinant proteins (Mehboob *et al.*, 2001), with minima at 222 and 208 nm. Helical contents were ~75%, in good agreement with published results (Lecomte *et al.*, 1993).

4.2.2 ITC Results

The ITC isotherm of I-C/ II-N system at 25 °C showed that sufficient heat (-0.45 µcal/sec) was released during titration of II-N into I-C (Fig 4.1), with an average K_d value of 6.9 ± 0.5 nM ($n = 3$). The K_d value was 6.7 ± 0.3 nM for I-C/ II-N-V22F, 35 ± 4 nM for I-C/ II-N-V22M and 93 ± 28 nM for I-C/ II-N-V22W. However, for I-C/ II-N-V22D system, there was insufficient heat released either when II-N-V22D (30 µM) was titrated with I-C (3 µM) (Fig 4.1), or when I (30 - 100 M) was titrated with II-N-V22D (3 µM), indicating that the K_d value for this system is larger than 100 M.

Some difficulties evolved during experiments before we were able to get reliable data (Fig 4.1). Some proteins precipitated during the titration experiment. Therefore, the concentration had to be lowered to prevent from aggregate formation. In order to obtain the reliable K_d value the accurate determination of exact protein concentration is essential.

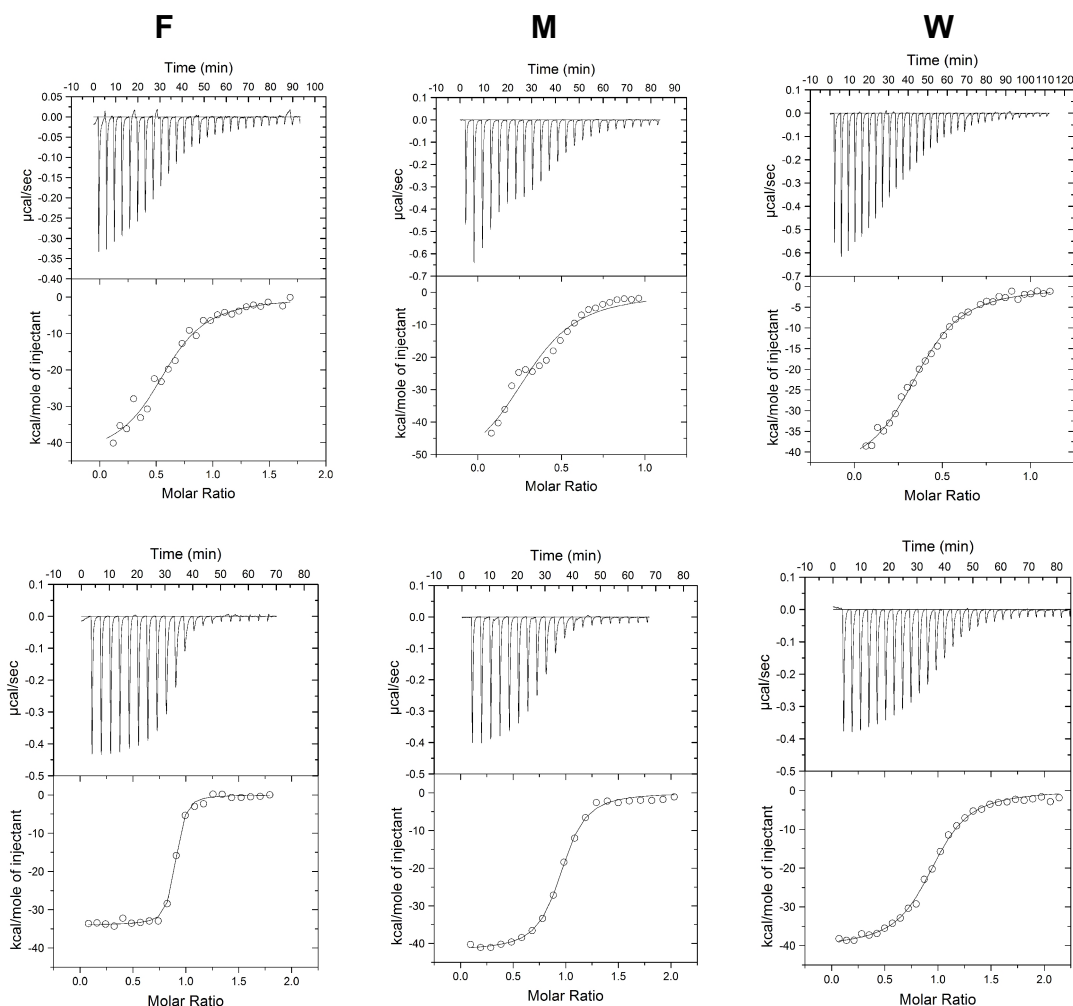


Fig 4.1 ITC Measurements for V22 mutants with I-C1. Top three titrations represent the initial experimental results. Bottom three represent the published data after optimizing the conditions. Recombinant protein samples of I-C, II-N-V22F (F), II-N-V22M (M) and II-N-V22W (W) were dialyzed together in 5 mM phosphate buffer with 150 mM sodium chloride at pH 7.4 and degassed thoroughly prior to ITC measurements. For the bottom three titrations II-N proteins (29 - 35 M) were each individually titrated into the sample cell containing I-C protein (3 M).

4.3 Discussion

The ITC results show that the K_d values for V22F and the wild type were about the same, with a K_d of about 7 nM. However, V22M and V22W both exhibited lower affinity than the wild type, with K_d values of 35 nM and 93 nM, respectively. The ITC results of V22D titration with I-C showed little interaction, with K_d values larger than 100 M.

Spectrin tetramer formation involves the bundling of three helices, one from (Helix C') and two from (Helix A' and Helix B'), forming a triple helical bundle (Mehboob *et al.*, 2010; Li and Fung, 2009). Mutations that affect the triple helical bundling lead to lower affinity.

Sequence alignment shows that II V22 corresponds to V31 in erythroid spectrin (I). I V31 has been identified as a hot spot that leads to severe clinical symptoms (Lecomte *et al.*, 1993). In triple helical bundling of II and II helices, an N-terminal hydrophobic cluster involves three residues in the II Helix C' (I15, V22, and L23) and two residues in the II Helix A' (V2019 and F2022), and one residue in the II Helix B' (F2073) (Mehboob *et al.*, 2010). Thus, it is not surprising that mutations at the V22 position may affect non-erythroid spectrin tetramer formation. Since V22 is involved in a hydrophobic cluster during helical bundling to form tetramers, a mutation from V to a charged residue D clearly weakens the hydrophobic cluster and thus severely reduces the ability of V22D to interact with Helices A' and B' in II-C. Mutation of V22 to other hydrophobic residues such as V22F did not affect its interaction with II-C.

Tetramerization is clearly important for spectrin function. At present, no clinical mutations in II spectrin, including the tetramerization region, have been identified. A reduced level of spectrin tetramers and abnormal spectrin-based membrane skeleton could cause abnormal neural activities in cells.

CHAPTER 5

QUANTITATIVE STUDIES OF CASPASE-3 CATALYZED II-SPECTRIN BREAK-DOWN WITH ELECTROPHORESIS AND FLUORESCENCE METHODS

*Manuscript submitted for publication under the same title by Witek and Fung in Jan 2013.

5.1 Introduction

Caspases, cysteine-aspartic acid proteases, cleave their substrates after aspartic acid and are members of the ICE/CED-2 protease family (Crawford and Wells, 2011; Fuentes-Prior and Salvesen, 2004; Alnemri *et al.*, 1996). Caspase-3 is the most abundant caspase in cells (around 200 nM), and the activity of other caspases is frequently overpowered by caspase-3 activity (Denault and Salvesen, 2001). While many proteins are cleaved during apoptosis, a prominent target of caspase-3 action is α -spectrin (also referred to as α -fodrin; Moon and McMahon, 1990). α -spectrin (Machnicka *et al.*, 2012) has long been recognized to be a significant substrate for caspase-3 during apoptosis in lymphocytes, hematopoietic cells, and neurons (Wang *et al.*, 1998; Janicke *et al.*, 1998, Cryns *et al.*, 1996; Martin *et al.*, 1995). However, the physiological importance of the spectrin break-down products (SBDP) has not been recognized until recently. Numerous studies report that the SBDP - of molecular mass 150 kDa (SBDP150) and, particularly, 120 kDa (SBDP120) - to name a few, are detected in several brain related injuries, such as traumatic brain injury (Hyman and Yuan, 2012; Hall *et al.*, 2005; Kupina *et al.*, 2003; Pike *et al.*, 2003; d'Avella *et al.*, 2002; Beer *et al.*, 2000; Newcomb *et al.*, 1997), mechanical stretch injury (Pike *et al.*, 2000), ischemia (Zhang *et al.*, 2002; Nath *et al.*, 1998), and degenerative brain diseases, such as Alzheimer's Disease, as well as other age-related degenerative diseases (Hyman and Yuan, 2012; Cotman *et al.*, 2005; Marx, 2001). SBDPs have been proposed to be potential biomarkers for neurodegenerative diseases (Yan and Jeromin, 2012). Furthermore, SBDP120, or its antibody activity, has been shown in the salivary gland, and plays a crucial role as an auto-antigen in the development of primary Sjögren's Syndrome (Haneji *et al.*, 1997). SBDP120 is also found in the sera of patients with normal tension glaucoma (Grus *et al.*, 2008). There is also increased evidence for non-apoptotic roles of caspase-3 in the brain, including the regulation of synaptic plasticity (Crawford and Wells, 2011)

and of neuronal morphology via local remodeling of the spectrin cytoskeleton (Westphal *et al.*, 2010). A recent “fragment generation” hypothesis suggests that Ca^{++} activated calpain/caspase fragmentations of spectrin, as well as of other proteins, play a role in sleep since the process decreases during sleep while fragment-destroying pathways are up-regulated (Varshavsky, 2012). Furthermore, it has been shown that cleavages of specific neuronal proteins play a role in long-term memory (Li *et al.*, 2010; Shimizu *et al.*, 2007, Lynch and Baudry, 1984). Thus, caspase-3 catalyzed α -spectrin break-down reactions are physiologically relevant, well regulated, complicated and sometimes confusing. Yet studies to provide molecular and quantitative understanding of these reactions are comparatively scarce.

We have followed the cleavage of α -spectrin by caspase-3 in detail with gel electrophoresis and fluorescence methods on model proteins of α -spectrin fragments of five different lengths. Our results show that fragmentation at two sites in the middle of α -spectrin are independent of each other, and exhibit very different caspase-3 catalytic rates. The cleavage after residue D1185, leading to SBDP150 in intact spectrin, is unusually efficient but not necessarily essential to the cleavage after residue D1478, leading to SBDP120 and SBDP of 37 kDa (SBDP37) from intact spectrin. The findings that the two cleavages are independent of each other and with very different rates suggest that the spectrin break-down products, SBDP150 and SBDP120, may be involved in different cellular processes. Furthermore, we speculate that SBDP37 is a well folded fragment that may also be involved in cellular functions.

5.2 Experimental Procedures

Chemicals - Ampicillin, dithiothreitol (DTT), EDTA, 3[(3-cholamidopropyl)dimethylammonio]-propane sulfonic acid (CHAPS), sucrose, 4-(2-hydroxyethyl)piperazine-1-ethanesulfonic acid (HEPES), and sodium dodecyl sulfate (SDS) were obtained from Thermo Fisher Scientific (Waltham, MA). Imidazole and

piperazine-N,N'-bis(2-ethanesulfonic acid) were obtained from Sigma-Aldrich (St. Louis, MO). All other reagents were either similar to those used in our previous studies of spectrin (e.g., Mehboob *et al.*, 2010), or are specified below.

5.2.1 DNA Plasmids Preparation

Two plasmids from ATCC (Manassas, VA): (1) pCMV-SPORT6 vector (product no 10436486) with the cDNA of human α -spectrin (GenBank BC053521) and (2) pET-23b vector (product no 99625) with the cDNA of pro-caspase-3 (GenBank U26943) were obtained. Five α -spectrin plasmids, using the spectrin cDNA from the pCMV-SPORT6 vector, were cloned into pDEST-15 vector (Invitrogen, Grand Island, NY), following the methods provided by the company's user manual, to give five spectrin model protein fragments in the region of residues 780-1556 (Table 1) consisting of residues (1) L780-F1344 (D8-D11), (2) L1087-F1344 (D10-D11), (3) L1087-F1556 (D10-D13), (4) H1335-F1556 (D12-D13) and (5) L1441-F1556 (D13) were prepared. The boundaries of these fragments were designed to ensure stable protein folding (see below). A thrombin recognition site (LVPRGS) between GST and the spectrin fragment was introduced in the primer sequence. All primers were purchased from Integrated DNA Technologies (Coralville, IA). A pDEST-15 plasmid with D1185E mutation (D10-D13(D1185E)) was also prepared, using primer-based site directed mutagenesis methods (Mehboob *et al.*, 2010). In addition, several plasmids for mutants of D10-D11 and D13 were prepared to replace tryptophan with phenylalanine residues. In D10-D11, residues 1106, 1192, 1215, 1248 and 1321 are tryptophan. The following mutants were prepared: (1) 1106F-1215F-1248F-1321F (only residue 1192 remained as W; designated as D10-D11 Δ_w -1), (2) 1215F-1248F-1321F (residues 1106 and 1192 remained as W; D10-D11 Δ_w), (3) 1106F-1248F-1321F (residues 1192 and 1215 remained as W; D10-D11 Δ_w -2). In D13, W1533 was mutated to F, leaving only residue 1460 as W (D13 Δ_w). All DNA constructs were verified

by DNA sequencing analysis (services provided by the Research Resources Center (RRC) at the University of Illinois at Chicago).

5.2.2 Protein Design, Expression, Purification and Characterization

5.2.2.1 Spectrin Model Proteins

In the design of the model proteins, the boundaries of each triple helical structural domain (31, 32) were predicted, first using the program in the FASTA package (EMBOSS Needle) for sequence analysis to align residues 780-1556 to α -spectrin residues 1-147 (D1), which is the first structural domain of α -spectrin with known atomic structure (Mehboob *et al.*, 2010). Furthermore, the alignment was also guided by the fact that the 16th and 88th residues in each typical spectrin triple helical domain are tryptophan residues (Mehboob *et al.*, 2010). After sequence alignment, the secondary structural elements (helices and loops) of α -spectrin D1 were assigned to the aligned regions in D8-D13. Each model protein consisted of predicted spectrin domain(s) plus the previous 4 residues and GS from thrombin cleavage to give a 6-residue overhang at the N-terminus and the 6 residues following the predicted boundary of the last structural domain to give an overhang at the C-terminus (Table 1) to enhance proper protein folding.

All plasmids, stored in DH5 *E. coli* cells (Zymo Research Corporation; Irvine, CA), were extracted and transformed into *E. coli* BL21-CodonPlus (DE3)-RIL competent cells (Agilent; Santa Clara, CA) for protein expression.

The spectrin model proteins, expressed as fusion proteins with an N-terminal GST tag followed by a thrombin cleavage site, were prepared with standard procedures developed in our laboratory (Mehboob *et al.*, 2010; Li and Fung, 2009).

5.2.2.2 Caspase-3

Full-length procaspase-3 was expressed with C-terminal His₆-affinity tag from pET-23b

vector in *E. Coli* BL21(DE3) cells (Agilent; Santa Clara, CA). Full length caspase-3 should be expressed as C-terminal fusion protein because the N-terminal peptide is proteolytically removed during expression. Cells were grown in 2xYT media supplemented with 200 μ g/ml ampicillin and 50 μ g/ml chloramphenicol at 37 °C to an OD₆₀₀ of 0.8. Over-expression of active caspase-3 was induced with 0.2 mM IPTG at 30 °C for 3 hrs. Cells were immediately harvested and resuspended in ice cold 100 mM Tris, pH 8.0, 100 mM NaCl (buffer A) and subjected to lysis by sonication. The cell lysate was clarified by centrifugation and soluble fraction was loaded onto a 5 ml Ni-NTA affinity column (Sigma Aldrich; St. Louis, MO) pre-equilibrated with buffer A and eluted with buffer A containing 200 mM Imidazole. The eluted protein was diluted two-fold with buffer B (20 mM Tris, pH 8.0) and purified by anion-exchange chromatography (Mono-Q, GE Healthcare; Waukesha, WI) with a 30-column volume gradient to 50 % of buffer B containing 1M NaCl. Fractions corresponding to pure caspase-3 were concentrated to 2 mg/ml (\sim 80 μ M), aliquoted and frozen. An average of 5 mg of caspase-3 from 1 L of *E.coli* was obtained using 2 L benchtop fermentor (New Brunswick; Edison, NJ).

The electrophoretic mass and the purity of proteins were determined by 16% SDS-PAGE (Li and Fung, 2009). Protein concentrations were determined using absorbance values at 280 nm, with extinction coefficients determined from the sequence of each protein. The mass of each protein, including D10-D11Dw and D13 Δ_w , was analyzed by mass spectrometry, with a LTQ-FT Ultra mass spectrometer, at the RRC. Only those proteins with the mass values within 1.5 Da of the expected mass values, as calculated from the sequence were used.

The folding of each protein (10 mM in 5 mM phosphate buffer containing 150 mM sodium chloride at pH 7.4, PBS) was analyzed by circular dichroism spectroscopy methods (JASCO 810; Easton, MD), scanning from 200 to 250 nm at 20 °C with a 0.1-cm path-length. Mean residue molar ellipticity values at 222 nm were used to calculate the helical content using a value of

36,000 deg cm²dmol⁻¹ for a 100% helical content (Mehboob *et al.*, 2010).

5.2.2.3 Caspase-3 Activity Assay

Recombinant caspase-3 activity was determined in a standard "caspase activity buffer" (20 mM piperazine-N,N'-bis-(2-ethanesulfonic acid)) with 100 mM NaCl, 10 mM DTT, 1 mM EDTA, 0.1% CHAPS, and 10% sucrose at pH 7.2) with fluorogenic substrate, Z-DEVD-AFC (EMD Biosciences; Billerica, MA), following a published method (Denault and Salvesen, 2008).

5.2.3 Cleavage of Spectrin Fragments by Caspase-3

5.2.3.1 SDS-PAGE Detection

A previously published gel electrophoresis method (Stennicke and Salvesen, 1999; Timmer *et al.*, 2009), including the published caspase-3 concentrations (Timmer *et al.*, 2009), was followed to allow for the study of a wide range of caspase-3 cleavage efficiency in spectrin model proteins. Briefly, a sample, 1 M final concentration, of each of the six spectrin proteins (D8-D11, D10-D11, D12-D13, D13, D10-D13, and D10-D13(D1185E)) was incubated with various amounts of caspase-3 (final concentration ranging from 0 to 500 nM) for exactly 1 hr ($t = 1$ hr) at 37 °C in the "caspase activity buffer." The reaction was terminated by boiling the sample for 10 min in the presence of the loading dye. Samples were loaded to 4 - 20% SDS-PAGE Precise Protein Gels (Thermo Fisher Scientific), and the electrophoresis was done in a running buffer (0.1 M Tris Base, 0.1 M HEPES, and 0.1% (w/v) SDS at pH 8) with constant current (50 mA). The protein staining was carried out using AcquaStain from Bulldog Bio (Portsmouth, NH). The protein band intensities at different caspase-3 concentrations ([casp-3]) were determined with Alphaimager HP (Protein Simple; Santa Clara, CA). The intensity values for samples with [casp-3] = 0.005, 0.01 and 0.05 nM were essentially the same as those without caspase-3 ([casp-3] = 0). Thus, the band intensities of these four points was averaged and set to represent the band intensity without caspase-3 (100%). The values for samples consisting

of [casp-3] > 0.05 nM were converted to fractions (%) accordingly. For the samples consisting of high [casp-3], such as 500 nM, (Fig 5.2 A and C, Fig 5.3 A and C, and Fig 5.4 A and C), the 13 and 17 kDa bands of caspase-3 were also visible on the gel. For band intensity analysis, the caspase-3 bands at corresponding concentrations were subtracted from each lane accordingly. A plot of the fraction of the remaining intact protein, or of the cleaved product(s), as a function of [casp-3] was made, and the value of [casp-3] corresponding to 50% of a spectrin protein disappeared/remained, or cleaved product appeared, $[E]_{1/2}$, was read from the plot directly, and the apparent value for k_{cat}/K_M was then determined with the half-life equation: $k_{cat}/K_M = \ln 2 / t[E]_{1/2}$, where $t = 1$ hr (Timmer *et al.* 2009).

The masses of some cleaved products were also determined by high-resolution mass spectrometry methods at the RRC (see Table 5-1).

5.2.3.2 Fluorescence Detection

In fluorescence studies, a substrate protein (spectrin model proteins) with tryptophan fluorescence signal sensitive to caspase cleavage is needed. Thus, we monitored the fluorescence intensities of tryptophan mutants D10-D11 Δ_w , D10-D11 Δ_w -1, D10-D11 Δ_w -2 and D13 Δ_w (see above, "Protein Design, Expression, Purification and Characterization" section) at 347 nm (with excitation at 295 nm) as a function of time in the "caspase activity buffer" in the presence of caspase-3 at 37 °C. The measurements were done with a Jasco Fluorometer (FP-6200; Easton, MD). Those model proteins sensitive to caspase-3 cleavage were selected for kinetics studies. A selected protein (D10-D11 Δ_w) was also studied by SDS-PAGE method to verify that the mutation does not affect the catalytic rate.

For kinetics studies, fluorescence spectra of the selected proteins at various concentrations in the "caspase activity buffer," incubated with caspase-3, were obtained as a function of time. The initial cleavage rate (V) at each protein concentration was measured from the linear portion of the plot of fluorescence intensity versus time. From the Lineweaver-Burk

plot ($1/V$ vs. $1/[\text{protein}]$), where $[\text{protein}]$ was the concentration of spectrin model protein, we obtained $1/V_{\text{max}}$ value from the y-intercept of the linear fit of the data and $-1/K_M$ from the x-intercept. The k_{cat} value was obtained since $k_{\text{cat}} = V_{\text{max}}/[\text{casp-3}]$. OriginPro 8.5 software was used for data processing both in gel electrophoresis and in fluorescence studies.

5.2.3.3 Structure Prediction

In addition to the prediction of domain boundaries and secondary structural elements as mentioned above, the sequence of Domain 10 (D10) was also analyzed for the probability of forming coiled coil structure using COILS (Lupas *et al.*, 1991) and the sequence of a part of D10 (L1157-E1210) was analyzed for structural dis-orderness using PONDR (Romero *et al.*, 2001).

5.3 Results

5.3.1 Protein Characterization

5.3.1.1 Spectrin

All spectrin model protein samples (Table 5-1) used in the studies were more than 90% pure, as indicated by SDS gel electrophoresis data. As noted in our previous publication (Lusitani *et al.*, 1994), spectrin fragments with proper boundaries consisting of full triple helical bundle structural domain(s) are stable and represent the full-length spectrin of particular regions well for functional studies (Mehboob *et al.*, 2010).

Sequence alignment of D10 showed that residues L1087 to F1238 aligned with residues L40 to Y154 in D1, with 22 % sequence identity and 41% similarity (Fig 5.1 A). In this alignment, the region V1167-H1200 did not align with the sequence in the template, and appeared to be an insertion. However, when the insertion region is removed, the alignment scores improved to 29% identity and 52% similarity (Fig 5.1 B). Secondary structural prediction showed Helix A (following the nomenclatures in Mehboob *et al.*, 2010) in D10 as residues K1092-L1114, Helix B as residues V1126-E1160, followed by an unusually long, 40-residue loop (residues G1161-H1200) (Fig 5.1 C) and then Helix C as residues T1201-G1230 (Fig 5.1 B). It should be

noted that the two conserved tryptophan residues found in Helices A and C in most triple helical bundles were aligned with those in D1. More importantly, with these predictions, the reported cleavage site D1185 was in the middle of this long loop (Fig 5.1 C) between Helix B and Helix C.

TABLE 5-1

The mass predicted from sequence (mass_{seq}), obtained from gel electrophoresis (mass_{ele}) and obtained from high-resolution mass spectrometry methods (mass_{ms}) of II-spectrin model proteins used in the study (left aligned, in bold). Each protein consisted of predicted spectrin domain(s) from sequence alignment plus overhang residues at both ends as well as GS as the first two residues in each protein (see Experimental Procedures). The first set of fragments obtained from caspase-3 cleavage (center aligned) and the fragments from a subsequent cleavage of a fragment, if any, (right aligned) are also listed.

Protein	Sequence	Mass_{seq} (Da)	Mass_{ele}	Mass_{ms} (Da)
D8-D11	L780-F1344	62,358.4	66	62,357.6
	L780-D1185	44,171.3	46	
	S1186-F1344	18,205.0	19	
D10-D11	L1087-F1344	29,830.0	36	29,829.9
	L1087-D1185	11,642.9	17	
	S1186-F1344	18,205.0	19	
D10-D13	L1087-F1556	54,265.5	62	54,265.6
	L1087-D1185	11,642.9	17	11,642.2
	S1186-F1556	42,640.5	45	
	S1186-D1478	33,690.3	37	33,689.8
	S1479-F1556	8,968.2	10	8,967.7
D10-	L1087-F1556	54,279.5	62	54,279.8
	L1087-D1478	45,329.3	53	45,330.1
	L1087-E1185	11,657.0	17	11,655.7
	S1186-D1478	33,690.3	37	
	S1479-F1556	8,968.2	10	8,967.8
D12-D13	L1335-F1556	25,766.8	28	25,766.1
	L1335-D1478	16,816.6	17	
	S1479-F1556	8,968.2	10	8,967.8
D13	L1441-F1556	13,550.1	15	13,549.9
	L1441-D1478	4,600	5	4,599.1
	S1479-F1556	8,968.2	10	8,967.8

A

40 68 108

D1 **LEDS-YRFQF FQDAEELEK WIQEK-LQIA SDENYKDPTN LQGKLQKHQA FEAEVQANS GAIVKLDETGN LMISEGHFAS**

1087 1116 1156

118 132 154

D1 **E-----TIRT-RLMELHRQW ELLEKMKREK GIKLLQAQKL VQY**

1166 1206 1238

B

1087 1165

D10' LEKSCCKKFML F-REANELQQ WINEKEAALT SEEVGADL-E QVEVLQKKFD DFQKDLKANE SRLKDINKVA EDLESEGLMAEE

D1 **LEDS-YRFQF FQDAEELEK WIQEK-LQIA SDENYKDP-T NLQGKLQKHQ AFDAEVQANS GAIVKLDETGN NLMISEGHFA (SE)**

D13 LDQC-LELQL FHRDCEQAEN WMAAR-EAFL NTEDKGDSL D SVEALIKKHE DFDKAINVQE EKIAALQAFD DQLIAAGHYA

1441 1469

1201 1209 1238

D10' TVATFNSI KELNERWRSL QQLAEERSQL LGSAGEVQRF

D1 **SETIRT--RL MELHRQWELL LEKMKREKGIK LLQAQKLVQY**

D13 KGDISS--RR NEVLDRWRRL KAQMIEKRSK LGESQTLQQF

1519 1527 1556

C

D10 Long loop

1161 1200

GLMAEEVQAV QQQEVYGMMP RDETDSKTAS PWKSARLMVH

Fig 5.1 (A) Sequence alignment of D10 (L1087-F1238, See Table 5-1) with D1 (L40-Y154), with D10 exhibiting 22% sequence identity and 41% similarity. The D1185 residue (bold and double underline) is located in the middle of the long, 34-residue segment (V1167-H1200, dotted line) that does not align with D1. Two conserved tryptophan residues found in Helices A and C are shown in grey. (B) D10', excluding residues from V1167-H1200, sequence aligned with D1 exhibiting 29% sequence identity and 52% similarity. The high sequence homology with D1 allows us to predict that Helix A in D10 as residues K1092-L1114 (underlined), Helix B as residues V1126 - E1160, and Helix C as residues T1201-G1230. Also shown is the sequence alignment of D13 (L1441-F1556) with D1. The alignment shows 28% identity and 49% similarity between D13 and D1. We assigned L1445-F1467 in D13 as Helix A (underlined), V1480-A1514 as Helix B, and K1519-G1548 as Helix C. The D1478 residue (bold, and double underline) is at the end of the segment connecting Helix A and Helix B. (C) A 40-residue segment (G1161 - H1200) located between Helix B and Helix C in D10.

The COILS program predicted regions similar to those mentioned above as coiled helices except for the region consisting of L1162-F1205. This region exhibited a very low probability (<3%) of forming coiled helix, whereas 20 residues prior to this region, for example, exhibited very high probability (>90%) of forming coiled helix. The PONDR analysis of the region from G1161 to P1191 predicted this region to be disordered. Thus, we believe that domain 10 in II-spectrin is folded into a triple helical bundle similar to other structural domains in spectrin, but with a very long loop between Helices B and C, with D1185 in the middle of this loop. It should be noted that some published spectrin structural predictions name D10 as "repeat 11" with different boundaries (e.g., Cianci *et al.*, 1999).

For D13, the sequence alignment was relatively straightforward, with L1441-F1556 aligned with L40-Y154 to give 28% identity and 49% similarity, and we assigned L1445-F1467 as Helix A, V1480-A1514 as Helix B, and K1519-G1548 as Helix C in D13 (Fig 5.1 B). Again the conserved tryptophan residues were also found in D13. The other reported D1475 and D1478 cleavage sites were found at the end of the 12-residue (LNTEDKGD*SLD*S) loop between Helix A and Helix B. In summary, simple structural prediction suggested that D10 folds into a triple helical coiled coil structure as in other spectrin domains, but with a very long unstructured loop between Helix B and Helix C. The D1185 residue was in the middle of this long loop. D13 was also predicted to fold into a triple helical coiled coil structure, but with D1475 and D1478 residues at the end of a shorter loop between Helix A and Helix B. Obviously, the actual structures of these two domains await experimental data.

The CD spectra showed that the helical contents of spectrin model proteins were between 60 - 70% (spectra not shown), in good agreement with previously published values for similar (triple helical bundles) spectrin model proteins (Mehboob *et al.*, 2010), suggesting that the proteins used were well folded into a triple helical domain. It should be mentioned that an SH3

domain (residues 965-1025) is nested in D9 (Musacchio *et al.*, 1992; Rotter *et al.*, 2004).

5.3.1.2 Caspase-3

The CD spectra for the recombinant caspase-3 used in this study showed two minima with similar signal amplitudes at 208 and 215 nm (spectra not shown), in good agreement with published spectra (Pop *et al.*, 2001). Using the substrate Z-DEVD-AFC, the k_{cat} value of our caspase-3 was 10.6/sec, with K_M 16 M, and k_{cat}/K_M 662,500 M⁻¹sec⁻¹, values in good agreement with published values (k_{cat} of 11.63/sec, K_M of 21.1 M, and k_{cat}/K_M value of 551,342 M⁻¹sec⁻¹) where a similar substrate, Ac-DEVD-AFC, was used (Timmer *et al.*, 2009).

5.3.2 Cleavage of Spectrin Proteins by Caspase-3

5.3.2.1 Gel Electrophoresis Studies

For the sample D10-D11 in the presence of caspase-3, the band at 36 kDa clearly decreased as [casp-3] increased above 0.5 nM (Fig 5.2 A). No significant changes were detected in samples with lower [casp-3] = 0, 0.005, 0.01, and 0.05 nM. Two bands at 17 and 19 kDa were clearly detected with [casp-3] = 3 nM. The band intensity plot as a function of [casp-3] (log scale for presentation convenience) (Fig 5.2 B) showed the gradual disappearance of D10-D11 upon increasing [casp-3]. The $[E]_{1/2}$ value determined from this plot was about 3 nM. The average value of several runs was 2.9 ± 0.6 nM ($n = 3$), and the corresponding average value of k_{cat}/K_M was found to be $67,700 \pm 13,200$ M⁻¹sec⁻¹ (Table 5-2).

For the larger model protein, D8-D11 (66 kDa), two bands at 19 and 46 kDa were also clearly detectable at [casp-3] = 3 nM (Fig 5.2 C). From the 66 kDa-band intensity plot (the disappearance of D8-D11) as a function of [casp-3] (Fig 5.2 D), the $[E]_{1/2}$ value was found to be about 10 nM. The average value was 7.7 ± 1.4 nM ($n = 2$), which corresponded to k_{cat}/K_M of $25,400 \pm 4,300$ M⁻¹sec⁻¹ (Table 5-2).

For the model protein D13 (15 kDa), only one product band was detected at the 10-kDa

position, with a smaller fragment presumably migrating off the gel (Fig 5.3 A). As [casp-3] increased, the intensity of the 10 kDa band was seen to increase, while that of the parent band at 15 kDa decreased (Fig 5.3 A). From the 15 kDa-band intensity plots (a typical plot is shown in Fig 5.3 B), the average value of $[E]_{1/2}$ value for the disappearance of D13 was found to be 57.8 ± 3.1 nM ($n = 3$), corresponding to a k_{cat}/K_M value of $3,300 \pm 200$ M⁻¹sec⁻¹. Mass spectrometry analysis of the cleaved products showed two fragments of 8,967.8 and 4,599.1 Da (Table 5-1) indicating that D13 was cleaved after D1478 (7, 44) and not after D1475 (44) since the C-terminal fragment of the D1475 site cleavage, S1476-F1556 with an expected mass from the sequence as 9,283.5 Da, was not found.

Upon cleavage of the larger D12-D13 protein (28 kDa), two fragments (10 and 17 kDa) were generated (Fig 5.3 C, [casp-3] = 50 nM, for example). From the band intensity plots (e.g., Fig 5.3 D), the average $[E]_{1/2}$ value for the disappearance of D12-D13 was found to be 62.2 ± 10.6 nM ($n = 2$), corresponding to a k_{cat}/K_M value of $3,100 \pm 500$ M⁻¹sec⁻¹. These values were very similar to those found for the D13 protein ($[E]_{1/2}$ of 57.8 nM and k_{cat}/K_M of 3,300 M⁻¹sec⁻¹, Table 5-2).

Finally, the D10-D13 protein (62 kDa) (Fig 5.4 A) generated various fragments upon caspase-3 cleavage. For [casp-3] = 0.5 nM, fragments of 17 and 45 kDa appeared (Fig 5.4 A). When [casp-3] > 10 nM, the 45 kDa band began to disappear while two other fragments at 10 and 37 kDa appeared. The mass spectrometry analysis of the final three cleaved products (10, 17 and 37 kDa; Table 5-1) indicated that D10-D13 was cleaved after D1185 and after D1478, in good agreement with the previously published studies (Wang *et al.*, 1998). Cleavage after D1475 (44) was again not observed. A typical plot of the relative intensity of the 62 kDa-band (Fig 5.4 B) showed an $[E]_{1/2}$ of about 3 nM. The average $[E]_{1/2}$ value was 4.3 ± 1.2 nM ($n = 3$) (Table 5-2). With this value, the k_{cat}/K_M was found to be $47,200 \pm 15,000$ M⁻¹sec⁻¹. The $[E]_{1/2}$ value for the appearance of 37 kDa was about 58.2 ± 10.1 nM ($n = 3$) and the k_{cat}/K_M value was $3,400 \pm 650$

$\text{M}^{-1}\text{sec}^{-1}$. For comparison, the relative intensity plot of D10-D11 (Fig 5.2 B) was also plotted in Fig 5.4 B to show that caspase-3 cleaved D10-D11 similarly to the D1185 site cleavage in D10-D13, with comparable $[\text{E}]_{1/2}$ and $k_{\text{cat}}/K_{\text{M}}$ values (Table 5-2). The $k_{\text{cat}}/K_{\text{M}}$ values for D10-D11 and D8-D11 agreed well with the values of the D1185 site cleavage for D10-D13, and the values for D13 and D12-D13 agreed well with the values of the cleavage, after the D1478 site for D10-D13. This finding indicated that the efficiency of caspase-3 cleavage of these two sites were very different, and they were independent of each other.

For the D10-D13(D1185E) mutant, its 62 kDa band intensity decreased at much higher values of [casp-3] and the first set of fragments detected were 10 and 53 kDa (Fig 5.4 C and D). The $[\text{E}]_{1/2}$ value was $73.0 \pm 22.8 \text{ nM}$ ($n = 2$) (Fig 5.4 D), and the $k_{\text{cat}}/K_{\text{M}}$ value was $2,800 \pm 900 \text{ M}^{-1}\text{sec}^{-1}$. These values were very similar to those found in the D13 protein ($[\text{E}]_{1/2}$ of 57.8 nM and $k_{\text{cat}}/K_{\text{M}}$ of $3,300 \text{ M}^{-1}\text{sec}^{-1}$), and in wild-type D10-D13 ($[\text{E}]_{1/2}$ of 58.2 nM and $k_{\text{cat}}/K_{\text{M}}$ of $3,400 \text{ M}^{-1}\text{sec}^{-1}$) (Table 5-2). The 53 kDa fragment was further cleaved into two fragments (17 and 37 kDa) at [casp-3] $> 50 \text{ nM}$. The average $[\text{E}]_{1/2}$ value for this cleavage (from the appearance of 37 kDa plot) was $172.7 \pm 27.0 \text{ nM}$ ($n = 3$) with a corresponding $k_{\text{cat}}/K_{\text{M}}$ of $1,100 \pm 180 \text{ M}^{-1}\text{sec}^{-1}$ (Table 5-2). The efficiency for the E1185 site cleavage was lower than that for the D1478 site. The mass spectrometry analysis of the cleaved products indicated that D10-D13(D1185E) was cleaved after E1185 and D1478 to give 10, 17, and 37 kDa fragments (Table 5-1). Again cleavage after D1475 (Dix *et al.*, 2008) was not observed in this mutant, suggesting that cleavage at this site, if occurring, would be even less efficient than at the E1185 site, under the conditions we used.

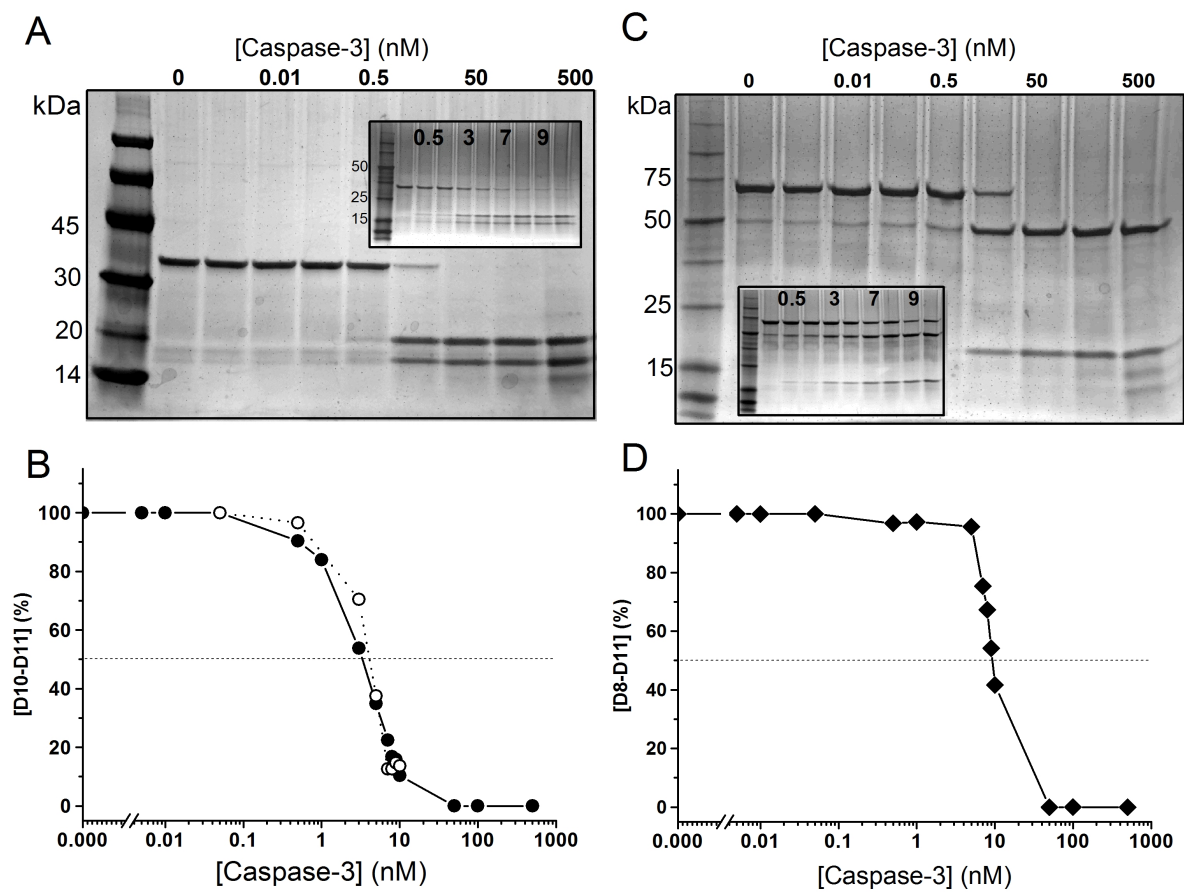


Fig 5.2 (A) A typical SDS-PAGE for the substrate D10-D11 ($1 \text{ } \mu\text{M}$) in the presence of various [casp-3] (0, 0.005, 0.01, 0.05, 0.5, 10, 50, 100, and 500 nM). Each sample of D10-D11 and caspase-3 was incubated at $37 \text{ }^{\circ}\text{C}$ for 1 hr precisely before gel electrophoresis runs (see text). Polyacrylamide gel (4-20% in Tris-HEPES-SDS, from Pierce) was used. See Table 5-1 for the masses of the proteins and fragments obtained from sequence, gel electrophoresis and mass spectrometry methods. Molecular markers are shown in the left most lane. At low concentrations of caspase-3, the 36 kDa (D10-D11) band is clearly seen. For samples with higher concentrations of caspase-3, bands at 17 and 19 kDa are detected. For the sample consisting of 500 nM caspase-3, the bands of caspase-3 at 17 kDa (corresponding to a mass of 16,614.8 Da) and 13 kDa (12,960.7 Da) are also visible. Similar caspase-3 bands at 500 nM were observed in samples without D10-D11 (data not shown). The insets are gels with [casp-3] = 0.05, 0.5, 1, 3, 5, 7, 8, 9, and 10 nM. (B) The intensities of the 36 kDa band in (A), converted to fractions of that without caspase-3 (%) (solid circle), at different [casp-3] show the disappearance of D10-D11 at [casp-3] > 0.05 nM. The value of [casp-3] to give 50% of D10-D11 (dash line), $[E]_{1/2}$, was read from the plot directly with the plotting software (Origin) as 3.3 nM. The $k_{\text{cat}}/K_{\text{M}}$ value was then determined with the half-life equation $k_{\text{cat}}/K_{\text{M}} = \ln 2/t [E]_{1/2}$ (see text) with $t = 1 \text{ hr}$ or 3600 sec, as $58,346 \text{ M}^{-1} \text{ sec}^{-1}$. The open circle symbols correspond to the data for D10-D11_w used in fluorescence studies. The $[E]_{1/2}$ value for D10-D11_w, from the plot, is 4.0 nM to give a $k_{\text{cat}}/K_{\text{M}}$ value of $48,135 \text{ M}^{-1} \text{ sec}^{-1}$. (C) A typical SDS-PAGE for the substrate D8-D11 ($1 \text{ } \mu\text{M}$). Details are similar to (A). (D) The intensities of the 66 kDa band in (C) at different [casp-3] were converted to fractions of that without caspase-3 (%) (solid diamond). The $[E]_{1/2}$ value from the plot is 9.0 nM with a $k_{\text{cat}}/K_{\text{M}}$ value of $21,393 \text{ M}^{-1} \text{ sec}^{-1}$.

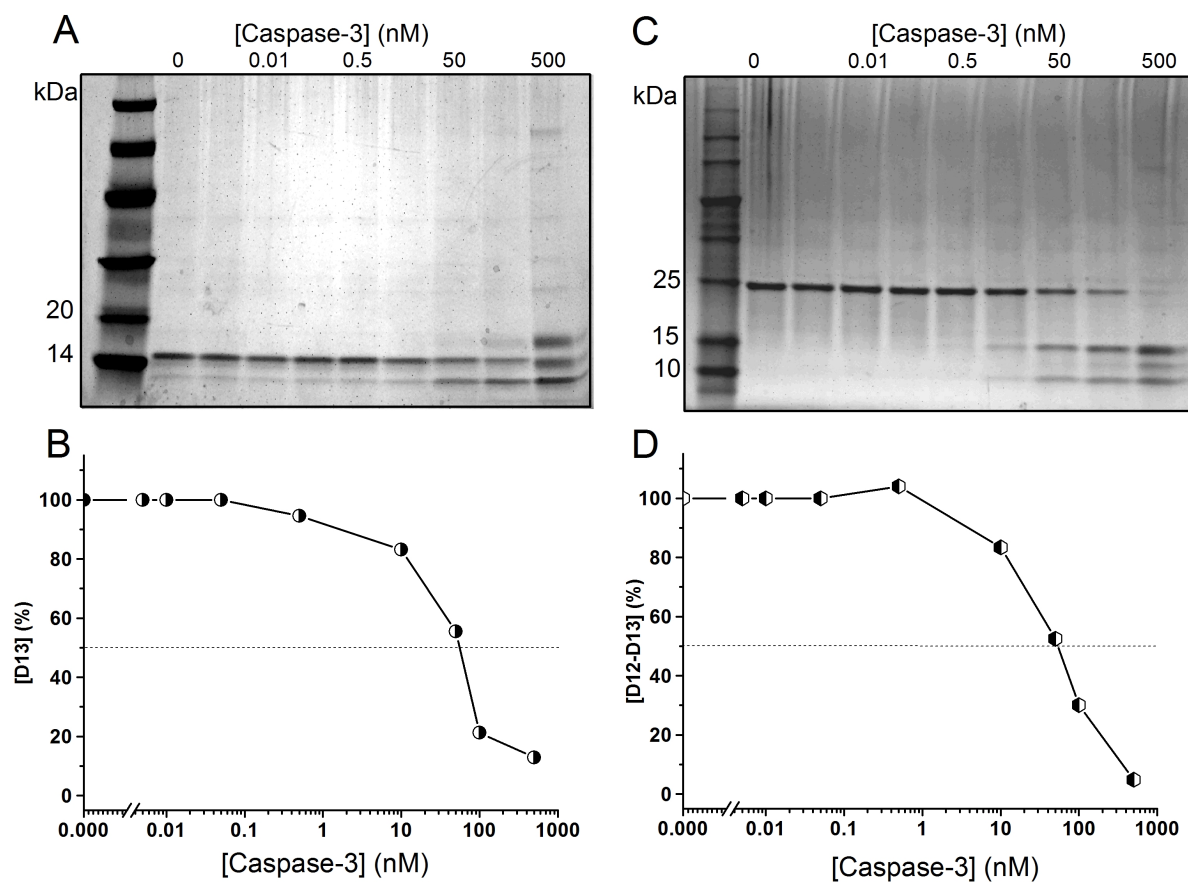


Fig 5.3 (A) A typical SDS-PAGE for the substrate D13 ($1 \text{ } \mu\text{M}$) in the presence of various [casp-3] with conditions similar to those in Fig 5.2 A. See Table 5-1 for the masses of proteins and fragments obtained from sequence, gel electrophoresis and mass spectrometry methods. Molecular markers are shown in the left most lane. At low concentrations of caspase-3, the 15 kDa (D13) band is clearly seen. For higher concentrations of caspase-3, a band at 10 kDa is detected. For the sample consisting of 500 nM caspase-3, the bands of caspase-3 at 17 kDa (corresponding to a mass of 16,614.8 Da) and 13 kDa (12,960.7 Da) are also visible. (B) The intensities of the 15 kDa band in (A), converted to fractions of that without caspase-3 (%) (right-half shaded circle), at different [casp-3] show the disappearance of D13 at [casp-3] > 100 nM. The [casp-3] value to give 50% fraction (dash line) of D13 ($[E]_{1/2}$) was read from the plot directly with the plotting software (Origin) to give a value of 57.2 nM. The k_{cat}/K_M value was then determined to be $3,366 \text{ M}^{-1} \text{ sec}^{-1}$. (C) A typical SDS-PAGE for the substrate D12-D13. Details are similar to (A). (D) The intensities of the 28 kDa band in (C) at different [casp-3], converted to fractions of that without caspase-3 (%), as a function of [casp-3] (left-half shaded hexagon). The $[E]_{1/2}$ value from the plot is 55.6 nM with a k_{cat}/K_M value of $3,463 \text{ M}^{-1} \text{ sec}^{-1}$.

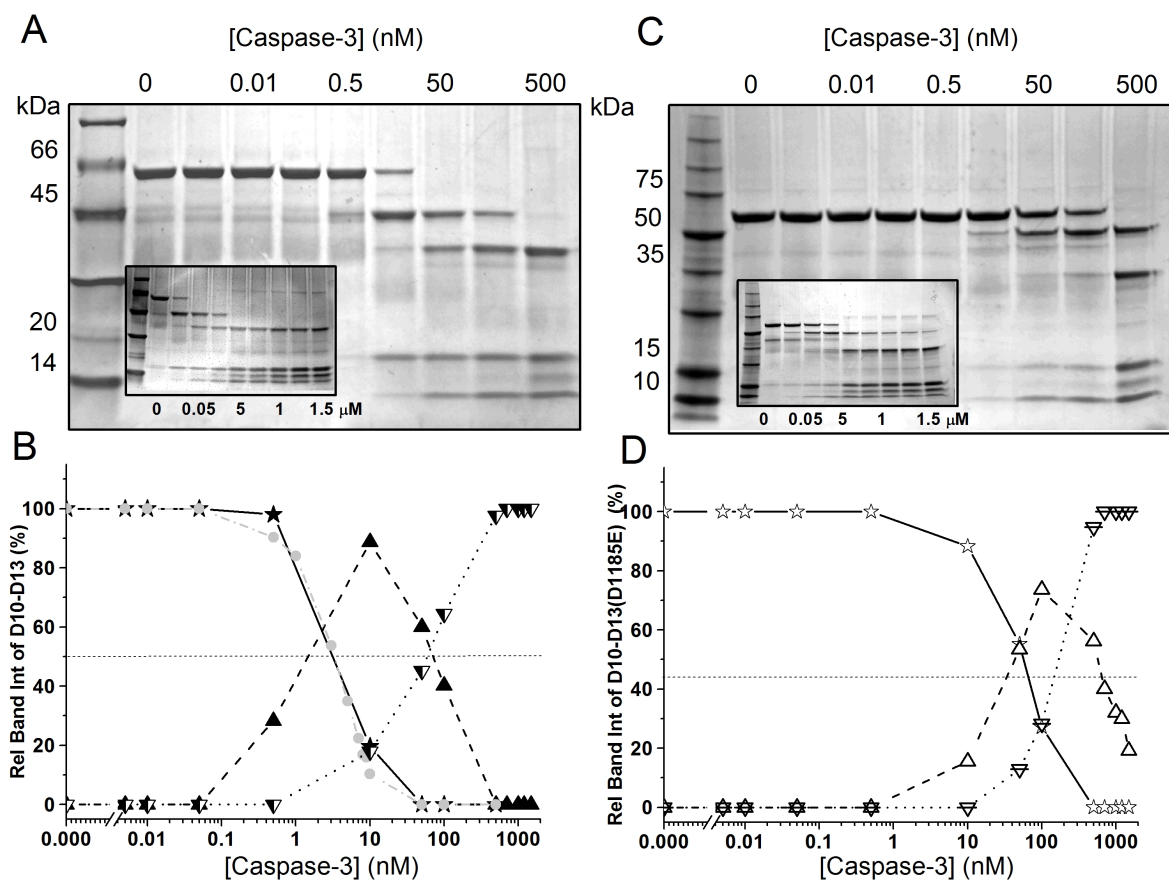


Fig 5.4 (A) A typical SDS-PAGE for the substrate D10-D13 ($1 \text{ } \mu\text{M}$) in the presence of various [casp-3], with conditions similar to Fig 5.2 A. See Table 5-1 for the masses of the proteins and fragments obtained from sequence, gel electrophoresis and mass spectrometry methods. Molecular markers are shown in the left most lane. At low [casp-3] values, the 62 kDa (D10-D13) band is clearly seen in each lane. For higher [casp-3] values, bands at 45, 37, 17, and 10 kDa are detected. Again, for the sample consisting of 500 nM caspase-3 or higher, the bands of caspase-3 at 17 kDa and 13 kDa are also visible. The inset gels are with [casp-3] = 0, 10, 50, 100, 500, 700, 1000, 1200 and 1500 nM. (B) The intensities of the 62 kDa band in (A), converted to fractions of that without caspase-3 (%), at different [casp-3] (solid stars) show the disappearance of D10-D13 at [casp] > 10 nM. The $[E]_{1/2}$ value was read from the plot directly with the plotting software to give a value of 3.1 nM with a k_{cat}/K_M value of $62,110 \text{ M}^{-1}\text{sec}^{-1}$. Also plotted are the appearance a 45 kDa fragment (solid triangle). When the [casp-3] > 10 nM, the concentration of the 45 kDa fragment decreases. A fragment at 37 kDa band (upside down left-half shaded triangle) becomes visible at [casp-3] ~ 10 nM, and its concentration continues to increase as [casp-3] increases. For comparison, the relative intensity plot of D10-D11 (solid circle) from Fig 5.2 A was also plotted. (C) A typical SDS-PAGE for the substrate D10-D13(D1185E), with conditions similar to (A). (D) The intensities of the 62 kDa band in (C) at different [casp-3], converted to fractions of that without caspase-3 (%) as a function of [casp-3] (open star). The $[E]_{1/2}$ value from the plot is 57.4 nM with k_{cat}/K_M value of $3,354 \text{ M}^{-1}\text{sec}^{-1}$. Also plotted are the appearance of a 53 kDa fragment as a function of [casp-3] (open triangle). When the [caspase-3] > 100 nM, the concentration of the 53 kDa fragment decreases. The 37 kDa band (upside down open triangle) becomes visible at [casp-3] ~ 100 nM, and its concentration continues to increase as [casp-3] increases.

5.3.2.2 Fluorescence Studies

The fluorescence intensities at 347 nm of D10-D11D Δ_w -1 and D10-D11D Δ_w -2 samples (see the Methods section for the identities of these proteins) showed no change with the addition of caspase-3, at either $t = 0$ or $t = 10$ min at 37 °C (Fig 5.5). However, the intensity of the D10-D11D Δ_w sample (at ~ 0.7 M, with [casp-3] = 100 nM) decreased as a function of time (Fig 5.6 A). Similarly, the intensity of the D13D Δ_w sample (at ~ 0.9 M, with [casp-3] = 700 nM) also decreased as a function of time (Fig 5.7 A). No intensity decreases in both samples occurred in the absence of caspase-3 (Figs 5.7 B and 5.6 B). Thus D10-D11D Δ_w and D13D Δ_w appeared to be good model proteins to be used to follow the kinetics of caspase-3 cleavage at D1185 and D1478 sites, respectively. We also checked the caspase-3 cleavage of D10-D11D Δ_w by gel electrophoresis and found the average value for $[E]_{1/2}$ to be 4.2 ± 0.5 nM with a k_{cat}/K_M of $46,800 \pm 3,900$ M⁻¹sec⁻¹ (Fig 5.2 B; Table 5-2), very similar to the values for D10-D11. Thus, tryptophan-residue replacement in this protein did not appear to affect the caspase-3 cleavage.

A plot of the relative fluorescence intensity at 347 nm as a function of time for samples of D10-D11D Δ_w at a series of concentrations (from ~ 0.7 to 11.7 M), each with [casp-3] = 100 nM, showed corresponding decreases in intensities (Fig 5.6 B). The initial cleavage rate (V) for D10-D11D Δ_w at 0.7 M, determined from the slope of the linear fit of the data in Fig 5.6 C, was 0.1335 M/min. The V values at other concentrations of D10-D11D Δ_w were determined, and the Lineweaver-Burk plot ($1/V$ vs $1/[D10-D11D\Delta_w]$) (Fig 5.6 D) showed that the data exhibited linear dependence, indicating that the kinetics of caspase-3 cleavage of D10-D11D Δ_w followed Michaelis-Menten kinetics. The V_{max} from the y-intercept was 1.6 M/min, with a K_M from the x-intercept of 7.8 M, and a k_{cat} from $V_{max}/[casp-3]$ of 16/min, or 0.27/sec. The k_{cat}/K_M value was then 35,000 M⁻¹sec⁻¹ (Table 5-2). This value agreed well with the gel electrophoresis finding of 25,000 - 68,000 M⁻¹sec⁻¹ for cleavage at the D1185 site.

Similarly, Figure 5.7 B shows a series of curves for D13_w samples with concentrations ranging from 0.9 to 8.2 μM , and $[\text{casp}] = 700 \text{ nM}$, each with intensity decreasing as a function of time. The V value obtained from Fig 5.7 C for $[\text{D13}\Delta_w] = 0.9 \text{ }\mu\text{M}$ was 0.08759 $\mu\text{M}/\text{min}$. The Lineweaver-Burk plot (Fig 5.7 D) was again linear, demonstrating Michaelis-Menten kinetics for caspase cleavage of D13 Δ_w . The V_{max} value was 0.7 $\mu\text{M}/\text{min}$, with the K_M 7.3 μM , and the k_{cat} of 1/min. The k_{cat}/K_M value was then 2,900 $\text{M}^{-1}\text{sec}^{-1}$ (Table 5-2). This value agreed well with the gel electrophoresis finding of 2,800 - 3,400 $\text{M}^{-1}\text{sec}^{-1}$ for the cleavage at the D1478 site, values much lower than those for the cleavage at the D1185 site.

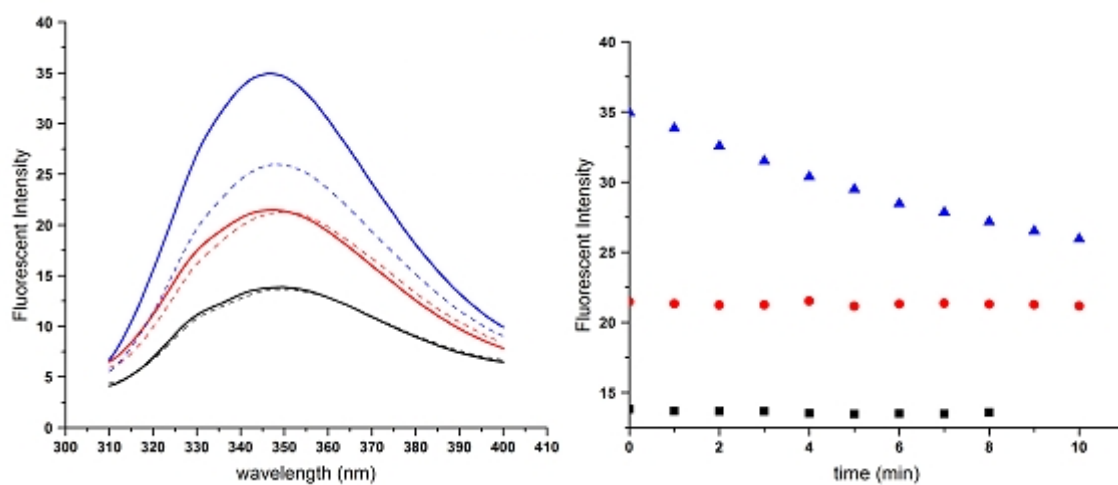


Fig 5.5 Fluorescence Spectra of D10-D11 w (blue), D10-D11 w-1 (black), D10-D11 w-2 (red) samples with the addition of caspase-3 at either $t = 0$ (solid line) or $t = 10$ min (dotted line) at 37°C . On the right, the fluorescence intensities at 347 nm as a function of time. No change in the intensity was observed for D10-D11 w-1 (black) or D10-D11 w-2 (red) with the caspase-3 addition.

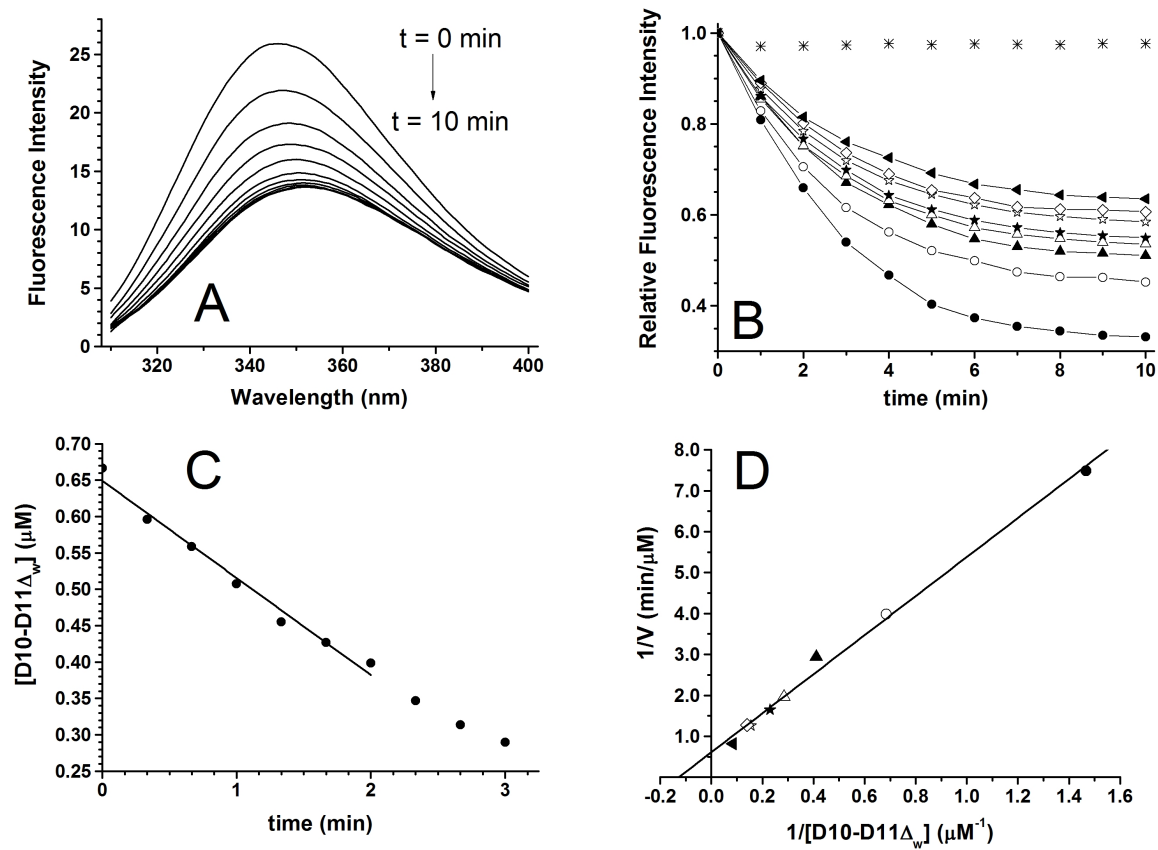


Fig 5.6 (A) Intrinsic tryptophan fluorescent spectra of a sample D10-D11_w (see the Methods and Table 5-1) at 0.7 M with [casp-3] = 100 nM at 37 °C show that the intensity decreases as a function of time (at 1 min interval), with slight λ_{max} shift, from 347 to 351 nm. The excitation wavelength was 295 nm. (B) Relative intensities at 347 nm of the spectra in (A), of [D10-D11_w] = 0.7 M (solid circles), as a function of time, with the intensity at t = 0 as 1. Also shown are those for [D10-D11_w] = 2.4 (open circles), 3.5, 4.4, 6.5, 7.1, and 11.7 M (solid triangle). The data for D10-D11_w without caspase-3 (*) show no decrease in intensity as a function of time. (C) A linear decrease of [D10-D11_w], converted from the intensities at 347 nm of the sample in (A) at a time interval of 20 sec, was found for the first 2 min. The linear fit ($R^2 = 0.98$) gives a slope, or the initial rate V, of 0.13352 M/min. (D) The Lineweaver-Burk (1/V vs 1/[D10-D11_w]) plot of the data from (B). The V_{max} value from the y-intercept was 1.4 M/min, the K_M value from the x-intercept was 6.3 M, and the k_{cat} from $V_{max}/[casp-3]$ was 14/min, or 0.23/sec. The k_{cat}/K_M value was then 37,000 M⁻¹sec⁻¹.

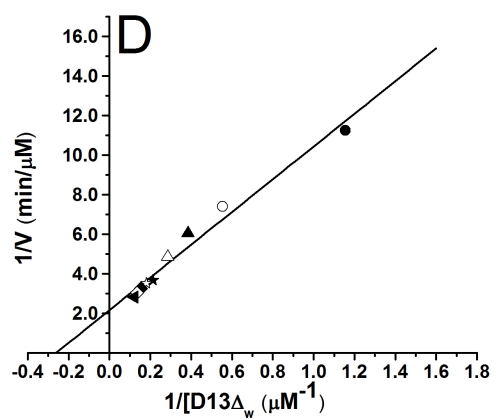
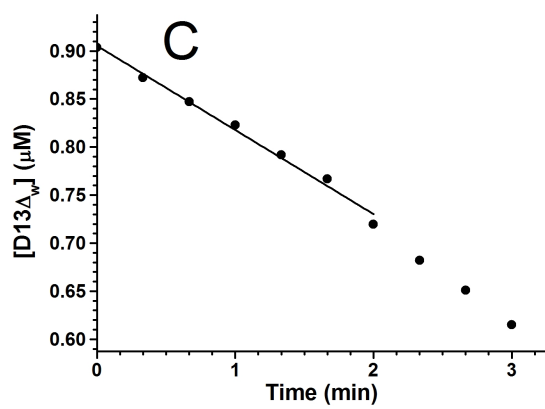
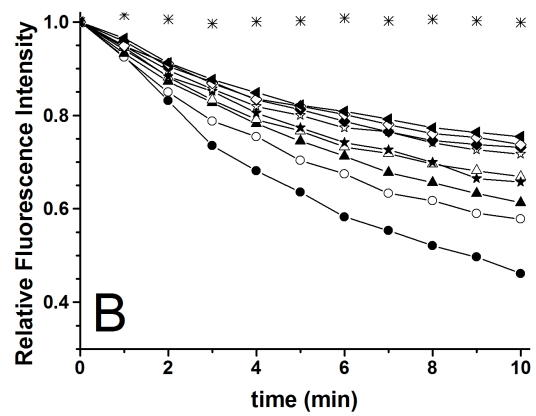
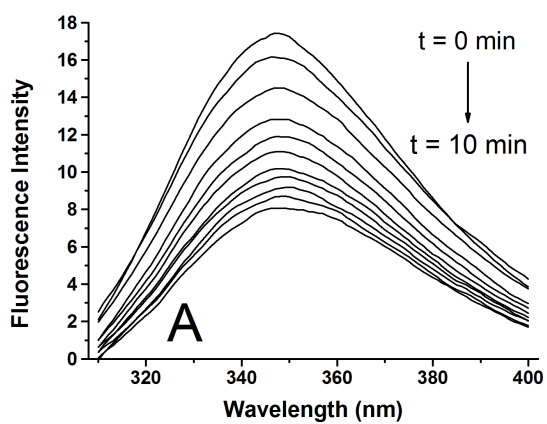


Fig 5.7 (A) Intrinsic tryptophan fluorescent spectra of D13_w at 0.9 M with [casp-3] = 700 nM at 37 °C show decreasing intensity as a function of time (at 1 min interval), with slight λ_{max} shift, from 347 to 349 nm. The excitation wavelength was 295 nm. (B) Relative intensities at 347 nm of the spectra in (A), with the intensity at $t = 0$ as 1 (solid circles, [D13_w] = 0.9 M). Also shown are those for [D13_w] = 1.8 (open circles), 2.6, 3.5, 4.7, 5.5, 6.5, 7.4, and 8.2 M (solid triangle). The data for D13_w without caspase-3 (*) show no decrease in intensity as a function of time. (C) A linear decrease of [D13_w], converted from the intensities at 347 nm of the sample in (A) at a time interval of 20 sec, was found for the first 2 min. The linear fit ($R_2 = 0.99$) gives a slope, or the initial rate V , of 0.08759 M/min. (D) The Lineweaver-Burk ($1/V$ vs $1/[D13_w]$) plot of the data from (B). The V_{max} from the y-intercept was 0.5 M/min, the K_M from the x-intercept was 3.8 M and the k_{cat} from $V_{\text{max}}/[\text{casp-3}]$ was 0.7/min, or 0.01/sec. The k_{cat}/K_M value was then 2,900 $\text{M}^{-1}\text{sec}^{-1}$.

TABLE 5-2

Equilibrium ($[E]_{1/2} = [\text{Caspase-3}]$ to give 50% cleavage of a spectrin model protein) and kinetic (k_{cat}/K_M) results of caspase-3 cleavage at a specific site in spectrin model proteins, as detected by gel electrophoresis and tryptophan fluorescence methods. See text for details in experimental set-up. The number of runs to give the listed average values and standard deviations was 3.

Cleavage Site	Proteins	$[E]_{1/2}$ (nM)	k_{cat}/K_M ($M^{-1}\text{sec}^{-1}$)	
			Electrophoresis	Fluorescence
D1185	D10-D11	2.9 ± 0.6	$67,700 \pm 13,200$	
	D8-D11	7.7 ± 1.4	$25,400 \pm 4,300$	
	D10-D13 ^a	4.3 ± 1.1	$47,200 \pm 15,000$	
	D10-D11 _w	4.2 ± 0.5	$46,800 \pm 3,900$	35,000
E1185	D10-D13(D1185E)	172.7 ± 27.0	$1,100 \pm 180$	
D1478	D13	57.8 ± 3.1	$3,300 \pm 200$	
	D12-D13	62.2 ± 10.6	$3,100 \pm 500$	
	D10-D13 ^b	58.2 ± 10.1	$3,400 \pm 650$	
	D10-D13(D1185E) ^c	73.0 ± 22.8	$2,800 \pm 900$	
	D13 _w			2,900

^aD10-D13 protein also consisted of the D1478 site.

^bD10-D13 protein also consisted of the D1185 site.

^cD10-D13(D1185E) protein also consisted of the E1185 site.

TABLE 5-3

Caspase/Caspase-3 cleavage site predictions on II-spectrin (L780-V1560) using algorithms from Cascleave (Song *et al.*, 2010), CAT3 (Caspase Analysis Tool 3) (Ayyash *et al.*, 2012), and SitePrediction (SP) (Verspurten *et al.*, 2009) servers.

Predicted Structural			P1	P4 - P4'	WT - D1185			D1185E		
Features			Res #		Cascleave ^b	CAT3 ^c	SP ^c	Cascleave ^b	CAT3 ^c	SP ^c
Domain	Helix	Loop			Score ^d	Score ^e	Score ^f	Score ^d	Score ^e	Score ^f
8	A		795	DVED*EETW	0.85	9	3	0.75	9	3
8-9	CA		888	DLED*SLQA	1.04	31	137	0.83	31	137
9		AB	917	GSTD*YGKD	0.37	3	5	0.57	3	5
9		AB	923	KDED*SAEA	0.28	1	3	0.03	1	3
9	B		936	LMSD*LSAY	0.37	-	1	0.01	-	1
SH3			977	ALYD*YQEK	0.00	-	0	0.22	-	0
9	C		1050	EQID*NQTR	0.67	2	5	0.63	2	5
10		BC	1185	DETD*SKTA	1.10	98	3012	0.06	0	6
11	B		1281	FERD*LAAL	0.22	-	2	0.34	-	2
11	C		1309	SAED*LQEK	0.07	-	1	0.10	-	1
11-12	CA		1340	DSHD*LQRF	1.05	31	8	1.12	31	8
12	A		1350	DFRD*LMSW	0.81	21	2	0.87	21	2
12		AB	1365	VSSD*ELAK	0.17	3	1	0.21	3	1
12	B		1389	TEID*ARAG	0.94	11	21	1.04	11	21
12	C		1424	DILD*QERA	0.70	21	2	0.72	21	2
13		AB	1475	DKGD*SLDS	0.70	46	22	0.65	46	22
13		AB	1478	DSL D*SVEA	1.05	76	940	1.03	76	940
13	B		1481	DSVE*ALIK	0.07	-	2	0.03	-	2
13	B		1491	EDFD*KAIN	0.22	-	1	0.42	-	1
13	C		1531	EVLD*RWRR	0.02	3	0	0.23	3	0

^astructural predictions based on the amino acid sequence alignment with D1 (see results for details); ^bfor all caspases; ^cspecific to caspase-3; ^dCascleave - cleavage probability score; ^eCAT3 - score; ^fSitePrediction - average score.

5.4 Discussion

Our results from well-folded α -II-spectrin model proteins of five different lengths that contained various reported caspase-3 cleavage sites, individually or together, clearly showed two specific cleavage sites in α -II-spectrin, one cleaved after the D1185 residue (D1185 site) and another after the D1478 residue (D1478 site), in good agreement with previous results from cellular studies (Wang *et al.*, 1998; Dix *et al.*, 2008). Thus, these model proteins represented intact spectrin well, in the break-down reactions catalyzed by caspase-3. It has been reported that the rank-order of substrate cutting in lysate is similar to that in apoptotic cells, suggesting that cellular structures do not dramatically alter substrate accessibility (Agard *et al.*, 2012), providing justification and confidence in using model proteins to study SBDP in cells.

Recently, several algorithms have become available to predict caspases or caspase-3 cleavage sites. These algorithms were developed based on knowledge from the well studied structural features of caspase substrates, such as preferred primary structure (sequence logo DxxD) (Timmer *et al.*, 2009; Dix *et al.*, 2008; Pop and Salvesen, 2009; Mahrus *et al.*, 2008; Weber *et al.*, 2008; Luthi and Martin, 2007; Timmer and Salvesen, 2007; Fischer *et al.*, 2003; Nicholson, 1999; Talanian *et al.*, 1997; Schneider and Stephens, 1990), secondary structure (unstructured loop) (Garay-Malpartida *et al.*, 2005), solvent accessible surface (Pop and Salvesen, 2009; Xu *et al.*, 2001), and phosphorylation at the P3 position (Dix *et al.*, 2012). It should be specifically noted that these authors found that phosphorylation on spectrin does not affect caspase-3 cleavage), etc. We found that three of these algorithms predicted D1185 and D1478 sites with high scores (Table 5-3). An observed D1475 site (Dix *et al.*, 2008) is predicted to be the third highest by one method (CAT3, Table 5-3). However, we did not observe any cleavage after this D1475 residue. Another method (SitePrediction, Table 5-3) scored the D888 site higher than the D1475 site while the D1340 site was scored as high as the D1478 site, with

the D888 site just slightly lower (Cascleave, Table 5-3). We did not observe any cleavage after the D888, D1340, or D1475 residue in our model protein studies. More interestingly, we observed cleavage at E1185 (the mutated site of D1185), with a k_{cat}/K_M value of $\sim 1,000 \text{ M}^{-1}\text{sec}^{-1}$. However, when we input the mutated sequence for prediction by these algorithms, the score for E1185 site was much lower than those for the D888, D1340, or D1475 sites (Table 5-3). Yet we did not observe any cleavage at these sites in our mutant. It appears that our current understanding of caspase-3 cleavage site preferences is still limited and could not be reliably used to predict the sites for spectrin in particular, and probably for other proteins in general, without experimentation.

It has been suggested that, for spectrin, the cleavage proceeds in a two-step mechanism, first at the D1185 site to cause conformational changes to expose the D1478 site for subsequent cleavage (Wang *et al.*, 1998; Williams *et al.*, 2003). This suggestion is consistent with studies reporting the SBDP150 as an intermediate product leading to eventual SBDP120 detection (Yan and Jeromin, 2012; Dix *et al.*, 2008; Agard *et al.*, 2012; Weiss and Baumgartner, 2011; Zhang *et al.*, 2009). However, it is not compatible with an *ex vivo* experiment, in which the D1478 cleavage occurs during apoptosis independently of the D1185 site, since proteins with the D1185 site deleted were still cleaved after the D1478 residue (Meary *et al.*, 2007). Our results quantitatively and unequivocally showed that, in spectrin model protein with both sites and in proteins with only a single site, the cleavage efficiencies (k_{cat}/K_M values) at each site were quantitatively comparable. The k_{cat}/K_M values for the D1185 site were about $40,000 \text{ M}^{-1}\text{sec}^{-1}$. More importantly, for the D1478 site, in proteins with or without the domain consisting of the D1185 site, the k_{cat}/K_M values were all about $3,000 \text{ M}^{-1}\text{sec}^{-1}$. A similar value for the D1478 site was also obtained in the protein with the D1185E mutation. Thus, our results showed that the cleavages at the D1185 site and the D1478 site were clearly unrelated to, or independent of, each other, and support the earlier finding that the cleavage after the residue D1478 occurs even

when the D1185 region is deleted (Meary *et al.*, 2007).

Recent proteomic studies (Agard *et al.*, 2012) find that only 2% of the substrate proteins studied (4 out of 179 proteins) exhibit efficiency between 40,000 - 70,000 $\text{M}^{-1}\text{sec}^{-1}$, and most (76%) substrate proteins are less than 5,000 $\text{M}^{-1}\text{sec}^{-1}$. For spectrin, we found 40,000 and 3,000 $\text{M}^{-1}\text{sec}^{-1}$, for the D1185 site and D1478 site, respectively. Thus, the D1185 site in α -II-spectrin is an unusually efficient site, whereas the D1478 site is like many others, with an average efficiency/rate. The cleavage rate after the D1185 residue was much faster than the cleavage rate after the D1478 residue. In the proteomic studies referenced above, the rates of substrate hydrolysis for individual caspases are found to vary greater than 500-fold, indicating a sequential process (Agard *et al.*, 2012). For spectrin, this caspase-3 initiated sequential process will mean that the break-down product formation is sequential, but the two cleavage events are not sequential to each other. The formation of the second product (SBDP120) does not depend on the formation of the first product (SBDP150). We suggest that, in the presence of caspase-3, both break-down products, SBDP150 and SBDP120, will form. However, due to the difference in the catalytic rates, the accumulation of SBDP120 will be much slower than that of SBDP150. Further cleavage of SBDP150 at the D1478 site will also produce SBDP120, as well as SBDP37. Our results imply that the cleavage after residue 1185 in intact spectrin will cut α -II-spectrin into two halves, with the N-terminal half slightly smaller (134,563.7 Da from sequence) than the C-terminal half (147,735.9 Da). The C-terminal half should be the SBDP150. The cleavage after residue 1478 in intact spectrin will give a larger N-terminal fragment (168,236.0 Da) harboring the D1185 site and a C-terminal fragment (114,063.6 Da). This C-terminal segment should be the SBDP120. However, since the rate of cleavage at this site is much slower than that at the D1185 site, this N-terminal fragment (residues 1-1478) will not accumulate, but will subsequently be fragmented at the D1185 site into an N-terminal fragment and the SBDP 37 fragment with

high efficiency.

With the great variation in cleavage rates (Agard *et al.*, 2012), it has been suggested that transient caspase activation occurs during cellular differentiation, including the transformations of monocytes to macrophages and pluripotent stem cells to more specialized cell types and perhaps these rapidly cleaved substrates are also important during transient caspase activation in differentiation (Fujita *et al.*, 2008; Sordet *et al.*, 2002). Since the caspase-3 cleavages at the D1185 and D1478 sites were independent of each other with substantially different rates, the cleavages at these two sites may represent different cellular events, with SBDP150 and SBDP120 involved in different functions.

Furthermore, we speculate that SBDP37 (S1186-D1478), the N-terminal fragment which pairs with the SBDP120 (the C-terminal fragment) from the break-down of SBDP150, is well folded with the 15-residue segment (S1186-H1200, see Fig 5.1) prior to Helix C in D10 as unstructured. This region of α -II-spectrin has been reported to be a calmodulin binding site (Simonovic *et al.*, 2006). In a crystallographic study, residue 1174 - residue 1210, prepared as a recombinant fragment, is found to bind to calmodulin and residues 1191-1210 undergo conformational changes, from unstructured to helical (Simonovic *et al.*, 2006). The SBDP37, after being cleaved off from SBDP150, if indeed consisting of a 15-residue unstructured segment (S1186-H1200) followed by a coiled coil helix as we speculated, may then bind to calmodulin with the 15-residue segment inserting into the calmodulin cavity as reported (Simonovic *et al.*, 2006). At this time, we are not able to speculate on the functional consequence of this interaction, if detected. We suggest that future studies of SBDP37 may provide useful insights and discoveries

Recent studies show that the vast majority of proteolyzed proteins yielded persistent fragments that correspond to discrete protein domains, suggesting that the generation of active effector proteins may be a principal function of apoptotic proteolytic cascades (Dix *et al.*, 2008).

Additional functional and structural studies of both the N-terminal and C-terminal fragments of spectrin break-down at both the D1185 and D1478 sites, including SBDP37, will allow us to further understand the cellular processes that we mentioned earlier, both the apoptotic and non-apoptotic events, e.g., traumatic brain injury, mechanical stretch injury, ischemia, and brain diseases, such as Alzheimer's Disease, as well as other age-related degenerative diseases, Sjögren's Syndrome, normal tension glaucoma as well as the regulation of synaptic plasticity and of neuronal morphology via local remodeling of the spectrin cytoskeleton.

CHAPTER 6

CRYSTALLIZATION OF SPECTRIN MODEL PROTEINS CONTAINING CASPASE-3

RECOGNITION SITE

6.1 Introduction

Unlike the stringent specificity of restriction endonucleases, proteases are enzymes with varying degrees of specificity and selectivity that are not exclusively influenced by the amino acid sequence of a substrate's recognition site. There are several determinants influencing which substrates a protease cleaves and where the cleavage sites are. One of the best known proteases is the caspase-3. It has been proposed that a peptide containing sequence P4-P3-P2-P1-P1', with the bond between P1 and P1' as the scissile bond, is a caspase substrate when (1) the P1 residue is Asp, (2) the P1' residue is small and uncharged (Gly, Ser, Ala), (3) P4-P3-P2 residues are complementary for interactions with the catalytic groove, and (4) the substrate cleavage site (P4-P1') is exposed to the aqueous environment (Pop and Salvesen, 2009). Furthermore, rates of proteolysis are well known to be enhanced by substrate denaturation (Fontana *et al.*, 2004). This suggests that "loops" and "turns" are prone to be proteolyzed. In contrast, numerous cleavage sites were found residing also in α -helices (Timmer *et al.*, 2009).

The presence of a sequence that satisfies the above four criteria is not sufficient for a protein substrate to be cut. This could be seen comparing well known caspase-3 site in D13 of spectrin II, which is 100% identical in sequence from P5 through P5' to that in D5 of spectrin II, but no cleavage was reported in D5 (Fig 6.4). In contrast, several natural caspase substrates containing non-canonical cleavage recognition sequences were found (Timmer and Salvesen, 2007). Thus, a protein with a preferred cleavage site sequence is not necessary to be cleaved.

Primary structure is only one aspect of caspase substrate recognition; secondary, tertiary, and quaternary structure effects, as well as localization, are also important. Even though there are still many questions to answer, few substrate structures have been solved that include regions involved in the caspase-3 catalysis.

We have shown that the cleavage after residue D1185 is unusually efficient, whereas the D1478 site is like many others, with an average efficiency/rate. We have now solved the crystal structure of D13 containing the D1478 caspase-3 recognition site. Using the x-ray structural information, together with our previous biophysical and biochemical studies of spectrin model proteins involved in caspase-3 catalysis, we examined structure - sequence correlation and its effect on the cleavage efficiency. We identified the residue D1478 being at the end of the 12-residue A₁₃B₁₃ loop. Unfortunately, we have not yet obtain a high resolution structure containing the D1185 site. However, previous study (Witek and Fung, submitted paper) suggests that the D1185 is in the middle of an unusually long, 40-residue loop. It is known that disordered regions are inherently difficult to crystalize. This might be one of the reasons we were not able to get highly ordered well diffracting crystal.

6.2 Experimental Procedures

6.2.1 DNA Plasmid Preparation

The cDNA of human α -II-spectrin was purchased from ATCC (Manassas, VA). Four α -II-spectrin plasmids were cloned into pDEST-15 vector (Invitrogen; Grand Island, NY), following the methods provided by the company's user manual, to give four spectrin model protein fragments, L780-F1344 (D8-D11), L1087-F1344 (D10-D11), L1087-F1556 (D10-D13), and L1441-F1556 (D13). All plasmids, stored in *E.coli* DH5 cells (Zymo Research), were extracted and transformed into *E.coli* BL21-CodonPlus (DE3)-RIL competent cells (Agilent) for protein expression.

The spectrin model proteins, expressed as fusion proteins with an N-terminal GST tag followed by a thrombin cleavage site, were prepared as in chapter five. The eluted proteins from GSH affinity column were diluted with 20 mM Tris pH 8 and further purified by anion-exchange chromatography (HiTrapQ HP, GE Amersham) with a 30-column volume gradient to 50% of buffer B containing 1 M NaCl. D8-D11 elutes with 240 mM NaCl, D10-D11 elutes with 250 mM NaCl, D10-D13 with 270 mM NaCl, and D13 protein with 200 mM NaCl. Spectrin proteins were concentrated and frozen drop-wise in liquid nitrogen and stored in -80 °C.

6.2.2 Crystallization of Spectrin Model Proteins

Crystallization of four spectrin model proteins was accomplished by using the hanging-drop, vapor diffusion method at 16 °C. Each protein solution was mixed with an equal volume of reservoir solution, to give 2 μ L droplet.

Also the Tecan Freedom Evo 200 robotic system was used for high-throughput protein crystallization to obtain initial crystal growth conditions (RRC, UIC) for D8-D11, D10-D13, and D10-D11 proteins. Crystallization plates contain 96 wells, with 3 sitting drop compartments per well, with a 1 μ L protein and 1 μ L crystallization reagent per each compartment. We tested three plates, 288 of different buffer conditions for each spectrin model protein. 1st plate contained crystallization screen from PEG/Ion (Hampton Research), 2nd plate contained Classics II crystallization screen (Qiagen; Valencia, CA) and for the 3rd plate we used JCSG+ screen (Qiagen).

6.2.2.1 D8-D11

D8-D11 spectrin model protein was concentrated to 27 mg/ml (~400 μ M) in 20 mM Tris and 240 mM NaCl buffer at pH 8). Crystals were obtained for five different conditions using PEG/Ion screen (solution #1 through #96). (1) A reservoir solution containing a mixture of 20% of PEG3350 and 0.2 M ammonium fluoride (#3), (2) 20% PEG3350 and 0.2 M ammonium

chloride (#9), (3) 20% PEG3350 and 0.2 M ammonium formate (#23), (4) 20% PEG3350 and 0.2 M ammonium sulfate (#35), and (5) 20% PEG3350 and 0.2 M ammonium tartrate dibasic (#38). Crystals from all conditions diffracted poorly ($\sim 5 \text{ \AA}$). Several different conditions for crystal growth were tried. Concentrations of 8 and 16 mg/ml, temperature of 25 °C, and the additive screen from Hampton Research containing 96 solutions were used. However no improvement in the resolution was obtained. Most crystals formed layers that were difficult to separate for mounting for diffraction experiments.

6.2.2.2 D10-D11

Needle shape crystals were grown using 16 mg/ml ($\sim 500 \text{ \mu M}$) in 20 mM Tris and 250 mM NaCl buffer at pH 8. A reservoir contained the mixture of 0.2 M potassium sulfate with 20% PEG 3350. Crystals were too small for diffraction.

6.2.2.3 D10-D13

D10-D13 was concentrated to 16 mg/ml ($\sim 300 \text{ \mu M}$) in 20 mM Tris and 250 mM NaCl buffer at pH 8 with 2 mM DTT. Large rectangular shaped crystals were formed for the reservoir mixture of 0.2 M potassium sodium tartrate tetrahydrate with 20% PEG 3350 and 0.1 M calcium chloride dihydrate after 10 days of incubation at 16 °C. To reduce radiation damage, D10-D13 crystals used for diffraction experiments were frozen at 100 K, with 30 % glycerol added as cryoprotectant.

6.2.2.4 D13

Protein concentration used for crystallization was 16 mg/ml ($\sim 1.2 \text{ mM}$). Crystals were formed in the reservoir mixture of 0.2 M lithium acetate, 20% PEG3350, 0.1 M TCEP hydrochloride, with mixture of additives (0.2% D-sorbitol, 0.2% glycerol, 0.2% glycine, 0.2% myo-inositol, 0.2% sarcosine, 0.02 M Hepes sodium pH 6.8). Crystals appeared nine days after set up at 16 °C.

6.2.3 X-ray Data Collection and Analysis

Diffraction for D13 crystal was collected at SER-CAT 22-ID (Southeastern Regional Collaborative Access Team, Advanced Photon Source, Argonne National Laboratory). The facility provided a 300 mm MAR CCD detector for image collection. Images were collected at a crystal-to-detector distance of 150 mm with an exposure time of 3 min per 0.5° oscillation. XDS (Kabsch, 1993) was used for indexing, integrating and scaling. D1 crystal structure (pdb code: 3f31) (Mehboob *et al.*, 2010) was used as the starting model. The model was manually build using the program Coot (Emsley and Cowtan, 2004) and validated using MolProbity (Chen *et al.*, 2010). Refinement of coordinates was performed using REFMAC5.5 within CCP4 (Winn *et al.*, 2011).

Data for D10-D13 was collected at LS-CAT 21-ID-F (Argonne National Laboratory) using a 225 mm MarMosaic detector for image collection. HKL-2000 was used for indexing. Partial data set was collected at 2.1 Å resolution.

6.3 Results

6.3.1 D13 Spectrin Model Protein

The SDS gel electrophoresis data showed that all spectrin model proteins used for crystallization studies were >95% pure. All of the molecular masses of the proteins used in this study were within 1 Da of the expected values (Table 5-3).

D13 spectrin structure was determined at 2.03 Å resolution, and crystallized in the $P2_12_12_1$ space group with a single molecule in the asymmetric unit. Poor electron density was observed for 11 C-terminal residues (K1546-F1556). Three helices, A_{13} (residues S1440-L1468), B_{13} (residues V1480-A1513), and C_{13} (residues K1519-K1543) were bundled with helices A_{13} and B_{13} connected by a long 11-residue $A_{13}B_{13}$ loop, and Helices B_{13} and C_{13} connected by a short $B_{13}C_{13}$ loop (5 residues) (Fig 6.1). The most flexible region is the long $A_{13}B_{13}$ loop, which exhibits B -factors more than 30 Å² for residues 1466-1478 (Fig 6.2). D1478 residue was in $A_{13}B_{13}$ loop thus the caspase-3 recognition site (DSLDS) is located at the end of this loop.

TABLE 6-1 Data collection and refinement statistics of II-D13. Values in parenthesis are for the highest resolution shell.

Data collection	
Space group	P_{212121}
Unit-cell parameters (Å)	$a = 33.11, b = 42.7, c = 79.18$
Resolution range (Å)	19.79-2.02 (2.15-2.02)
# of unique reflections	7218
Completeness (%)	97.85 (82.9)
$\langle I / \langle I \rangle \rangle$	24.73 (8.79)
R_{merge} (%)	5.0 (15.8)
Wilson B factor (Å ²)	26.6
Refinement	
# of protein residues	105
# of water molecules	140
$R_{\text{work}}/R_{\text{test}}$	18.9/19.3
<i>R.m.s.d. from ideal values</i>	
Bond lengths (Å)	0.018
Bond angles (°)	1.570
Torsion angles (°)	5.35
Chiral centers (Å ³)	0.101
Planes (Å)	0.007
Average B factor (Å ²)	25.8
<i>Ramachandran plot</i>	
Favorable	97 [92.4%]
Acceptable	2 [1.9%]
Outliers	2 [1.9%]

For Educational Use Only

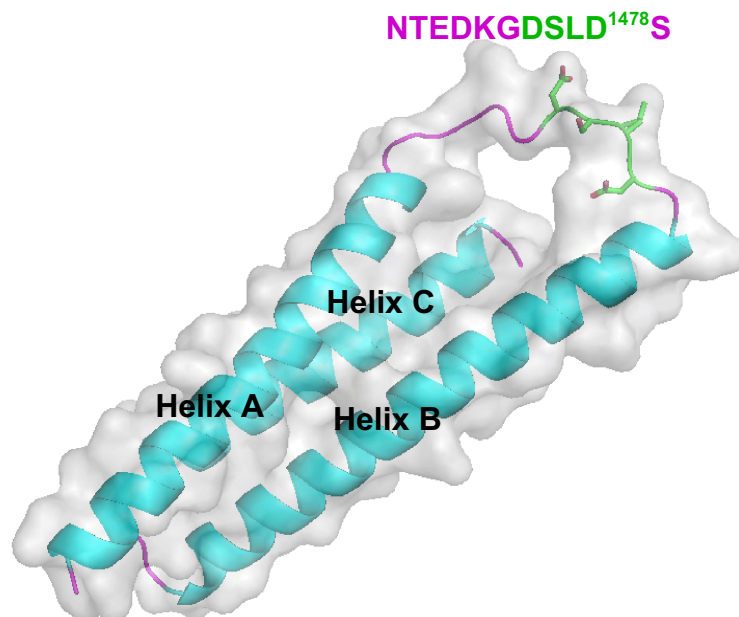


Fig 6.1 II-D13 crystal structure. α -helices A, B, and C are colored blue with loops in magenta. The sequence of the 11-residue AB loop is written from N-terminus to C-terminus. Caspase-3 canonical DxxD (P4-P1) recognition site is shown in green. The cartoon image was prepared with PyMOL.

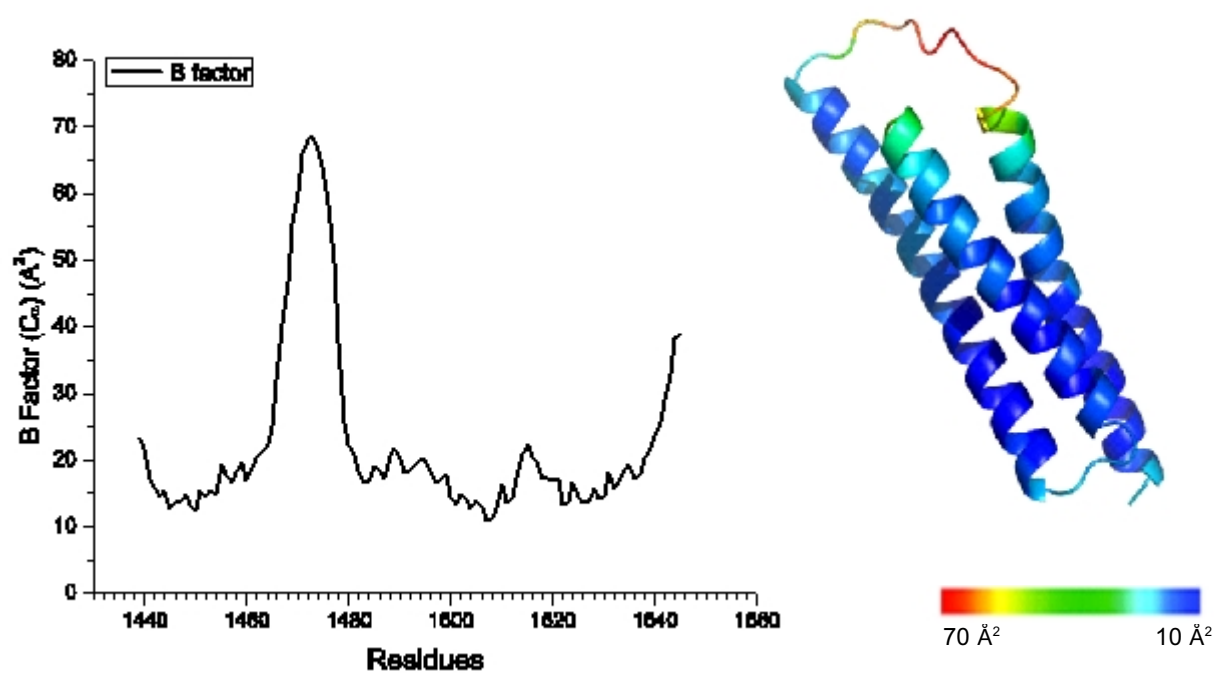


Fig 6.2 B-factors for D13. The most flexible region is the long $A_{13}B_{13}$ loop, which exhibits B-factors more than 30 \AA^2 for residues 1466-1478. Caspase-3 recognition site (DSL^{D1478}S) is located at the very end of this loop.

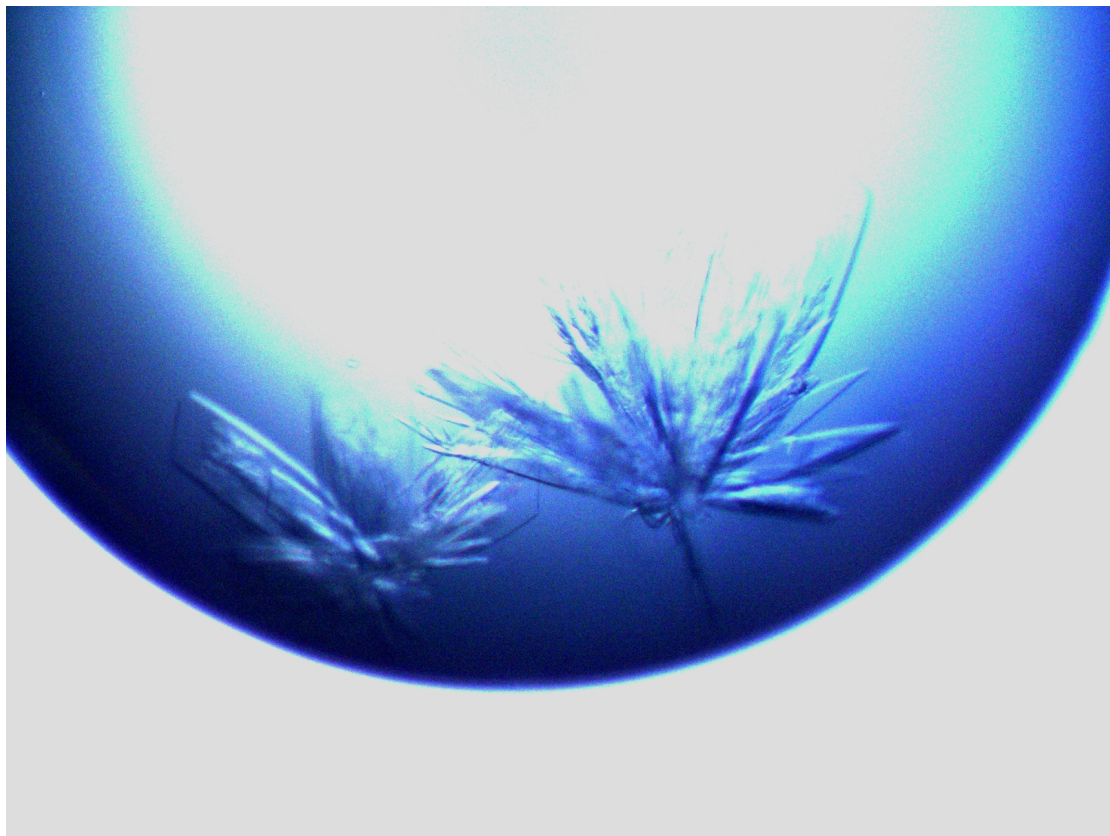


Fig 6.3 Crystals for D10-D13 spectrin model protein after 36 days of incubation at 12 °C (50x magnification).

```

      10      20      30      40      50      60
•   D 5      D Y E Q C M D L Q L F Y R D T E Q V D N W M S K Q E A F L L N E D L G D S L D S V E A L L K K H E D F E K S L S A Q E E
•           : . . . . . : . . . . . : . . . . . : . . . . . : . . . . . : . . . . . :
•   D 13      D L D Q C L E L Q L F H R D C E Q A E N W M A A R E A F L N T E D K G D S L D S V E A L I K K H E D F D K A I N V Q E E
•
      70      80      90      100     110
•   D 5      K I T A L D E F A T K L I Q N N H Y A M E D V A T R R D A L L S R R N A L H E R A M R R R A Q L A D S
•           : . . . . : : . : . : . : . . . . : . . : . : . . . . . :
•   D 13      K I A A L Q A F A D Q L I A A G H Y A K G D I S S R R N E V L D R W R R L K A Q M I E K R S K L G E S

```

Fig 6.4 Alignment of D5 with D13 shows 10 residues starting from P5 (Gly) to P5' (Leu) (boxed region) to be identical for two sequences. In red D1478 residue is shown. Underlined are the tryptophan residues located at “16th” and “88th” position in a typical 106 amino acid long spectrin domain (for more info see Chapter 2.1.5).

6.4 Discussion

Substrate specificity of caspase-3 is influenced by the sequence of amino acids extending in both the N- and C-terminal directions from the cleavage site. The preferred primary structure cleaved by caspase-3 has the sequence logo DxxD. However, it is known that the sequence preference alone cannot explain the selectivity that is observed in spectrin proteolysis. There are 10 DxxD's recognition sequences found in II spectrin but caspase-3 cleaves only at two sites, D1185 (D10) and D1478 (D13).

Hubbard *et al.* (1994) suggested that in order to interact with a protease the substrate must adopt the extended conformation that requires a propensity for local unfolding for at least 12 residues around the cleavage site. Eleven spectrin structures have been published with 7-10 residues in AB loop, with an average of eight, and 5-6 residues in BC loop. However, loops in these structures do not contain DXXD sequence. The published spectrin domains include D14 of *Drosophila* spectrin (Yan *et al.*, 1993; PDB code: 2SPC), human erythroid I-D1 (Park *et al.*, 2003; 1OWA), I-D8-D9 (Kusunoki *et al.*, 2004; 1S35) and I-D14-D15 (Stabach *et al.*, 2009; 3EDU and 43; 3F57), non-erythroid II-D14-D16 (Davis *et al.*, 2009; 3EDV), and chicken brain II-D15-D17 (Kusunoki *et al.*, 2004; 1U5P & 1U4Q, 2; 1CUN and Pascual *et al.*, 1997; 1AJ3). Therefore, 11-residue AB loop in D13 and 40-residues long BC loop in D10 are longer than most spectrin structural domains. With that length of the loop and the DxxD sequence contained within, it is a good combination for caspase-3 to approach spectrin and cleave.

We have shown previously (Witek and Fung, submitted) that the cleavage rate after the D1185 residue is $\sim 30,000 \text{ M}^{-1}\text{sec}^{-1}$ which is 10-fold faster than the cleavage rate after the D1478 residue ($3,000 \text{ M}^{-1}\text{sec}^{-1}$). An extended loop conformation by addition of extra five residues on each site of P1' in engineered carA mutants improved $k_{\text{cat}}/K_{\text{M}}$ by 10 fold (Timmer, 2009). Therefore, we suggest that the size of the disordered region flanking the cleavage site affects

the rate, with D10 being more efficiently cleaved by caspase-3 than D13 site.

Our current understanding of caspase-3 cleavage site preferences is still limited and could not be reliably used to predict the sites and their cleavage rates without experimentation. The increasing number of structural information of caspase-3 substrates can be incorporated into substrate-predictions algorithms making predictions more reliable.

REFERENCES

1. Agard, N.J., Mahrus, S., Trinidad J. C., Lynn, A., Burlingame, A. L., and Wells, J. A. (2012) Global kinetic analysis of proteolysis via quantitative targeted proteomics. *Proc. Natl. Acad. Sci. U. S. A.* **109**, 1913-1918
2. Alnemri, E. S., Livingston, D. J., Nicholson, N. A., Salvesen, G., Thornberry, N. A., Wong, W. W., and Yuan, J. (1996) Human ICE/CED-3 protease nomenclature. *Cell* **87**, 171
3. An, X., Zhang, X., Salomao, M., Guo, X., Yang, Y., Wu, Y., Gratzer, W., Baines, A.J. and Mohandas, N. (2006) Thermal Stabilities of Brain Spectrin and the Constituent Repeats of Subunits *Biochemistry*. **45**, 13670-13676
4. Ayyash, M., Tamimi, H., and Ashhab, Y. (2012) Developing a powerful *In Silico* tool for the discovery of novel caspase-3 substrates: a preliminary screening of the human proteome. *BMC Bioinformatics* **13**, 1-14
5. Baines, A. J. (2009). Evolution of spectrin function in cytoskeletal and membrane networks. *Biochem Soc Trans* **37**, 796-803
6. Beer, R., Franz, G., Srinivasan, A., Hayes, R. L., Pike, B. R., Newcomb, J. K., Zhao, X., Schmutzhard, E., Poewe, W., and Kampfl, A. (2000) Temporal profile and cell subtype distribution of activated caspase-3 following experimental traumatic brain injury. *J. Neurochem.* **75**, 1264-1273
7. Beechem, J. M. and L. Brand (1985). Global analysis of fluorescence decay: applications to some unusual experimental and theoretical studies. *Photochem Photobiol* **44**, 323-329
8. Begg, G. E., Morris, M. B., and Ralston, G. B. (1997) Comparison of the salt-dependent self-association of brain and erythroid spectrin. *Biochemistry* **36**, 6977-6985
9. Bennett, V., and Healy, J. (2008) Organizing the fluid membrane bilayer: diseases linked to spectrin and ankyrin, *Trends Mol Med.* **14**, 28-36
10. Benz, P.M., Blume, C., Moebius, J., Oschatz, C., Schuh, K., Sickmann, A., Walter, U., Feller, S.M., and Renne, T. (2008) Cytoskeleton assembly at endothelial cell-cell contacts is regulated by II-spectrin-VASP complexes. *J. Cell Biol.* **180**, 205-219
11. Bignone, P.A., King, M.D., Pinder, J.C., and Baines, A.J. (2007) Phosphorylation of a threonine unique to the short C-terminal isoform of II-spectrin links regulation of -spectrin interaction to neuritogenesis. *J. Biol. Chem.* **282**, 888-896

12. Chan, S. L. and M. P. Mattson (1999). Caspase and calpain substrates: roles in synaptic plasticity and cell death. *J Neurosci Res* **58**, 167-190
13. Chen, V. B., W. B. Arendall (2010) MolProbity: all-atom structure validation for macromolecular crystallography. *Acta Crystallogr D Biol Crystallogr* **66**, 12-21
14. Ciani, C. D., Zhang, Z., Pradhan, D., and Morrow, J. S. (1999) Brain and muscle express a unique alternative transcript of β II spectrin. *Biochemistry* **38**, 15721-15730
15. Cotman, C. W., Poon, W. W., Rissman, R. A., and Blurton-Jones, M. (2005) The role of caspase cleavage of tau in Alzheimer disease neuropathology. *J. Neuropathol. Exp. Neurol.* **64**, 104-112
16. Crawford, E. D., and Wells, J. A. (2011) Caspase substrates and cellular remodeling. *Annu. Rev. Biochem.* **80**, 1055-1087
17. Cryns, V. L., Bergeron, L., Zhu, H., Li, H., and Yuan, J. (1996) Specific cleavage of alpha-fodrin during Fas- and tumor necrosis factor-induced apoptosis is mediated by an interleukin-1beta-converting enzyme/Ced-3 protease distinct from the poly(ADP-ribose) polymerase protease. *J. Biol. Chem.* **271**, 31277-31282
18. D'Amelio, M., V. Cavallucci (2011). Caspase-3 triggers early synaptic dysfunction in a mouse model of Alzheimer's disease. *Nat Neurosci* **14**, 69-76
19. d'Avella, D., Servadei, F., Scerrati, M., Tomei, G., Brambilla, G., Angileri, F. F., Massaro, F., Cristofori, L., Tartara, F., Pozzati, E., Delfini, R., and Tomasello, F. (2002) Traumatic intracerebellar hemorrhage: clinico-radiological analysis of 81 patients. *Neurosurgery* **50**, 16-25
20. Davis, L., Abdi, K., Machius, M., Brautigam, C., Tomchick, D.R., Bennett, V. and Michaely, P. (2009) Localization and structure of the ankyrin-binding site on beta2-spectrin. *J. Biol. Chem.* **284**, 6982-7
21. Denault, J.-B., and Salvesen, G. S. (2001) Caspases. *Curr. Protocols in Protein Sci.* **21**, 8.1-8.16
22. Denault, J.-B., and Salvesen, G. S. (2008) Apoptotic caspase activation and activity. *Methods in Mol. Biol.* **414**, 191-220
23. Dix, M. M., Simon, G. M., and Cravatt, B. F. (2008) Global mapping of the topography and magnitude of proteolytic events in apoptosis. *Cell* **134**, 679-691
24. Dix, M. M., Simon, G. M., Wang, C., Okerberg, E., Patricelli, M. P., and Craves, B. F. (2012) Functional interplay between caspase cleavage and phosphorylation sculpts the

- apoptotic proteome. *Cell* **150**, 426-440
25. Emsley, P. and K. Cowtan (2004). Coot: model-building tools for molecular graphics. *Acta Crystallogr D Biol Crystallogr* **60**, 2126-2132
 26. Falconer, R. J., A. Penkova, *et al.* (2010). Survey of the year 2008: applications of isothermal titration calorimetry. *J Mol Recognit* **23**, 395-413
 27. Fischer, U., Janicke, R. U., and Schulze-Osthoff, K. (2003) Many cuts to ruin: a comprehensive update of caspase substrates. *Cell Death Differ.* **10**, 76-100
 28. Fontana, A., P. P. de Laureto, *et al.* (2004) Probing protein structure by limited proteolysis. *Acta Biochim Pol* **51**, 299-321
 29. Freire, E., A. Schon, *et al.* (2009). Isothermal titration calorimetry: general formalism using binding polynomials. *Methods Enzymol* **455**, 127-155
 30. Freyer, M. W. and E. A. Lewis (2008). Isothermal titration calorimetry: experimental design, data analysis, and probing macromolecule/ligand binding and kinetic interactions. *Methods Cell Biol* **84**, 79-113
 31. Fuentes-Prior, P., and Salvesen, G. S. (2004) The protein structures that shape caspase activity, specificity, activation and inhibition. *Biochem. J.* **384**, 201-232
 32. Fujita, J., Crane, A., Souza, M., Dejosez, M., Kyba, M., Flavell, R. Thomson, J. and Zwaka, T. (2008) Caspase activity mediates the differentiation of embryonic stem cells. *Cell Stem Cell* **2**, 595-601
 33. Garay-Malpartida, H. M., Occhiucci, J. M., Alves, J., and Belizario, J. E. (2005) CaSPredictor: a new computer-based tool for caspase substrate prediction. *Bioinformatics* **21**, 169-176
 34. Greenfield, N. and Fassman, G. D. (1969) Computer circular dichroism spectra for the evaluation of protein conformation. *Biochemistry* **8**, 4108-4116
 35. Grus, F. H., Joachim, S. C., Sandmann, S., Thiel, U., Bruns, K., Lackner, K. J., and Pfeiffer, N. (2008) Transthyretin and complex protein pattern in aqueous humor of patients with primary open-angle glaucoma. *Mol. Vis.* **14**, 1437-1445
 36. Gulyaeva, N. V. (2003). Non-apoptotic functions of caspase-3 in nervous tissue. *Biochemistry (Mosc)* **68**, 1171-1180
 37. Hall, E. D., Sullivan, P. G., Gibson, T. R., Pavel, K. M., Thompson, B. M., and Scheff, S. W. (2005) Spatial and temporal characteristics of neurodegeneration after controlled cortical impact in mice: more than a focal brain injury. *J. Neurotrauma* **22**, 252-265

38. Haneji, N., Nakamura, T., Takio, K., Yanagi, K., Higashiyama, H., Saito, I., Noji, S., Sugino, H., and Hayashi, Y. (1997) Identification of α -fodrin as a candidate autoantigen in primary Sjögren's Syndrome. *Science* **276**, 603-607
39. He, J., J. Zhao, *et al.* (2008) Mucosal administration of α -fodrin inhibits experimental Sjogren's syndrome autoimmunity. *Arthritis Res Ther* **10**, R44
40. Hubbard, S. J., F. Eisenmenger, *et al.* (1994). Modeling studies of the change in conformation required for cleavage of limited proteolytic sites. *Protein Sci* **3**, 757-768
41. Hyman, B. T. and Yuan, J. (2012) Apoptotic and non-apoptotic roles of caspases in neuronal physiology and pathophysiology. *Nature Reviews - Neuroscience* **13**, 395-406
42. Ipsaro, J. J., L. Huang, *et al.* (2009). Structures of the spectrin-ankyrin interaction binding domains. *Blood* **113**, 5385-5393
43. Janicke, R. U., Ng, P., Sprengart, M. L., and Porter A. G. (1998) Caspase-3 is required for α -fodrin cleavage but dispensable for cleavage of other death substrates in apoptosis. *J. Biol. Chem.* **273**, 15540-15545
44. Jin, M., S. M. Hwang, *et al.* (2011) Autoantibodies in Sjogren's syndrome patients acutely inhibit muscarinic receptor function. *Oral Dis* **18**, 132-139
45. Kabsch, W. (1993) Automatic processing of rotation diffraction data from crystals of initially unknown symmetry and cell constants. *J. Appl. Cryst.*, **26**, 795-800
46. Kabsch, W., and Sander, C. (1983) Dictionary of protein secondary structure: pattern recognition of hydrogen-bonded and geometrical features. *Biopolymers* **22**, 2577-2637
47. Kang, J., Song, Y., Sevinc, A., Fung, L.W.-M. (2010) Important residue (G46) in erythroid spectrin tetramer formation. *Cell Mol. Biol. Lett.* **15**, 46-54
48. Kelly, S. M., T. J. Jess, *et al.* (2005) How to study proteins by circular dichroism. *Biochim Biophys Acta* **1751**, 119-139
49. Kumar, S., and Nussinov, R. (1999) Salt bridge stability in monomeric proteins. *J. Mol. Biol.* **293**, 1241-1255
50. Kumar, K. and X. L. Wu (1994). Post-ischemic changes in protein kinase C RNA in the gerbil brain following prolonged periods of recirculation: a phosphorimaging study. *Metab Brain Dis* **9**, 323-331
51. Kupina, N. C., Detloff, M. R., Bobrowski, W. F., Snyder, B. J., and Hall, E. D. (2003) Cytoskeletal protein degradation and neurodegeneration evolves differently in males and females following experimental head injury. *Exp. Neurol.* **180**, 55-73

52. Kusunoki, H., MacDonald, R. I., and Mondragon, A. (2004) Structural Insights into the Stability and Flexibility of Unusual Erythroid Spectrin Repeats. *Structure* **12**, 645-656
53. Kusunoki, H., Minasov, G., MacDonald, R. I., and Mondragon, A. (2004) Independent movement, dimerization and stability of tandem repeats of chicken brain alpha-spectrin. *J. Mol. Biol.* **344**, 495-511
54. Lam, V.Q., Antoniou, C., Rolius, R., Fung, L.W. (2009) Association studies of erythroid alpha-spectrin at the tetramerization site. *Br. J. Haematol.* **147**, 392-395
55. Laskowski, R. (2009) PDBsum new things. *Nucleic Acids Res.* **37**, D355-D459
56. Lecomte, M.C., Garbarz, M., Gautero, H., Bournier, O., Galand, C., Boivin, P., Dhermy, D. (1993) Molecular basis of clinical and morphological heterogeneity in hereditary elliptocytosis (HE) with spectrin alpha I variant. *Br. J. Haematol.* **85**, 584-595
57. Li, Q., and Fung, L. W.-M. (2009) Structural and dynamic study of the tetramerization region of non-erythroid α -spectrin: a frayed helix revealed by site-directed spin labeling electron paramagnetic resonance. *Biochemistry* **48**, 206-215
58. Li, Z., Jo, J., Jia, J.-M., Lo, S.-C., Whitcomb, D. J., Jiao, S., Cho., K., and Sheng, M. (2010) Caspase-3 activation via mitochondria is required for long-term depression and AMPA receptor internalization. *Cell* **141**, 859-871
59. Long, F., McElheny, D., Jiang, S., Park, S., Caffrey, M. S., and Fung, L.W.M. (2007) Conformational change of erythroid α -spectrin at the tetramerization site upon binding β -spectrin, *Protein Sci.* **16**, 2519-2530
60. Lupas, A., Van Dyke, M., and Stock, J. (1991) Predicting coiled coils from protein sequences. *Science* **252**, 1162-1164
61. Lusitani, D. M., Qtaishat, N., LaBrake, C. C., Yu, R. N., Davis, J., Kelley, M. R., and Fung, L. W.-M. (1994) The first human α -spectrin structural domain begins with serine. *J. Biol. Chem.* **269**, 25955-25958
62. Lusitani, D., Menhart, N., Keiderling, T. A., and Fung, L. W.-M., (1998) Ionic Strength Effect on the Thermal Unfolding of α -Spectrin Peptides. *Biochemistry* **37**, 16546-16554
63. Luthi, A. U., and Martin, S. J. (2007) The CASBAH: a searchable database of caspase substrates. *Cell Death Differ.* **14**, 641-650
64. Lynch, G. and Baudry, M. (1984) The biochemistry of memory: a new and specific hypothesis. *Science* **224**, 1057-1063.
65. MacDonald, R. I., A. Musacchio, *et al.* (1994). Invariant tryptophan at a shielded site

- promotes folding of the conformational unit of spectrin. *Proc Natl Acad Sci U S A* **91**, 1299-1303
66. Machnicka, B., Grochowalska, R., Boguslawska, D. M., Sikorski, A. F. and Lecomte, M. C. (2012) Spectrin-based skeleton as an actor in cell signaling. *Cell. Mol. Life Sci.* **69**, 191-201
 67. Mahrus, S., Trinidad, J. C., Barkan, D. T., Sali, A., Burlingame, A. L., and Wells, J. A. (2008) Global sequencing of proteolytic cleavage sites in apoptosis by specific labeling of protein N termini. *Cell* **134**, 866-876
 68. Martin, S. J., O'Brien, A. G., Nishioka, W. K., McGahon, A. J., Mahboubi, A., Saido, T. C., and Green, D. R. (1995) Proteolysis of fodrin (non-erythroid spectrin) during apoptosis. *J. Biol. Chem.* **270**, 6425-6428
 69. Marx, J. (2001) New leads on the 'how' of Alzheimer's. *Science* **21**, 2192-2194
 70. Meary, F., Metral, S., Ferreira, C., Eladari, D., Colin, Y., Lecomte, M.-C., and Nicolas, G. (2007) A mutant β -spectrin designed to resist calpain and caspase cleavage questions the functional importance of this process *in vivo*. *J. Biol. Chem.* **282**, 14226-14237
 71. Mehboob, S., Jacob, J., May, M., Kotula, L., Thiyagarajan, P., Johnson, M. E. and Fung, L. W.-M. (2003) Structural analysis of the N-terminal region of erythroid and nonerythroid spectrins by small-angle X-ray scattering. *Biochemistry* **42**, 14702-14710
 72. Mehboob, S., Song, Y., Witek, M., Long, F., Santarsiero, B. D, Johnson, M. E., and Fung, L. W.-M. (2010) Crystal structure of the nonerythroid β -spectrin tetramerization site reveals differences between erythroid and nonerythroid spectrin tetramer formation. *J. Biol. Chem.* **285**, 14572-14584
 73. Mehboob, S., B. H. Luo, *et al.* (2001) Alpha beta Spectrin coiled coil association at the tetramerization site. *Biochemistry* **40**, 12457-12464
 74. Moody, M., M. Zipp, *et al.* (2001) Salivary anti-spectrin autoantibodies in Sjögren's syndrome. *Oral Surg Oral Med Oral Pathol Oral Radiol Endod* **91**, 322-327
 75. Moon R. T, and McMahon, A. P. (1990) Generation of diversity in nonerythroid spectrins. *J. Biol. Chem.* **265**, 4427-4433
 76. Musacchio, A., Noble, M., Pauptit, R., Wierenga, R., and Saraste, M. (1992) Crystal structure of Src-homology 3 (SH3) domain. *Nature* **359**, 851-855
 77. Nath, R., Probert, A., Jr., McGinnis, K. M., and Wang, K. K. W. (1998) Evidence for activation of caspase-3-like protease in excitotoxin- and hypoxia/hypoglycemia-injured

- neurons. *J. Neurochem.* **71**, 186-195
78. Newcomb, J. K., Kamfl, A., Posmantur, R. M., Zhao, X., Pike, B. R., Liu, S. J., Clifton, G. L., and Hayes, R. L. (1997) Immunohistochemical study of calpain-mediated breakdown products to alpha-spectrin following controlled cortical impact injury in the rat. *J. Neurotrauma* **14**, 369-383
 79. Nicholson, D. W. (1999) Caspase structure, proteolytic substrates, and function during apoptotic cell death. *Cell Death Differ.* **6**, 1028-1042
 80. Pantazatos, D. P. and R. I. MacDonald (1997) Site-directed mutagenesis of either the highly conserved Trp-22 or the moderately conserved Trp-95 to a large, hydrophobic residue reduces the thermodynamic stability of a spectrin repeating unit. *J. Biol. Chem.* **272**, 21052-21059
 81. Park, S., Caffrey, M. S., Johnson, M. E. & Fung, L. W. (2003) Solution structural studies on human erythrocyte alpha-spectrin tetramerization site. *J. Biol. Chem.* **278**, 21837-44
 82. Park, S., Mehboob, S., Luo, B. H., Hurtuk, M. G., Johnson, M. E., and Fung, L.W. (2001) Molecular Studies of the Erythrocyte Spectrin Tetramerization Region. *Cell Mol Biol Lett.* **6**, 224
 83. Park, S., M. E. Johnson, *et al.* (2002). Nuclear magnetic resonance studies of mutations at the tetramerization region of human alpha spectrin. *Blood* **100**, 283-288
 84. Parry, D. A., T. W. Dixon, *et al.* (1992). Analysis of the three-alpha-helix motif in the spectrin superfamily of proteins. *Biophys J* **61**, 858-867
 85. Pascual, J., Pfuhl, M., Walther D., Saraste, M., and Nilges, M. (1997) Solution structure of the spectrin repeat: a left-handed antiparallel triple-helical coiled-coil. *J. Mol. Biol.* **273**, 740-751
 86. Pelton, J. T. and L. R. McLean (2000) Spectroscopic methods for analysis of protein secondary structure. *Anal Biochem* **277**, 167-176
 87. Pierce, M. M., C. S. Raman, *et al.* (1999). Isothermal titration calorimetry of protein-protein interactions. *Methods* **19**, 213-221
 88. Pike, B. R., Flint, J., Dave, J. R., Lu, X.-C. M., Wang, K. K. K., Tortella, F. C., and Hayes, R. L. (2003) Accumulation of calpain and caspase-3 proteolytic fragments of brain-derived II-spectrin in cerebral spinal fluid after middle cerebral artery occlusion in rats. *J. Cerebral Blood Flow & Metabolism* **24**, 98-106

89. Pike, B. R., Zhao, X., Newcomb, J. K., Glenn, C. C., Anderson D. K., and Hayes, R. L. (2000) Stretch injury causes calpain and caspase-3 activation and necrotic and apoptotic cell death in septo-hippocampal cell cultures. *J. Neurotrauma* **17**, 283-298
90. Pop, C., Chen, Y.-R., Smith, B., Bose, K., Bobay, B., Tripathy, A., Franzen, S., and Clark, C. A. (2001) Removal of the pro-domain does not affect the conformation of the procaspase-3 dimer. *Biochemistry* **40**, 14224-14235
91. Pop, C., and Salvesen, G. S. (2009) Human caspases: activation, specificity, and regulation. *J. Biol. Chem.* **284**, 21777-21781
92. Romero, P., Obradovic, Z., Li, X., Garner, E. C., Brown, C. J., and Dunker, A. K. (2001) Sequence complexity of disordered protein. *Proteins: Struct., Funct., Bioinf.* **42**, 38-48
93. Rotter, B., Kroviarski, Y., Nicolas, G., Dhermy, D., and Lecomte, M.-C. (2004) II-Spectrin is an in vitro target for caspase-2, and its cleavage is regulated by calmodulin binding. *Biochem. J.* **378**, 161-168
94. Royer, C. A. (2006) Probing protein folding and conformational transitions with fluorescence. *Chem Rev* **106**, 1769-1784
95. Schneider, T. D., and Stephens, R. M. (1990) Sequence logos: a new way to display consensus sequences. *Nucleic Acid Res.* **18**, 6097-6100
96. Shammass, S. L., J. M. Rogers, *et al.* (2012) Slow, reversible, coupled folding and binding of the spectrin tetramerization domain. *Biophys J* **103**, 2203-2214
97. Shimizu, K., Phan, T., Mansuy, I. M., and Storm, D. R. (2007) Proteolytic degradation of SCOP in the hippocampus contributes to activation of map kinase and memory. *Cell* **128**, 1219-1229
98. Silva, P. J. (2008) Assessing the reliability of sequence similarities detected through hydrophobic sequence analysis. *Proteins: Struct., Funct., Bioinf.* **70**, 1588-1594
99. Simonovic, M., Zhang, Z., Cianci, C. D., Steitz, T. A., and Morrow, J. S. (2006) Structure of the calmodulin II-spectrin complex provides insight into the regulation of cell plasticity. *J. Biol. Chem.* **281**, 34333-34340
100. Speicher, D. W., G. Davis, *et al.* (1983). Structure of human erythrocyte spectrin. II. The sequence of the alpha-I domain. *J. Biol. Chem.* **258**, 14938-14947
101. Stabach, P. R., I. Simonovic, *et al.* (2009) The structure of the ankyrin-binding site of beta-spectrin reveals how tandem spectrin-repeats generate unique ligand-binding properties. *Blood* **113**, 5377-5384

102. Stennicke, H. R., and Salvesen, G. S. (1999) Caspases: preparation and characterization. *Methods* **17**, 313-319
103. Sordet, O., Rebe, C., Plenchette, S., Zermati, Y., Hermine, O., Vainchenker, W., Garrido, C., Solary, E., and Dubrez-Daloz, L. (2002) Specific involvement of caspases in the differentiation of monocytes into macrophages. *Blood* **100**, 4446-4453
104. Song, J., Tan, H., Shen, H., Mahmood, K., Boyd, S. E., Webb, G. I., Akutsu, T., and Whisstock, J. C. (2010) Cascleave: towards more accurate prediction of caspase substrate cleavage sites. *Bioinformatics* **26**, 752-760
105. Song, Y, Pipalia, N.H., and Fung, L.W.M. (2009) The L49F mutation in alpha erythroid spectrin induces local disorder in the tetramer association region: Fluorescence and molecular dynamics studies of free and bound alpha spectrin. *Protein Sci.* **18**, 1916-1925
106. Stabach, P. R., Simonovic, I., Ranieri, M. A., Aboodi, M. S., Steitz, T. A., Simonovic, M., and Morrow, J. S. (2009) The structure of the ankyrin-binding site of {beta}-spectrin reveals how tandem spectrin-repeats generate unique ligand-binding properties. *Blood* **113**, 5377-5384
107. Sumandea, C. A. and Fung, L. W.-M. (2005) Mutational effects at the tetramerization site of nonerythroid alpha spectrin. *Mol. Brain Res.* **136**, 81-90
108. Susuki K. Rasband MN (2008) Spectrin and ankyrin-based cytoskeletons at polarized domains in myelinated axons. *Experimental Biology & Medicine.* **233**, 394-400
109. Talanian, R. V., Quinlan C., Trautz, S., Hackett, M. C., Mankovich, J. A., Banach, D., Ghayur, T., Brady, K. D., and Wong, W. W. (1997) Substrate specificities of caspase family proteases. *J. Biol. Chem.* **272**, 9677-9682
110. Timmer, J. C., Zhu, W., Pop, C, Regan, T., Snipas, S. J., Eroshkin A. M., Riedl, S. J., and Salvesen, G. S. (2009) Structural and kinetic determinants of protease substrates. *Nat. Struct. Mol. Biol.* **16**, 1101-1109
111. Timmer, J. C., and Salvesen, G. S. (2007) Caspase substrates. *Cell Death Differ* **14**, 66-72
112. Tyler, W. J. (2012) The mechanobiology of brain function. *Nature Reviews* **13**, 867-878
113. Varshavsky, A. (2012) Augmented generation of protein fragments during wakefulness as the molecular casue of sleep: a hypothesis. *Protein Sci.* **21**, 1634-1661
114. Verspurten, J., Gevaert, K., Declercq, W., Vandenabeele, P. (2009) SitePredicting the cleavage of proteinase substrates. *Trends Biochem Sci.* **7**, 319-23

115. Voas, M.G., Lyons, D.A., Naylor, S.G., Arana, N., Rasband, M.N., and Talbot, W.S. (2007) II-Spectrin is essential for assembly of the nodes of Ranvier in myelinated axons. *Curr. Biol.* **17**, 562-568
116. Wallace, A. C., Laskowski, R. A., and Thornton, J. M. (1995) LIGPLOT: a program to generate schematic diagrams of protein-ligand interactions. *Protein Eng.* **8**, 127-134
117. Wang, K. K. W., Posmantur, R., Nath, R., McGinnis, K., Whitton, M., Talanian, R. V., Glantz, S. B., and Morrow, J. S. (1998) Simultaneous degradation of II- and II-spectrin by caspase-3 (CPP32) in apoptotic cells. *J. Biol. Chem.* **273**, 22490-22497
118. Weber, I., Fang, B., and Agniswamy, J. (2008) Caspases: structure-guided design of drugs to control cell death. *Mini-Reviews in Medicinal Chemistry* **8**, 1154-1162
119. Weiss, E. S., and W. A. Baumgartner, W. A. (2011) Molecular and biochemical basis of brain injury following heart surgery - interventions for the future. *Brain Protection in Cardiac Surgery*. By Bonser, R. S., Pagano, D., and Haverich, A. London: Springer, 1-10
120. Westphal, D., Sytnyk, V., Schachner, M., and Leshchyn'ska, I. (2010) Clustering of the neural cell adhesion molecule (NCAM) at the neuronal cell surface induces caspase-8 and -3-dependent changes of the spectrin meshwork required for NCAM-mediated neurite outgrowth. *J. Biol. Chem.* **285**, 42046-42057
121. Williams, S. T., Smith, A. N., Cianci, C. D., Morrow, J. S., and Brown, T. L. (2003) Identification of the primary caspase 3 cleavage site in alpha II-spectrin during apoptosis. *Apoptosis* **8**, 353-361
122. Winkelmann, J. C., J. G. Chang, *et al.* (1990). Full-length sequence of the cDNA for human erythroid beta-spectrin. *J. Biol. Chem.* **265**, 11827-11832
123. Winn, M. D., C. C. Ballard, *et al.* (2011) Overview of the CCP4 suite and current developments. *Acta Crystallogr D Biol Crystallogr* **67**, 235-242
124. Wolan, D. W., Zorn, J. A., Gray, D. C., and Wells, J. A. (2009) Small-molecule activators of a proenzyme. *Science* **326**, 853-858
125. Xu, G., Cirilli, M., Huang, Y., Rich, R. L., Myszkowski, D. G., and Wu, H. (2001) Covalent inhibition revealed by the crystal structure of the caspase-8/p35 complex. *Nature* **410**, 494-497
126. Xu, D., Tsai, C.-J., and Nussinov, R. (1997) Hydrogen bonds and salt bridges across protein-protein interfaces. *Protein Eng.* **9**, 999-1012
127. Xu, K., Zhong, G., and Zhuang, X. (2013) Actin, Spectrin, and Associated Proteins Form

- a Periodic Cytoskeletal Structure in Axons. *Science* **339**, 452-456
128. Yan, X. and Jeromin, A. (2012) Spectrin breakdown products (SBDPs) as potential biomarkers for neurodegenerative diseases. *Curr. Tran. Geriatr. Gerontol. Rep.* **1**, 85-93
 129. Yan, Y., Winograd, E., Viel, A., Cronin T., Harrison, S. C., and Branton, D. (1993) Crystal structure of the repetitive segments of spectrin. *Science* **262**, 2027-2030
 130. Zhang, Z., Lerner, S. F., Liu M. C., Zheng, W., Hayes, R. L., and Wang, K. K. W. (2009) Multiple alpha II-spectrin breakdown products distinguish calpain and caspase dominated necrotic and apoptotic cell death pathways. *Apoptosis* **14**, 1289-1298
 131. Zhang, C., Siman, R., Xu, Y. A., Mills, A. M., Frederick, J. R., and Neumar, R. W. (2002) Comparison of calpain and caspase activities in the adult rat brain after transient forebrain ischemia. *Neurobiol. Dis.* **10**, 289-305

CURRICULUM VITAE

Contact Information:

Phone: 312-355-0566 (Work)

E-mail: mwitek2@uic.edu

Work address: Department of Chemistry
University of Illinois at Chicago
845 W. Taylor St.
Rm 4500 SES (MC 111)
Chicago, IL 60607

Education:

2007 - 2013 Doctor of Philosophy (PhD) in Chemistry (Biophysics and Biochemistry of Proteins) Department of Chemistry, University of Illinois at Chicago

2003 - 2007 Bachelor of Science (BS) in Biochemistry
(Institutional Honors, Cum Laude; Departmental Distinction)
University of Illinois at Chicago

2000 - 2002 School of Pharmacy, Medical University of Silesia, Sosnowiec, Poland

Awards and Fellowships:

2012 Merit Award - University of Illinois at Chicago

2009 - 2011 NIH-T32 Multidisciplinary Oral Science Training Fellowship (MOST)

2008 Bodmer International Travel Award - University of Illinois at Chicago

2007 Dean's list, SMART scholarship - University of Illinois at Chicago

2006 Sarah Madonna Kabbes Scholarship for undergraduate research - University of Illinois at Chicago

2006 Iota Sigma Pi (Honor Society for Women in Chemistry) - Frances Seabright
Award for undergraduate research oral presentation at DePaul University,
Chicago

Academic Achievements and Honors:

2007 - Phi Theta Phi
 2007 - Golden Key International Honor Society
 2007 - American Chemical Society (ACS) Member
 2007 - Member of the Biochemical Society
 2006 - Iota Sigma Pi - National Honor Society for Women in Chemistry
 2006 - Member of the Biophysical Society
 2005 - Chancellor's List
 2003 - Phi Theta Kappa

Funding:

2009 - 2011 Principal Investigator: Luisa DiPietro
 Trainee: Marta A. Witek
 Institution: University of Illinois at Chicago
 Type: 1T32DE018381
 Agency: NIH/NIDCR

Work Experience:

08/2007 - Graduate Research Assistant - PhD Student. Department of Chemistry, University of Illinois at Chicago (Advisor: Leslie W.-M. Fung, Ph.D.)
 Spring 2007 Chemistry tutor for the UIC Honors College
 Fall 2007 - Spring 2008 Teaching assistant, General Chemistry I - CHEM 112
 Fall 2008 - Spring 2009 Teaching assistant, Inorganic Chemistry - CHEM 314
 Spring 2011 Teaching assistant, Biochemistry - CHEM 452
 Summer 2011 Teaching assistant, General Chemistry II - CHEM 114
 Fall 2011 Teaching assistant, Biochemistry - CHEM452
 Fall 2012 Teaching assistant, Chemistry - CHEM101

Publications:

1. Crystal Structure of the Nonerythroid α -Spectrin Tetramerization Site Reveals Differences between Erythroid and Nonerythroid Spectrin Tetramer Formation. Shahila Mehboob, Yuanli Song, Marta Witek, Fei Long, Bernard D. Santarsiero, Michael E. Johnson, and Leslie W.-M. Fung, J. Biol. Chem. 2010, 285: 14572-14584.

The atomic structure of brain α -spectrin N-terminal segment was obtained by X-ray crystallography and molecular dynamic simulation methods, and the functional properties were obtained by isothermal titration calorimetry (ITC).

2. Yeast Two-Hybrid and ITC Studies of Alpha and Beta Spectrin Interaction at the Tetramerization Site. Akin Sevinc, Marta A. Witek, and Leslie W.-M. Fung, Cell. Mol. Biol. Lett. 2011, 16: 452-461.

The effects of single residue mutations on spectrin tetramer formation were studied with ITC methods. The following K_d (nM) values were obtained: 7 (\pm 1) for wild-type α -spectrin, 7 (\pm 1) for V22F, 35 (\pm 4) for V22M; 93 (\pm 28) for V22W, and no detectable binding for V22D. These results complement the findings in yeast 2-hybrid studies of similar mutations, done by another member of the group, and were published in 2011.

Manuscripts in Preparation:

1. Quantitative Studies of Caspase-3 Catalyzed α -Spectrin Break-Down with Electrophoresis and Fluorescence Methods. Marta A. Witek and Leslie W.-M. Fung. Submitted on Jan.28, 2013.

We have followed the cleavage of α -spectrin by caspase-3 in detail with gel electrophoresis and fluorescence methods on model proteins of α -spectrin fragments of five different lengths. Our results show that fragmentations at two sites in the middle of α -spectrin are independent of each other, and exhibit very different caspase-3 catalytic rates. These findings suggest that the spectrin break-down products, SBDP150 and SBDP120, may be involved in different cellular processes.

2. Structural Determinants of Spectrin Proteolysis by Caspase-3. Marta A. Witek and Leslie W.-M. Fung.

I have solved the atomic structure of the spectrin fragment containing caspase-3 recognition site obtained by X-ray crystallography.

Extensive experience in following areas:

Teaching skills:

Student Supervision

Train and supervise nine undergraduate students (Priya Patel, Mary Youkhana, Erika Pino, Esther Ng, Nichelle Simpkins, Kayleigh Tovar, Hina Dalal, Jagravi Thakkar, & Vicky Phan), two graduate students (Pauline Kabre, Bihn Nguyen), and one laboratory technician (Esther Ng). Specifically, teach lab techniques, manage their projects, help with manuscript preparations, and troubleshoot technical problems. Reviewing scientific manuscripts and responding to questions from other lab members concerning troubleshooting in their experimental design and manuscript preparation.

Computer programs:

Origin, Microsoft office, PyMOL, Chimera, X-ray structure building using COOT & refinement using CCP4, structural modeling using SpdViewer, molecular dynamics simulations using Gromacs.

Kinetic Studies:

SDS-PAGE, intrinsic tryptophan fluorescence

Molecular Biology Methods:

DNA manipulation and cloning, restriction dependent and independent cloning, PCR, site-directed mutagenesis, primer design, DNA/protein sequence analysis, and plasmid preparation. Familiar with Topo, Gateway, and In-fusion cloning techniques.

Protein Expression and Purification Techniques:

Protein expression in E. coli cell

Experience with challenging proteins through optimization of protocols and/or construct re-engineering. Experience in the use of protein purification systems such as AKTA Purifier. Column Chromatography (GST/His-tag affinity, SEC, IEX, HPLC, FPLC). Electrophoresis (SDS-PAGE).

Protein-Protein Interaction

Isothermal titration calorimetry

X-ray Protein Crystallography

Screen and optimize crystal growth conditions; collect data, initial model building and structure refinement.

Equipment used:

BioFlo benchtop fermentor for cell growth, PCR cycler, nanodrop spectrophotometer, ELISA/fluorescence plate reader, fluorescence spectrometer, circular dichroism, dynamic light scattering, isothermal titration calorimetry, FPLC-AKTA system.

Invited Talk:

1. ITC studies of alpha and beta brain spectrin interaction reveal the importance of single residues at the tetramerization region, "2012 Chicago Biacore and MicroCal User's Day" GE Healthcare-MicroCal Division; June 13, 2012 at University of Chicago Medical Center.

Oral Presentations:

1. Studies of the tetramerization site of spectrin using chimeric spectrin peptide. Iota Sigma Pi - Annual Undergraduate Research Presentation. April 8, 2006

Poster Presentations:

1. Structural and Kinetics Determinants of Controlled Spectrin Proteolysis by Caspase-3. Witek, M & Fung, L. W.-M. 26th Annual Symposium of the Protein Society in San Diego, CA - August 5-8, 2012.
2. Caspase-3 Action on Alpha II Spectrin. Witek, M & Fung, L. W.-M. 55th Annual Meeting of Biophysical Society in Baltimore, MD - March 5-9, 2011.
3. EPR Spectroscopic and X-Ray Crystallographic Studies of Non-Erythroid alpha-Spectrin Tetramerization Site. L. W.-M. Fung, S. Mehboob, Q. Li, Y. Song, M. Witek, F. Long, B. D. Santarsiero, and M. E. Johnson. 36th Lorne Conference on Protein Structure and Function 2011", Lorne, Victoria, Australia - February 6-10, 2011.
4. EPR Spectroscopic and X-Ray Crystallographic Studies of Non-Erythroid alpha-Spectrin Tetramerization Site. Witek, M. A., Li, Q., Fung, L.W.-M. EPR Workshop 2010: Cutting-Edge Biomedical EPR Methods, Medical College of Wisconsin, Milwaukee -

August 20-21, 2010.

5. Crystal Structure of the N-terminal Region of Brain Spectrin Reveals a Helical Junction Region and a Stable Structural Domain. Witek, M. A., Mehboob, S., Song, Y., Long, F., Santarsiero, B. D., Johnson, M. E., Fung, L.W.-M. 54th Annual Meeting of Biophysical Society in San Francisco, CA - February 20-24, 2010.
6. Crystal Structure of the N-terminal region of Alpha II-Spectrin Tetramerization Region. Mehboob, S., Witek, Marta., Long, F., Santarsiero, B., Johnson, M. E., Fung, L.W.-M. 10th Annual Neuroscience Day, sponsored by Brain Research Foundation, University of Chicago, IL - December 12, 2008.
7. Calorimetric Studies of the Tetramerization Site of Spectrin. Marta Witek and L. W-M. Fung.
European Membrane Skeleton Club and the Committee on Cell Biology, Polish Academy of Sciences - "Membrane Skeleton. Recent Advances and Future Research Directions." Zakopane, Poland - June 16-19, 2008.

Co-Curricular Activities:

- 2006 - Women in Science and Engineering (WISE)
- 2005 - National League of Artists
- 2002 - St. Peter and Paul Ski Team

Community Service Activities:

- Spring 2010 - Biochemistry Representative of the Chemistry Graduate Student Association, University of Illinois at Chicago
- Fall 2008 - 'Bring your daughter to work' day at UIC
- Fall 2005 - Reach Out and Read Program, Volunteer Aide

APPENDIX A

Crystal Structure of the Nonerythroid α -Spectrin Tetramerization Site Reveals Differences between Erythroid and Nonerythroid Spectrin Tetramer Formation.

Shahila Mehboob, Yuanli Song, Marta Witek, Fei Long, Bernard D. Santarsiero, Michael E. Johnson, and Leslie W.-M. Fung. *J. Biol. Chem.* 2010, 285: 14572-14584.

ABSTRACT

We have solved the crystal structure of a segment of non-erythroid α -spectrin (II) consisting of the first 147 residues, including the first structural domain (D1) and the important N-terminal partial domain, which is involved in the formation of functional spectrin tetramer, to a resolution of 2.3 Å. Molecular dynamics simulation of the II segment in explicit solvent shows the conformation to be stable. We find that the structure of this II segment is generally similar to a corresponding erythroid α -spectrin (I) segment, yet with unique differences. Specific features identified in the structures include (i) an irregular and frayed first helix (Helix C'), (ii) a helical conformation in the junction region connecting Helix C' with the first structural domain, (iii) a long A_1B_1 loop, and (iv) specific inter-helix hydrogen bonds/salt bridges that stabilize the first structural domain (D1). When comparing inter-helix interactions in D1, we find more hydrogen bonds and hydrogen bond networks in II than in I, suggesting that the difference in the extent of hydrogen bond networks contributes to structural domain stability, and thus rigidity, in II and flexibility in I. We suggest that the structural features in the region prior to D1 are important for α -spectrin association with β -spectrin. One important common feature is the structural flexibility in the first helix, Helix C', to allow association with the helices in β -spectrin to form spectrin tetramers. Another important feature unique to each is the conformation of the junction region connecting the first lone helix to the triple helical structural domain, with an unstructured conformation in I and a helical conformation in II. We suggest that these differences modulate the association affinity of α -spectrin. Isothermal titration calorimetry measurements of the association of α -spectrin with β -spectrin WT and with an α -spectrin junction region mutant, R37P, support the suggestion. We further suggest that mutations in α -spectrin affecting the Helix C' structural flexibility and/or the junction region conformation will alter the equilibrium between spectrin dimers and tetramers in cells. Mutations leading to reduced levels of functional tetramers in cells will potentially lead to abnormal

neuronal functions.

Spectrin isoforms are proteins associated with the cytoplasmic surface of plasma membranes of most cells. Spectrin associates with other cytoskeletal proteins, such as ankyrin and protein 4.1, to establish and maintain a diverse set of specialized plasma membrane domains (1). Non-erythroid, or brain, spectrin (spectrin II) exhibits high sequence homology with erythroid spectrin (spectrin I), despite their different cellular physiological functions (1). Due to their sequence homology, it is possible in theory to apply most of the molecular information obtained from the well-studied spectrin I (both α I and β I subunits) to the less studied spectrin II (α II and β II), or from one domain to another domain (2). Yet, the two spectrin isoforms exhibit quite different functional properties, such as the ability of (i) the spectrin I network to deform, or the spectrin II network to remain rigid, and (ii) the heterodimers to associate to form functional ($\alpha\beta$)₂ tetramers with much higher affinity in spectrin II than in spectrin I. Tetramer formation in non-erythroid spectrin is essential in the regulatory step for neuritogenesis (3). α II-spectrin has recently been reported to be essential for stabilizing nascent sodium-channel clusters (4), assembling the mature node of Ranvier (4), and regulating endothelial cell-cell contacts (5).

The C-terminus of α I, or α II, and the N-terminus of β I, or β II, associate to form heterodimers ($\alpha\beta$ I, or $\alpha\beta$ II) (6). Two dimers then associate with a pair of interactions at the opposite ends, the N-terminus of α I or α II, and the C-terminus of β I or β II, to form a functional ($\alpha\beta$ I)₂ or ($\alpha\beta$ II)₂ tetramer (1). The N-terminal partial domain region in α II shares over 60% sequence similarity and more than 50% identity with the corresponding region in α I (7, 8), and the C-terminal partial domain region in β II (residues 2010-2087) shares over 80% sequence similarity and over 70% identity with β I (residues 2002-2079). Yet, spectrin II exhibits about 15-fold higher affinity than spectrin I in its association at the tetramerization site (9). In model proteins (spectrin segments) used to study these regions of spectrins, the K_d value is around 10 nM for the spectrin II systems and around 1 M for the spectrin I systems (7, 10, 11). The molecular mechanism for this difference is not clear.

Thus, insight into the association mechanism may provide important clues about the pathophysiology of various neurological disorders (12).

In prior work, we have provided indirect evidence that the conformation of the region connecting the first structural domain and the partial domain region of α -spectrin plays an important role in the interactions between α and β spectrin leading to the formation of spectrin tetramers (7, 11, 13). Specifically, our NMR (14), small angle X-ray scattering (7) and spin label EPR (13) studies of I have shown that the junction region in I is unstructured, and that mutations in Helix C' produce decreased association that correlates with the severity of hereditary spherocytosis (15). More recently, our small angle X-ray scattering (7) and spin label EPR (8) studies of II suggest that the junction region in II is helical, while our spin label EPR studies show that the N-terminal end of Helix C' is frayed (8).

We have now solved the crystal structure of the segment consisting of the first 147 residues of II, including the first triple helical structural domain (D1) and the important N-terminal partial domain that is responsible for association with the C-terminal partial domain of α -spectrin. Using the structure of Helix C', we developed a homology model of the II Helix C' bundled with Helices A' and B' of α -spectrin to form a three helix-bundle (A'B'C') at the tetramerization site, followed by MD simulations. We compare the structures of A'B'C' spectrin I and II and find that the unstructured junction region in I and the helical junction region in II play an important role in the association of Helix C' of α -spectrin with Helices A' and B' of α -spectrin. We show that the analysis of inter-helix interactions in these predicted structures of A'B'C' of spectrin I and II is not productive.

The apparent stiffness or rigidity of spectrin molecules is correlated with its structural domain thermal stability (16). Using the X-ray structural information, together with our previous solution NMR structure of the corresponding N-terminal region of erythrocyte spectrin (14), we examine inter-helix interactions in the D1 of II (X-ray structure) and of I (NMR structure). We

identify more hydrogen bonds and hydrogen bond networks in II than in I, suggesting that they contribute toward the higher domain thermal stability in II than in I. Thus, brain spectrin with higher rigidity indeed shows greater inter-helix interactions in structural domains, at least in D1, compared to those in erythrocyte spectrin, despite the similarity in their primary structures.

EXPERIMENTAL PROCEDURES

Recombinant Proteins. An N-terminal segment of brain II-spectrin consisting of the first 147 residues (II-N1), similar to a well-studied erythroid α -spectrin segment consisting of the first 156 residues (I-N1) (14), was prepared from a similar recombinant protein with 149 residues (7), following standard procedures (8, 13, 17). This segment is predicted to include a partial domain that is responsible for associating with β -spectrin to form tetramers, followed by the first full structural domain of brain α -spectrin (7, 8).

The procedures for preparing L-seleno-methionine (seleno-Met)-labeled II-N1 samples were similar to those used for NMR samples (11) except with methionine-auxotroph and protease-deficient competent cells B834(DE3) (Novagen - EMD Chemicals, Gibbstown, NJ) with our spectrin construct, and cells were grown in the M9 medium with seleno-Met (60 mg/L, ACROS Organics, Thermo Fisher Scientific Inc., USA).

Three other recombinant model proteins -- I-N1, a C-terminal segment of erythroid I consisting of residues 1898-2083 (I-C1), and a non-erythroid II segment consisting of residues 1906-2093 (II-C1) -- were also prepared. The plasmid of II-N1 with R37P mutation was prepared using site-directed mutagenesis methods with mutated primers to prepare the DNA construct and transformed into *E. coli* cells for protein expression and purification. Circular dichroism (CD) spectra at 20 °C for all proteins were obtained using a CD spectrometer (J-810, JASCO, Japan) with a 0.1 cm path length sample cell. Mean residue molar ellipticity values at 222 nm were used to calculate the helical content of the proteins using a value of $-36,000 \text{ deg cm}^2$

dmol⁻¹ for a 100% helical conformation (18). The actual helicity values are probably higher, as we discussed recently (11) in comparing the helicity values from CD and NMR studies.

Crystallization and X-ray Data Collection. II-N1 and the seleno-Met-labeled II-N1 in 10 mM Tris buffer at pH 7.4 were concentrated to 7.5 mg/mL and used for crystallization with hanging-drop vapor-diffusion methods at 20 °C. Each protein solution was mixed with an equal volume of reservoir solution to give a 2 μ L droplet. The reservoir solution contained a mixture of PEG8000 (Hampton Research, Aliso Viejo, CA) and PEG1000 (1:2 molar ratio) for II-N1, or of a PEG 4000 and PEG1000 mixture for seleno-Met labeled II-N1, both with 4% butane-1,4-diol (Hampton Research). Crystals from solutions without butane-1,4-diol diffracted poorly. To reduce radiation damage, all crystals used for diffraction experiments were frozen at 100 K, with 20% (v/v) Paratone-N (Hampton Research) added as a cryo-protectant.

Diffraction intensities for the native II-N1 crystals were collected to a resolution of 1.95 Å on an R-Axis IV++ detector equipped with confocal optics. Cu-K α x-rays were generated using a Rigaku RUH2R rotating-anode generator. Images were collected at a crystal-to-detector distance of 150 mm with an exposure time of 5 min per 0.5° oscillation. Images were processed with XDS (19).

Diffraction intensities for the seleno-Met-labeled II-N1 crystals were collected at the Northeast Collaborative Access Team (NE-CAT) 24-ID beamline at the Advanced Photon Source, Argonne National Laboratory. X-ray data were processed to 3.0 Å resolution using HKL2000 (20).

Structure Solution and Refinement. The crystal structure of the seleno-Met-labeled II-N1 was solved by a single-wavelength anomalous diffraction (SAD) phasing using the automated search routine AUTOSOL from the Python-based Hierarchical Environment for Integrated Xtallography (PHENIX) program suite (21). The crystal structure of II-N1 was solved using the phase information from the crystal of the seleno-Met-labeled II-N1. The phases were applied to the

native data, and extended to 2.3 Å. Refinement of coordinates was then performed using *REFMAC5.5* and *PHENIX.refine*. Ten percent of the total observed unique reflections were randomly selected and used as a test set to calculate the free R value. The model was manually built using the program COOT (22) and validated using MolProbity (23). The coordinates and structure factors for the final model have been deposited with the protein data bank (PDB) with accession code: 3F31.

Structural Analysis. The secondary structural elements (24), protein-protein interface areas and molecular interactions were analyzed with PDBsum (25). For molecular interactions, PDBsum identifies non-bonded contacts (NBC), and within NBC, specific interactions were identified as hydrogen bonds using strict geometric criteria (26, 27). In addition, salt bridges (28) were identified separately.

Since PDBsum identifies protein-protein interactions as chain-chain interactions, we labeled each helix in our structure as a chain, including half of the loops connecting to the adjacent helices, in each PDB file to give inter-helical interactions. From these inter-helical interactions, we examined clusters of atoms involved in NBC, which consist of hydrogen bonds, and salt-bridges. We also identified hydrophobic clusters from the NBC atom pairs, considering F, I, L, M, V, W and Y residues as hydrophobic cluster members (29).

Protein Thermal Stability. Protein samples (10-15 M) of II-N1, seleno-Met labeled II-N1 and I-N1 in 5 mM phosphate buffer with 150 mM NaCl at pH 7.4 were used for thermal stability studies. CD signal intensities at 222 nm of a sample were monitored as a function of temperature with a thermostated cell, from 20 to 100 °C at an interval of 1 °C. Fractions of thermal unfolding as a function of temperature were obtained from curve fitting of mean residue molar ellipticity values as before (30) to give T_m and G values for each unfolding.

Molecular Dynamics (MD) Simulation. GROMACS (v.4.01) (31) with the 43A1 version of GROMOS

force field (32) was used for MD simulations of solvated protein molecules. We compared different force fields for MD simulations of spectrin system and found similar results (17). The particle mesh Ewald (PME) method (33) was used for long-range electrostatic interactions. Simulations were set up by solvating the protein molecule with water ("simple point charge" or SPC), followed by a 5000-step energy minimization with steepest descent minimization method and 100 ps simulations with position restraint on proteins before simulation for 10 ns. Coordinates and velocities were saved every 2 ps. The time step for integration was 2 fs. Simulation trajectories/structures were analyzed using tools from the GROMACS package. RMSF values are the average values of root mean square fluctuation of C α in each residue of the last 1,000 structures (the last 2 ns of the 10 ns simulation). The GROMACS "dominant structure", defined as the most representative structure with the smallest root mean square deviation (RMSD) values, from the last 2 ns (amongst the last 1,000 snapshot structures), was used as the "MD structure".

We note that, when PME mode was not used, the structures fell apart after 2 ns simulation, indicating the importance of appropriate electrostatic simulation parameters to give stable and reliable structures.

Structural images were produced using PyMOL (DeLano Scientific LLC, Palo Alto, CA). *Isothermal Titration Calorimetry (ITC)*. ITC measurements were performed at 25 °C with an isothermal titration calorimeter (VP ITC, MicroCal, LLC, Northampton, MA). Protein titration pairs (I-N1 and I-C1, I-N1 and II-C1, II-N1 and I-C1, II-N1 and II-C1, and II-N1-R37P and I-C1) were dialyzed together in 5 mM phosphate buffer with 150 mM sodium chloride at pH 7.4 to ensure identical solution conditions of the titration pairs to avoid introducing heat of dilution in the titration experiments. Each α -spectrin protein (about 400 μ M I-N1 or 60 μ M II-N1) was titrated into the sample cell containing one of the β -spectrin proteins (about 40 μ M in I or 6 μ M in II titration). The titration isotherm was analyzed by a single binding site model, provided by

MicroCal software, to obtain an association constant (K_a), which was converted to a dissociation constant (K_d), and the values of ΔH and ΔS of the association.

Homology Modeling.

Triple Helical Bundle A'B'C' Complex. The structure of the spectrin tetramer, (α)₂, at the partial domain association region was modeled by bundling the single α -spectrin partial domain helix (Helix C') with the two helices of the β -spectrin partial domain (Helices A' and B'). We built an A'B'C' complex consisting of Helix C' of α II and Helices A' and B' of β I or β II, using homology modeling methods similar to those used for the β I and β I complex (14, 17). In these models, the sequence of β I at the region predicted to be Helices A' and B' (34) is aligned with that of α -spectrin Helices A₁ and B₁ to determine the boundaries of Helices A' and B'. To assess the sensitivity of models to assumptions about structural details, we used two different templates to model the tetramer association region. The two templates, t I and t II, were used to position Helices A', B' and C' in the complex and to determine the length of each helix. t I is based on the first structural domain of β I, consisting of Helices A₁, B₁ and C₁ of the NMR structure (PDB code: 1OWA) (14). The NMR structure of β I consists of an ensemble of 10 structures. The average value of the C _{α} atom positional RMSD (C _{α} -RMSD) values of these structures is about 2 Å, indicating all structures are similar. The coordinates of the structural domain of structure 1 were arbitrarily selected as t I for homology modeling. t II was based on the crystal structure of the first structural domain of β II from this work. Note that Helix A₁ refers to Helix A in the structural domain 1, and Helix A' to that in the partial domain.

Since the Helix C' structure is now known for both β I and β II, we replaced Helix C₁ with Helix C' of either β I (in β I I complex, for example) or β II (in β II I complex) by overlaying Helix C' over Helix C₁ (e.g., residues 12 - 31 in β II Helix C' is overlaid with residues 117 - 136 of Helix C₁ in template t I), using operations in PyMOL. Helix C' in M1 and M2 (see below) assumes slightly

different structures in the crystal, and we selected the structure of M2 for II Helix C' since this structure, with the bend involving only one residue, is in better agreement with our EPR studies (8).

The lengths of Helices A' and B' of I, or II, in t I and t II vary slightly due to different helix lengths in the first structural domains of I and II. Helix A' is 5 residues longer and Helix B' is 4 residues shorter, both at the C-terminus, in t I than in t II. Details on helical boundaries of the three helices in the models are shown in Table 4. Note: the numbering systems for residues in I and II and in I and II differ, with residue 21 in I corresponding to residue 12 in II. Residue 2044 in I corresponds to residue 2052 in II.

We have previously published two different models of A'B'C' of I I with t I, with Helix C' terminating either at residue 45, as in free Helix C' (14), or at residue 52, as in bound Helix C' (17). In this study, since we use the crystal structure of free (unbound) Helix C' for II, we used the unbound Helix C' in the I I-t I model (14) for MD simulations (see below).

II-Mutations. We introduced a mutation in the model at position 37 of II Helix C', from Arg to Pro, in both the free form and the bound form (MD structure of A'B'C' of II I-t I, see below). We also introduced II mutations at positions 19 (R19C) and 40 (L40C) to the bound Helix C' in A'B'C', since mutations at these positions in recombinant model proteins show abnormal binding affinities (8).

RESULTS

Protein Characterization. The expected mass for II-N1 is 17,662.9 Da, and the experimental mass from the high resolution mass spectrometry is 17,662.2 Da. The expected mass for seleno-Met-labeled II-N1, with all four methionine residues labeled, is 17,850.6 Da, and the experimental mass is 17,850.3 Da. The II mutant R37P mass is 17,604.1 Da, with an expected mass of 17,603.9 Da. The helical content from CD measurements is about 70% for II-N1, 62% for the

seleno-Met-labeled II-N1, 48% for II-N1-R37P and 52% for I-N1. The values for II WT and I-N1 are similar to our published values (34). Dynamic light scattering experiments indicate that II-N1, at 2 mg/mL, is monomeric in solution, with a hydrodynamic radius (R_h) of about 30 Å (11).

Overall Structure of II-N1. X-ray diffraction data (Table 1) show that the asymmetric unit contains two crystallographically independent structures of II-N1, monomers 1 (M1) and 2 (M2). Each monomer consists of a short unstructured segment followed by an unpaired helix with either a bend or short α -turns plus a triple helical bundle (Fig 1). M1 and M2 are antiparallel to each other, with the triple helical bundle of M1 facing that of M2 by a pseudo twofold axis. The interfacial area between the paired monomers is 1,530 Å² for M1 (about 14% of total area 10,747 Å²) and 1,450 Å² for M2 (about 13% of 10,966 Å²).

N-Terminal Partial Domain Helix C'. M1 and M2 assume slightly differing conformations in the first 36 residues. This N-terminal region is critical for the association with the C-terminal partial domain of α -spectrin. In M1, we observe poor electron density for residues 1-10. Residues 11-13 form a turn (following the PDBsum secondary structure terminology) (Table 2). Residues 14-25 and 30-36 are helical segments, connected by a four-residue beta turn. In M2, residues 1-7 also exhibit poor electron density, and residues 8-11 form a turn. The helix starts at residue 12, and has a bend that involves only residue 33. To simplify the discussion when comparing structures with other spectrin isoforms (e.g., with the corresponding region in I-spectrin), we designate residues 14-36 in M1, or 12-36 in M2, as the lone Helix C', which bends at residues 26-29 in M1, or at residue 33 in M2 (Fig 2A; Table 2). A rotation of the N-terminal end of the M1 Helix C' at the bend by about 55° brings it largely into superposition with Helix C' in M2 (Fig 2A). After the bend, M1-Helix C' is very similar to that of M2. Thus, in summary, the conformations of Helix C' in M1 and M2 differ only slightly, with the start of the helix differing by two residues, and slightly differing bends at slightly different locations, but are otherwise quite similar.

The flexibility in Helix C' is also shown by the values of the C α B-factors, with M1 being less ordered than M2 (Fig 3). Helix C' is thus an irregular and frayed helix, capable of conformational mobility, at least going from that in M1 to that in M2. The flexible nature of Helix C' implies that this region may undergo conformational change upon interacting with neighboring molecules/atoms, as in the unit cell of crystals, and potentially with its interactor proteins in cells.

Helical Junction Region. The most interesting feature of our crystal structures is that residues 37-43, downstream of Helix C', are *helical* in both M1 and M2. Based on the secondary structural analysis and the homologous sequence alignment with I, we assign this region to be the junction region. However, there are no clear structural boundaries for this junction region, with the end of Helix C', the junction region and the start of the first helix in the structural domain being a long continuous helical segment. We have previously shown that the corresponding region in α -erythroid spectrin (I residues 46-52) is *unstructured* (14). Our previous hypothesis, that the differences in the association affinity between erythroid and non-erythroid spectrin in forming tetramers can be associated with differences in the junction regions of I and II (7), is thus shown to be correct.

First Structural Domain of II-Spectrin (D1- II). The regions after residue 43 in M1 and M2 superimpose very well, with an average C α -RMSD value of 0.57 Å, indicating essentially identical structures for residues 44-147. We define this region as the first triple helical structural domain of II-spectrin (D1- II), with the three helices being A $_1$ (residues 44-66), B $_1$ (residues 78-111 or 112), which has a bend around residues 94-96, and C $_1$ (residues 117-143 or 146) (Table 2). Helices A $_1$ and B $_1$ are connected by a long, 11-residue A $_1$ B $_1$ loop, while Helices B $_1$ and C $_1$ are connected by a short B $_1$ C $_1$ loop (4-5 residues) (Figs 1 and 2A; Table 2). The most flexible region in the structural domain is the long A $_1$ B $_1$ loop, which exhibits B-factors more than 100 Å² for residues 73-74 (Fig 3).

Thermal Stability and Inter-Helix Interactions. We observe similar thermal unfolding profiles for II-

N1 and seleno-Met- II-N1. The T_m values are 73.1 °C and 74.6 °C, while ΔG (25 °C) values are 9.1 and 8.5 kcal/mol, respectively (Fig 4). The unfolding profile of the corresponding I protein (residues 1-156; I-N1) showed a similar unfolding pattern, except at lower temperatures, with a T_m value of 56.0 °C and a ΔG of 5.3 kcal/mol (Fig 4). The difference in ΔG (ΔG) at 25 °C is 3.8 kcal/mol. Thus, II-N1 is more stable than I-N1 by about 4 kcal/mol, in good agreement with previous results on similar proteins (16, 35).

With an atomic resolution structure of D1- II, interaction analysis of inter-helical interactions shows multiple hydrogen bonds in M1 and M2. These hydrogen bonds satisfy the published, strict geometric criteria (26, 27) (see Experimental Procedures). The details of hydrogen bond atom pairs and their locations in the domain are shown in Fig 5B. These hydrogen bonds spread throughout the interfaces of the three helices to form hydrogen bond networks that stabilize the triple helical structural domain D1- II. No additional salt bridges are evident. Similar interaction analysis of D1- I of four randomly selected NMR structures (PDB code: 1OWA) shows only 1-2 inter-helix hydrogen bonds, and no hydrogen bond networks (Fig 5A). Also, no additional salt bridges were identified by the PDBsum program.

All structures of II and I show 17-19 residues to be involved in inter-helix hydrophobic clusters, with 4-8 of these residues having multiple close-distance partners. These hydrophobic clusters are distributed evenly in the hydrophobic core of the structural domain. In brief, D1- I and D1- II exhibit similar hydrophobic clusters, further suggesting that the higher stability in D1- II than in D1- I is due to specific inter-helix hydrogen bond interactions.

MD Structures of M1 and M2

MD simulations of the explicitly solvated M1/M2 crystal pair or separated monomers generally reach equilibrium after 2-3 ns, as indicated by the RMSD values (Fig 6), with larger RMSD values in monomers of separated M1 and M2 than in the M1/M2 crystal pair. All four (each

monomer in the pair and 2 from the separated monomers) MD structures (defined as the "dominant structures" of the last 2 ns simulations, see Experimental Procedures) are generally similar to each other and to the X-ray structures, with some differences at the N-terminus of Helix C'. The differences between monomers in the crystal structures of Helix C' (starting residue, bend position and bend length) are also found in MD structures. Helix C' starts at residue 11 in separated M2, but at residue 17 in separated M1 (Table 2), further demonstrating its flexibility (Figs 2, 3 and 6). The C RMSF values for residues and the corresponding B-factor values, converted from RMSF values following published methods (36) (Fig 3), show that the N-terminal residues at the frayed end of Helix C' exhibit different conformations, in good agreement with X-ray conformations, further suggesting that this region may undergo conformational exchange.

It is interesting to note that the converted MD B-factor values of the A₁B₁ loop are higher than those from X-ray in M1, but lower for M2, suggesting that the flexibility of this loop in solvated structures is modulated by interactions between this loop in M2 and Helix C' in M1 (Fig 1). We suggest that the long, flexible A₁B₁ loop is a special feature of this particular structural domain (D1-II), discussed further below.

Association Affinity at the Tetramerization Site. Typical ITC results for the titration of I-N1 or II-N1 with I-C1 or II-C1 (Fig 7) show that α -spectrin I and II do not contribute to the observed differences in dimer association to form tetramers; the differences are mostly due to differences in α -spectrin I and II. In fact, sequence alignment shows 54% sequence identity for I-N1 and II-N2 and 70% for I-C1 and II-C1. Our previously published K_d values are about 1 μ M for the association of I-N1 with I-C1 (7, 11, 37), and about 10 nM (8, 11) for II-N1 with I-C1.

To better characterize the thermodynamic contributions to association, we examined the accuracy of the K_d , H and S parameters obtained from ITC experiments. K_d values are obtained from fitting the amounts of heat evolved as various mole fractions of II-N1 are added to I-C1, and

can be obtained relatively accurately. ΔH can also be obtained relatively accurately in well designed experiments such that, at the start of the titration, most all of the titrating protein (proteins in our case) forms a complex with its partner (proteins), giving a relatively flat plateau (for example, see ΔH isotherm in Fig 7). With the heat determined from the initial titration and an accurate determination of protein concentration, an accurate value (kcal/mol) for ΔH can be obtained. The K_d and ΔH values are obtained directly from regression of the ITC data. However, the ΔS accuracy may be lower, since ΔS is a secondary parameter calculated from K_d and ΔH , and includes the uncertainties of both. Consequently, the ΔG values obtained from summing the experimental values of ΔH and $-T \Delta S$ (ΔG -sum) are not necessarily equal to the value calculated directly from K_d values (ΔG - K_d). As a consistency check, we examined 64 ITC data sets, and found that the ratios of the ΔG -sum/ ΔG - K_d can range from 0.6 to 1.4, although most are close to 1.0. Thus, we include only the results from experiments where the ΔG -sum/ ΔG - K_d ratios were within a range of 1.0 ± 0.05 , thus providing the most reliable ΔS values from ITC results.

For the I-N1 and I-C1 system at 298.15 K, the average value ($n = 4$) for K_d is ~ 900 nM, ΔH is -27.7 kcal/mol and $T \Delta S$ is -19.4 kcal/mol. For the II-N1 and I-C1 system, the average value for K_d is 8.5 nM, ΔH is -37.9 kcal/mol and $T \Delta S$ is -26.9 kcal/mol (Table 3). For II-N1-R37P the K_d is $\sim 11,000$ nM, with a ΔH of -16 kcal/mol and a $T \Delta S$ of -9.4 kcal/mol. Most of our K_d values generally agree with surface plasmon resonance studies of similar I, II, I and II model systems (10), although the ΔH and ΔS values for II II differ significantly for reasons that are unclear (with theirs being -58 kcal/mol and -48 kcal/mol, respectively (10)).

Model Structures of the A'B'C' Complex of II. We find that the MD structures of Helices A' and B' of either I, or II, complexed with Helix C' of II (A'B'C' complex) from either template (t I or t II) generally appear the same. The three helices remain a stable triple helical bundle after MD

simulations reach equilibrium. The most interesting structural feature of the A'B'C' complex is that the bend in the free Helix C' around residue 33 (Fig 8 A and B) straightens to give a more regular Helix C' in the complex (Fig 8 C and D). The conformational change in Helix C' upon binding Helices A' and B' to form the A'B'C' complex provides an inter-helix hydrophobic cluster at the C-terminal end, downstream from the bend, that involves II-L40 and V2044/2052-L2047/2055-I2048/2056 (with the first number for I and *the second italic number for II*) (Fig 8E). Note: hydrophobic residue clusters were identified from the NBC list in PDBsum (see Experimental Procedures). We also identify an N-terminal hydrophobic cluster that involves three residues in Helix C' (I15-V22-L23) (Fig 8 F and G), two residues in Helix A' (V2011/2019 and F2014/2022) (Fig 8F) and one residue in Helix B' (F2065/2073) (Fig 8G).

In addition to hydrophobic clusters near residue 33, there are five charged residues downstream of residue 33 (R36, R37, K39, E41 and D42) and seven charged residues at the N-terminal end of Helix B' (E2045/2053, K2046/2054, K2049/2057, R2050/2058, E2052/2060, E2055/2063 and K2056/2064). These charged side-chains might also be responsible for bringing the C-terminal end of Helix C' (such as R37 at the "e" position in the heptad) closer to the N-terminal end of Helix B' (such as E2052/2060 at the "b" position and E2055/2063 at "e" position) close together (Fig 8H).

In principle, the analysis of inter-helix hydrogen bonds in the A'B'C' complex will allow us to examine the stability of this complex, as we show above for D1 in I and II. However, the predicted (MD) structures of the complex lack the structural precision that would allow critical analysis of hydrogen bonds and their networks to predict stability with energy differences of only a few kcal/mol, in contrast to the analysis of either the X-ray or NMR structures. The numbers of inter-helix hydrogen bonds obtained from the analysis of A'B'C' structures of t I and of t II are quite different (data not shown). Thus, inter-helix interaction analysis of the complex awaits

determination of its atomic resolution structure. However, we believe that the MD structures provide good prediction of the conformation for Helix C' bound in the complex, and identify potential hydrophobic clusters, which are not distance dependent, though the van der Waals interactions of the atoms involved are distance dependent.

We have previously shown, with yeast-two-hybrid methods, that the mutant R37P in α II has an impaired ability to form tetramers with α II (38). A proline residue mutation is, of course, likely to disrupt the helical conformation that we observed in the α II WT junction region. Thus, we prepared an α II-N1-R37P model protein. The CD measurements show that the helical content value is 48% for R37P, a value not only lower than that of α II-N1, but also lower than that of α I-N1. The ITC results show a K_d value of about 10^{-6} M (Fig 7 and Table 3), a value much higher than that for WT, and even an order of magnitude higher than that for α I. The ΔH value is -16.2 kcal/mol and $\Delta T \Delta S$ is -9.4 kcal/mol. For α II-N1 association with α 1-C1, the ΔG is 4.2 kcal/mol between the WT and R37P systems.

Model Structure of Free R37P. With a helical conformation around R37P as the starting conformation (from homology modeling) (Fig 9A), the MD structure shows that 8 residues around residue 37 (residues 32-39) become unstructured (3 α -turns) (Fig 9B), consistent with the CD results. We also note that, for comparison, the unstructured junction region in α I (residues 46-52) remains unstructured after MD simulation (structure not shown). As a consequence of the conformational change, we identify only 2 intra-helix hydrogen bonds between residues 30-43 of Helix C' in R37P, as compared to 9 in WT and 4 in α I for the corresponding region (residues 39-52). Thus, these three α -spectrin models exhibit very different conformations at the C-terminal end of Helix C' and the junction region, which are likely responsible, at least in part, for the differences in the affinity (ITC) results reported above.

Model Structure of the A'B'C' Complex of R37P. When residue R37 in the A'B'C' homology model

is changed to P37, the neighboring residues (34-42), that are helical in the homology model, again become unstructured after MD simulation (Fig 9C). In contrast to an unstructured to helical conformational change upon binding α -spectrin in the junction region in I, the unstructured region (residues 32-39) in the free form (Fig 9B) remains unstructured. Furthermore, it lengthens (residues 32-43). Thus, despite the presence of potential inter-helix interactions provided by Helices A' and B' with residues in Helix C', the mutation causes this region in the complex to unwind.

Model Structure of the A'B'C' Complex of R19C and of L40C. We introduced two other mutations (R19C and L40C) to our A'B'C' complex model, since the association affinities of these two mutants with α -spectrin are lower than that for the WT (8). The A'B'C' model of the WT discussed above provides us with a possible mechanism for the effect of this mutation on the affinity. The MD structure of II I A'B'C' with the R19C mutation in Helix C' shows that the general conformations of Helices C' and A' both remain similar to those of the WT. However, Helix B' is considerably shortened, with the last residue reduced from T2072 to R2064, probably due to the inability of residue 19C to interact with the E2069 residue downstream of the helix, as in the R19 - E2069 WT interaction (Figs 8I and 10A). In the WT, this ion-pair keeps the C-terminal end of Helix B' close to the N-terminal ends of Helices A' and C', forming a stable triple helical bundle, whereas the C-terminal end of Helix B' in A'B'C' of R19C moves away from the N-termini of Helices A' and C' (Fig 10B).

For L40C, the general conformation of Helix C' remains similar to that of the WT. However, Helix B' exhibits a kink around residues K2049-H2051. Residues V2044, L2047 and I2048 are still able to form a hydrophobic residue cluster. However, this hydrophobic residue cluster has one less member (L40) than that in the WT (L40-V2044-L2047-I2048) (Figs 8E and 10D). Again, the A'B'C' model of the WT provides us a possible mechanism for the effect of this mutation on the affinity.

DISCUSSION

The perception that we largely understand spectrin structure-function relationship once the structural domains (often referred to as spectrin repeats) are found to be triple helical bundles far oversimplifies the details and may lead to inaccurate conclusions. The canonical triple helical bundle conformation does not reveal specific functions associated with either different domains, or different isoforms. We suggest that many α - and β -spectrin structural domains include unique structural features, such as the BC loop region of domain 15 of β -spectrin, which is a unique ankyrin binding site (39), and the different conformations in the junction regions of N-terminal α - and β -spectrin which affect tetramerization affinity (8, 13).

The atomic structures of 12 different spectrin domains have been published. These domains include D14 of *Drosophila* spectrin (40; PDB code: 2SPC), human erythroid α -D1 (14; 1OWA), α -D8-D9 (41; 1S35) and α -D14-D15 (42; 3EDU and 43; 3F57), non-erythroid β -D14-D16 (39; 3EDV), and chicken brain β -D15-D17 (44; 1U5P & 1U4Q, 2; 1CUN and 45; 1AJ3). The structures of four different spectrin domains have already been compared, and the results show extensive variation: helices are straight, curved, or bent; the lengths of the helices vary from 21 to 31 residues; and the length of the loops between helices also differs (46). The findings of structural domain variation are valid for all 12 published structures, as well as for the structure from the current study. The unique structural features in each domain may lead to different contributions to the overall functional properties of spectrin, such as spectrin's rigidity/flexibility in the cytoskeletal network of different cells.

The important specific features identified in the N-terminus of β -spectrin in this study include (i) the irregular Helix C' with a variable, flexible bending region, (ii) the helical conformation in the junction region connecting Helix C' with the first structural domain, (iii) the long A_1B_1 loop, and (iv) specific inter-helix hydrogen bonds/salt bridges that stabilize structural domain 1. We discuss

each of these features in detail below.

Irregular Helix C'

The irregular or frayed Helix C' with a bend seen in the X-ray structures is in good agreement with the heptad sequence analysis of this region, as well as with the solution structure by spin label EPR studies (8). The sequence of this region shows one heptad residue deletion after residue 30, with K30 at "e" and E31 at "g". This one-residue deletion in the heptad pattern in the sequence corresponds to two successive stammers in coiled coil helices (47), and is able to tighten up a coiled coil and shorten the local pitch length (48). The existence of a stammer is usually responsible for local flexibility of the helix (47). These structural features may enhance the interfacial interactions when associating with its binding partner (48) or may disrupt the interactions, and lead to diseases, such as an in-frame deletion in the desmin gene that leads to skeletal or cardioskeletal myopathy (49). Unwound, bent or broken helices have been shown to be important components in understanding variations in protein-protein interactions (50). Thus, Helix C', as an irregular and frayed helix, is capable of conformational mobility upon interacting with α -spectrin and/or an interactor protein in cells. It is possible that proteins other than α -spectrin may exhibit specific interaction with this irregular Helix C' to modulate/regulate the tight association between Helix C' of α -II and Helices A' and B' of β -II during specific cellular events. We have identified several proteins that interact with α -II, but do not interact with an α -II Helix C' mutant V22D, which also does not interact with α -spectrin (51). Thus, these proteins may interact specifically with the flexible Helix C' to modulate the affinity of α -spectrin in its association with α -spectrin in this region.

It is interesting to note that Helix C' becomes more regular in the model structure of the complex. We included the bend feature into the initial structure (homology model) of the complex, and yet Helix C' is observed without a significant bend in the structure resulting from MD simulation.

Helical Junction Region

We previously inferred a helical conformation for the junction region of α II from our low resolution small angle X-ray scattering (7) and spin label EPR (8) structural studies, and have now confirmed its existence in this study. Since we have shown that the corresponding junction region in α I-spectrin is unstructured in the absence of its α -spectrin binding partner (7, 14), but is helical in the presence of α -spectrin (11, 13), we now suggest that this helical junction plays an important role in the "on-rate" of the association. Indeed it has been shown that, in studies with α I and α II model systems slightly different from ours, the on rate for α I is slower than that for α II (10). We have shown that when the junction region in α I spectrin is not able to undergo the unstructured to helical conformational change upon binding α -spectrin, as in the α I L49F mutant, the association affinity with α -spectrin is low (17).

Long A₁B₁ Loop

The D1- α II structure includes a long A₁B₁ loop, with 11 residues, whereas the corresponding loop in D1- α I consists of 6 residues (14). The other 11 known spectrin domain loops consist of 7-10 residues (we used PDBsum to analyze the published structures for this information), with an average of 8 residues. We speculate that this long loop may provide binding sites for other, non-spectrin, proteins to recognize this specific site for interaction. The sequence of this loop is ASDENYKDPTN (residues 67-77), a combination of residues, many of which are polar, with differing side-chain properties, well suited for specific molecular recognition/interaction.

Specific Inter-Helix Hydrogen Bonds/Salt Bridges

Generally speaking, hydrogen bonds (27, 28) and salt-bridges stabilize protein structures (28). To use atom pairs for determining interactions quantitatively, salt bridges are two atoms of opposite charge within 4 Å but that do not qualify as hydrogen bonded (52). An increased temperature of stabilization is related to a structure with an increased number of hydrogen bonds/salt bridges and/or a better hydrophobic internal packing. Recently, it has been shown that

the replacement of a single amino acid residue that affects hydrogen bonds as well as other steric strains could affect the T_m by up to 16 °C and ΔG by 4-5 kcal/mol (52, 53). Similarly, a specific interaction between two helices in partial domain association may lead to differences in K_d values by two orders of magnitude, which corresponds to a ΔG value of 2-3 kcal/mole. Thus, it is clear that a single specific hydrogen bond or salt bridge is able to increase stability of specific domains in spectrin by 10-20 °C in T_m values. Various spectrin segments have been reported to have different T_m values (16, 35). Examination of specific interactions for both D1- I and D1- II shows more specific hydrogen bonds in D1- II than D1- I, but with similar hydrophobic internal packing and provides an atomic level of understanding of the different stabilities in these two structural domains.

Predicting Spectrin Tetramer Structure at the Association Region

In the absence of either NMR or X-ray structures of the A'B'C' complex structure in the spectrin tetramer, a general structure of the helical bundle A'B'C' is relatively simple to predict, due to heptad repeats in sequences of the three helices involved in spectrin tetramer formation, with the residues at the "a" and "d" positions of each helix facing each other to form a hydrophobic core of the bundle (17). Further, since the sequences of the partial domain Helices A', B' and C' are homologous to those in structural domains, it is reasonable to select a known spectrin structural domain structure as a template to model the structure of A'B'C'. This approach has been validated for helical membrane protein systems, due to the reduced degrees of freedom that a protein can adopt in a lipid bilayer (54), and our coiled coil helix system also has reduced degrees of freedom due to hydrophobic residues at heptad "a" and "d" positions forming hydrophobic clusters.

The structures from MD simulations of the homology models of the complex of II I, and of II II, show inter-helix hydrophobic clusters at both the N-terminal end and the C-terminal end of the helical bundle. Similar hydrophobic clusters are also found in the I I model structure (17).

Thus, hydrophobic clustering does not appear to be responsible for the differing association affinities of α I I and α II II, though mutations eliminating members of the cluster (e.g., L49C in α I and L40C in α II) do lead to reduced association affinities (8, 13).

The conformation of the junction region of α -spectrin, a region connecting the partial domain that is responsible for the association with the first structural domain, differs uniquely among three complexes studied (α II-WT/ α I, α II-R37P/ α I, and α I/ α I), ranging from a regular helical structure to completely unstructured. We showed that both in the free form and in the bound form, the C-terminal region of Helix C' and the junction region exhibit different degrees of helicity in α II, α II-R37P and α I. The junction region of α II is already in a helical conformation in the free form (with 9 intra-helix hydrogen bonds around the junction region), while that of α I is unstructured in the free form (with 4 intra-helix hydrogen bonds), but becomes helical in the bound form, whereas the region in α II-R37P is unstructured (with 2 intra-helix hydrogen bonds) in the free form and remains unstructured in the bound form. Thus, we suggest that the conformational entropy changes of the junction region play an important role in the differences observed between α -erythroid (α I) and non-erythroid (α II) spectrin association affinity of tetramer formation. We suggest that the helical conformation in the junction region controls the "on-rate" of the association. Indeed it has been shown that, in slightly different α I I and α II I model system studies, the on rate for α I is much slower than that for α II (10).

Strictly speaking, conformational entropy is the entropy associated with motions of the ligand and/or the protein, and the binding free energy includes a loss in conformational entropy due to the decrease in freedom of the ligand and the protein upon binding (55). Changes in conformational entropy on binding are often large, cancel much of the energy change that drives binding, and must be accounted for to obtain good correlations with measured affinities (56). In protein systems, the conformational entropy is introduced by local fluctuations in the neighborhood

of a well-defined structure as well as from the larger scale conformational variations that occur in less well defined structures (55). The complex conformational state is determined by its associated free energy, and a binding event shifts the population of the unbound conformational state to a bound conformational state (57). The change at the binding site is determined dynamically via residue-residue interactions to release the created strain energy if there is a conformational change at an allosteric site. Since ITC measurements, in principle, provide information on entropy change of spectrin association, we examined the ΔH and ΔS values of the association. We selected only the measurements that should provide the most reliable thermodynamic information for the association, and found that the entropy change in α II- α II association (with $T \Delta S$ about -27 kcal/mol) is indeed more favorable than that of α I- α I (-19 kcal/mol). However, the ΔH term in α II- α II (-38 kcal/mol) is also more favorable than that of α I- α I (-28 kcal/mol). Furthermore, it is impossible to separate the conformational entropy change from the solvation entropy change in the ΔS values obtained from ITC. Thus, at this time, we are not able to experimentally demonstrate the extent of conformational entropy change in spectrin association. However, our experimental data are consistent with the importance of a conformational entropy contribution to the association.

In the absence of structural differences in the junction region, mutations R19C and L40C in α II (8) or mutations R28C and L49C in α I (13) exhibit differing affinities due to small variations in local conformation, with similar effects in tetramers of either α I or α II. Other mutations that exhibit abnormal affinity and perturb local interactions, rather than the conformation in the junction region, have been reported for α I-R45S and R45T (15).

In conclusion, the canonical triple helical bundle conformation of structural domains in spectrin isoforms does not reveal specific functions associated with either different domains, or different isoforms. The unique structural features in each domain, and even each partial domain, lead to different contributions toward the overall functional properties of spectrin, such as spectrin's

rigidity/flexibility and the ability of dimers to associate to form tetramers, in the cytoskeletal network of different cells. In this study, we find that the N-terminal regions of α I and α II are generally similar, but with each exhibiting specific unique features. One important common feature is the structural flexibility in the first helix, Helix C', to allow association with the helices in β -spectrin to form spectrin tetramers. An important feature unique to each is the conformation of the junction region connecting the first lone helix to the triple helical structural domain, with an unstructured conformation in α I and a helical conformation in α II. These differences modulate the association affinity of α spectrin. α II α II tetramer formation is essential in the regulatory step for neuritogenesis (3). α II is essential for stabilizing nascent sodium-channel clusters (4), assembling the mature node of Ranvier (4), and regulating endothelial cell-cell contacts (5). Mutations affecting the Helix C' structural flexibility and the junction region conformation in α spectrin, as well as inter-helix electrostatic interactions, will alter the equilibrium between spectrin dimers and spectrin tetramers. Consequently, mutations in this region will lead to substantially reduced levels of functional tetramers in cells, and potentially abnormal functions of neurons, as similar mutations in erythroid spectrin lead to hematological disorders.

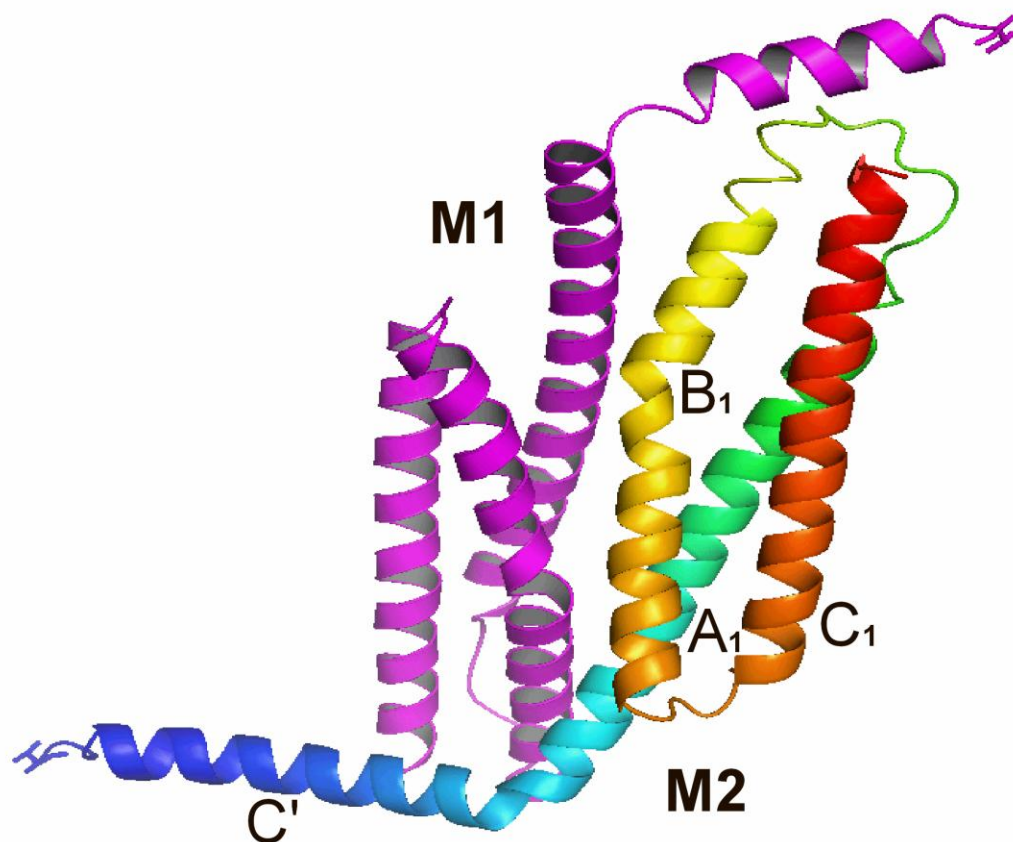


Figure 1. Crystal structure of α II-N1, the first 147 residues of α II-spectrin, at 2.3 Å resolution. Two monomers are observed in the asymmetric unit. The ribbon structure of Monomer 1 (M1) is shown in magenta and of Monomer 2 (M2) is shown in a spectrum of colors. The side chain of the first residue to mark the N-terminus is shown in each monomer. The first helix is marked as C', followed by helices of the (first) structural domain as A₁, B₁ and C₁. Structural images are produced with PyMOL.

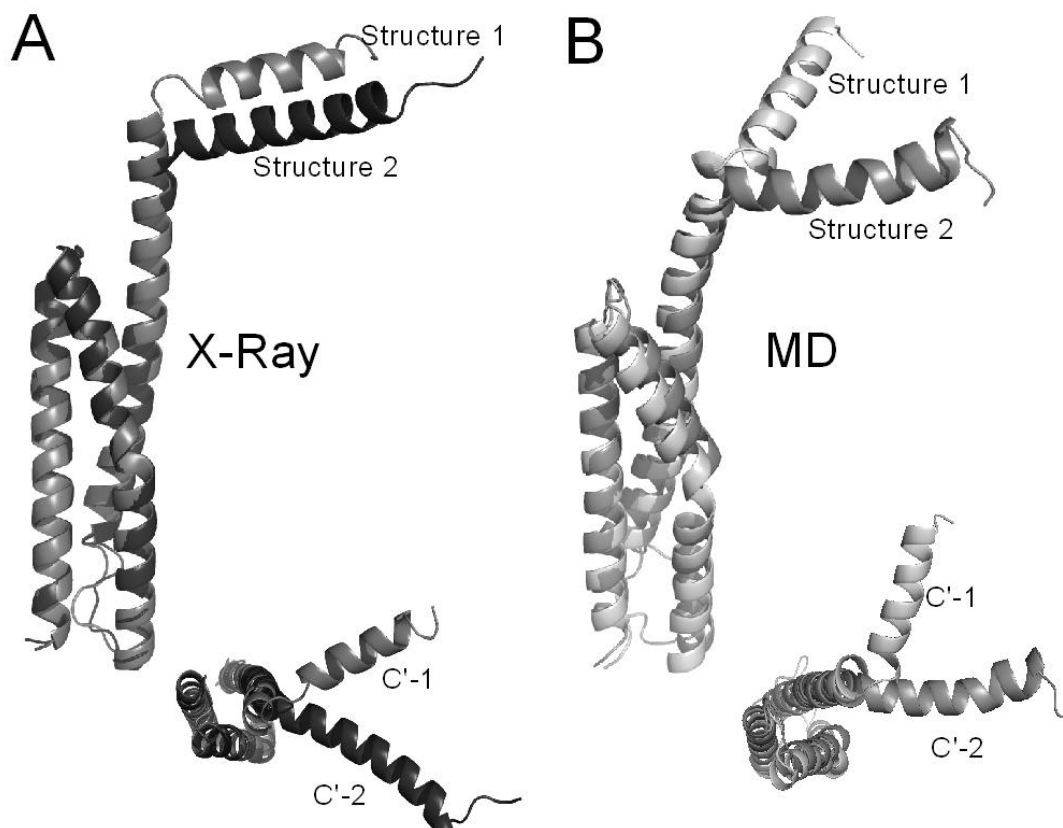


Figure 2. The superposition of structures from X-ray and MD simulation. Overlay of M1 (dark gray) with M2 (black) from the X-ray structure (**A**). The region after residue 43 in the two structures superimposes very well, with an average C_{α} -RMSD value of 0.57 Å, indicating that these regions in the two structures are essentially identical. A shift in the angle by about 54° of the first parts of Helix C' with respect to the triple helical bundle domain is clearly seen at the bottom of (**A**). Structural similarities and differences of M1 and M2 persist after MD simulations, as shown with the dominant MD structures of the last 2 ns (see Methods section for definition), with M1 in light gray and M2 in gray (**B**). The shift in Helix C' with respect to the triple helical bundle domain remains similar, as shown at the bottom of (**B**).

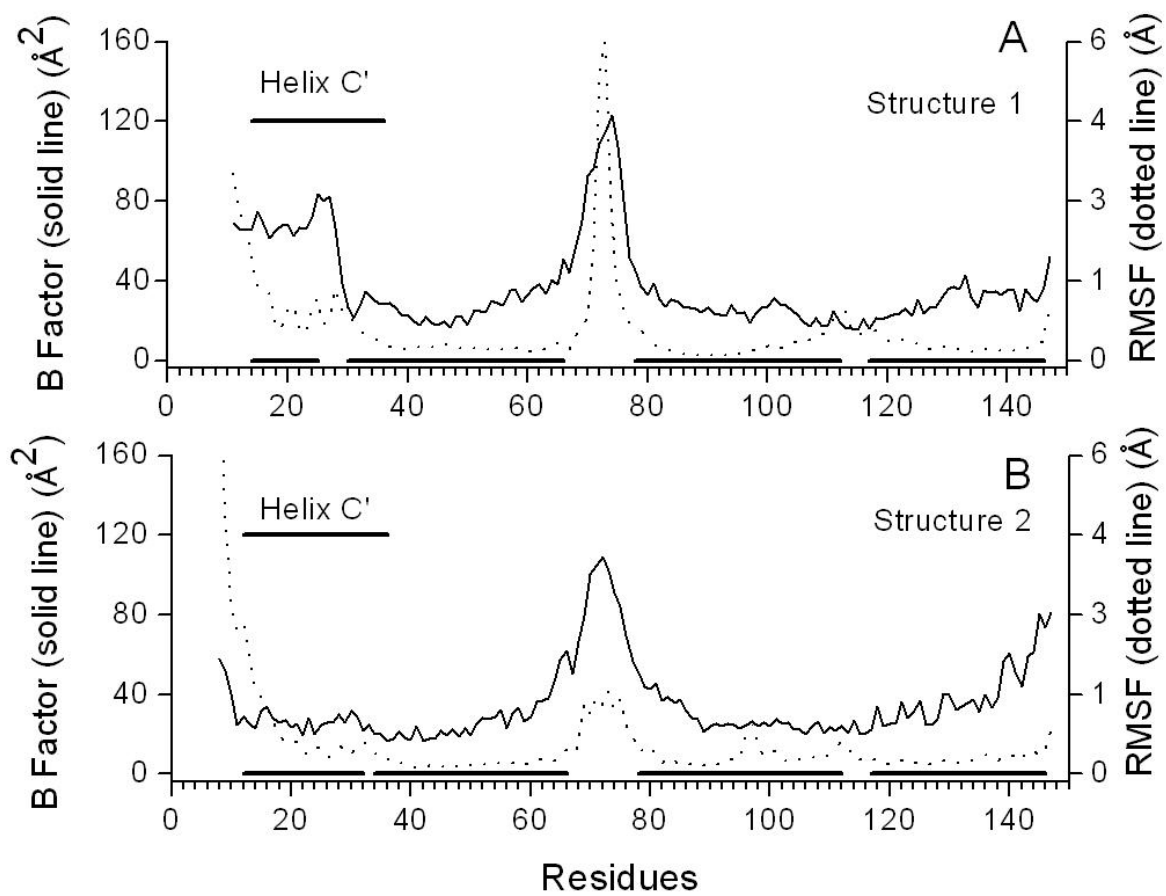


Figure 3. The B-factors of M1 (**A**, solid line) and M2 (**B**, solid line) are generally similar, except for some variation at the N-termini, with values for Helix C' in M1 (residues 14-36) higher than those in M2 (residues 12-36). The helical regions (marked by solid horizontal bars above the x-axis) generally show relatively low B-factor values ($< 30 \text{ \AA}^2$), indicating relatively minor disorder in these parts of the molecule. The values for residues 14-28 in Helix C' of M1 are above 50 \AA^2 , indicating a large disorder for this particular section of the molecule. The RMSF values for residues from MD simulations of the M1/M2 pair are also shown, with the scale on the right x-axis. The values were also converted to B-factor values for comparison, (left z-axis), following published methods (Li and Daggett, 1995). The converted B-factor values of the A₁B₁ loop are higher than those from X-ray for M1 but lower for M2, suggesting that the flexibility of this loop in solvated structures is modulated by interactions between this loop in M2 and Helix C' in M1.

Table 2

Secondary structure analysis of α II-N1 (residues 1–147), with helical regions boldface

See “Experimental Procedures” for definitions of secondary structural elements. M is monomer.

	α II-N1						α I-N1 ^a
	X-Ray		MD Simulations				EPR ^b
	M1	M 2	M1		M2		
			Paired ^c	Alone ^d	Paired	Alone	
Not seen/studied	1-10	1-7	1-10		1-7		1-8
Unstructured	11-13	8-11	11-12	11-16	8-14	8-10	9-10
Helix C'	14-36	12-36	13-36	17-36	15-36^e	11-36	11-36
Helix C' bend	26-29	33	29-33	27-29	33	31-33	33
Helical junction	37-43				37-43^f		37-43
Unstructured junction							46-52
Helix A₁	44-66		44-68	44-69	44-68	44-69	44-47^g
A ₁ B ₁ loop	67-77		69-77	70-77	69-77	70-77	82-87
Helix B₁	78-112	78-111	78-111		78-112		88-118
Helix B ₁ bend	94-96		94-95		94-96		
B ₁ C ₁ loop	113-116	112-116	113-116	112-116	113-116	113-118	119-122
Helix C₁	117-146	117-143	117-145		117-145	119-145	123-153
Unstructured	147	144-147	146-147		146-147		154-156

^a The solution structure of α I-N1 (PDB code IOWA) from NMR studies (14). Data are shown for comparison.

^b Results from EPR studies of α II-N3 (residues 1–359, scanning residues 9–47) (8). Data are shown for comparison.

^c Average structure of the last 2 ns of MD simulations of paired M1/M2.

^d Average structure of the last 2 ns of MD simulations of monomers 1 or 2 alone.

^e With a break at residue 19 for helical region with residues 15–18 and 20–32.

^f With a break at residue 40 for helical region with residues 34–39 and 41–43.

^g Studies do not include residues beyond residue 47.

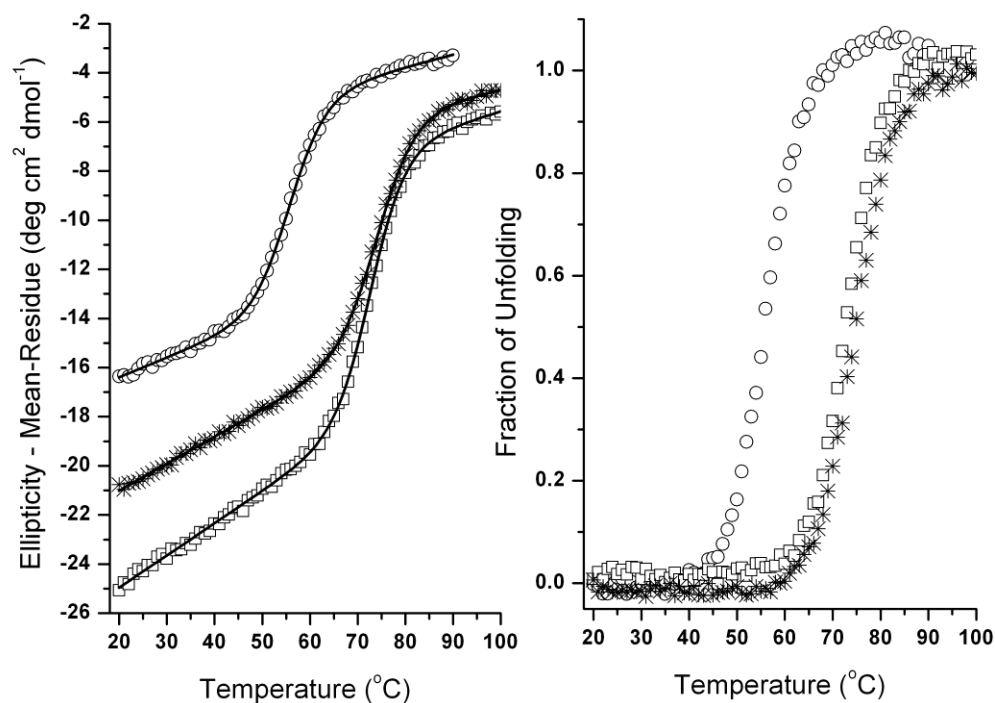


Figure 4. Fractions of thermal unfolding as a function of temperature (right panel) and values of T_m and ΔG for samples (\circ for α I-N1, \square for α II-N1, and $*$ for seleno-Met-labeled α II-N1) in PBS7.4 (~ 10 - 15μ M) were obtained from curve fitting of mean residue ellipticity values, calculated from CD signals at 222 nm, at different temperatures (left panel). The T_m values are 56.0 °C for α I-N1, 73.1 °C for α II-N1 and 74.6 °C for seleno-Met-labeled α II-N1, and the ΔG at 25 °C vales are 5.3 kcal/mol for α I-N1, 9.1 for α II-N1 and 8.5 kcal/mol for seleno-Met labeled α II-N1.

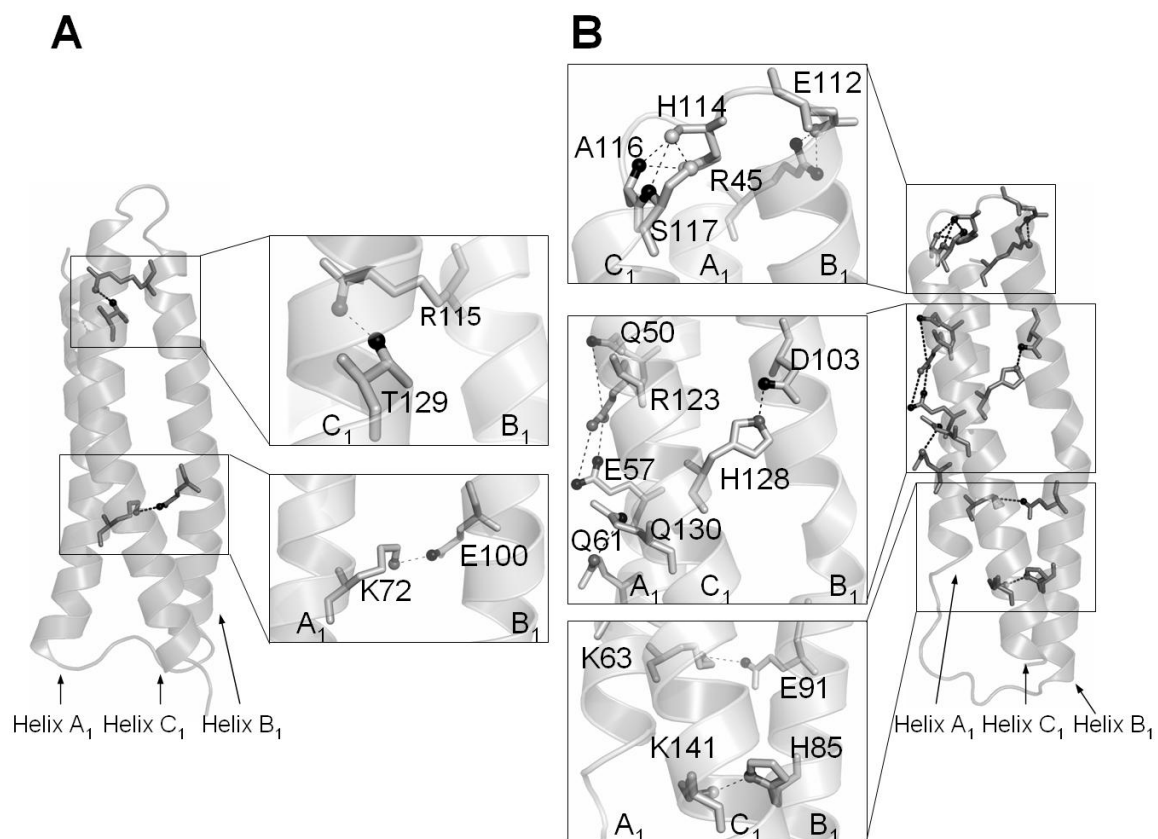


Figure 5. Hydrogen bonds of the first structural domain of α I and α II, as defined by PDBsum, see Experimental Procedures, of domain 1 (D1) of α I (PDB code: 1OWA) (**A**) and of D1 of α II (**B**), with structural display by PyMOL. The residues involved in hydrogen bonds are displayed as sticks, and the atoms are displayed as spheres, with O in black and N in dark gray. Dashed lines are drawn between atom pairs forming hydrogen bonds. D1- α I consists of only two hydrogen bonds: (i) K72 (NZ) of Helix A₁ and E100 (OE1) of Helix B₁, and (ii) R115 (NH1) of Helix B₁ with T129 (OG) of Helix C₁. However, multiple hydrogen bonds forming an extended hydrogen bond network are found in D1- α II. The hydrogen bonds in M1 and M2 often involve the same residues, but different atoms in the residues (e.g., either OE1 or OE2 in Glu). These hydrogen bonds are R45 (NE2, **NH1** or NH2) - E112 (**OE1** or OE2) (bolded atoms are shown in figure) and K63 (**NZ**) - E91 (**OE2**) in Helices A₁ and B₁ interface, Q50 (**OE1** or O) - R123 (**NH1**), E57 (**OE1** or **OE2**) - R123 (**NE** or **NH2**) and Q61 (**NE2**) - Q130 (**OE1**) in the Helix A₁ and C₁ interface and D103 (**OD1** or OD2) - H128 (**NE2**), H85 (**ND1**) - K141 (**NZ**) in the Helix B₁ and C₁ interface, as well as H114 (**O**) - S117 (**N**, **OG**) and H114 (**ND1**) - A116 (**N**) in the B₁C₁ loop.

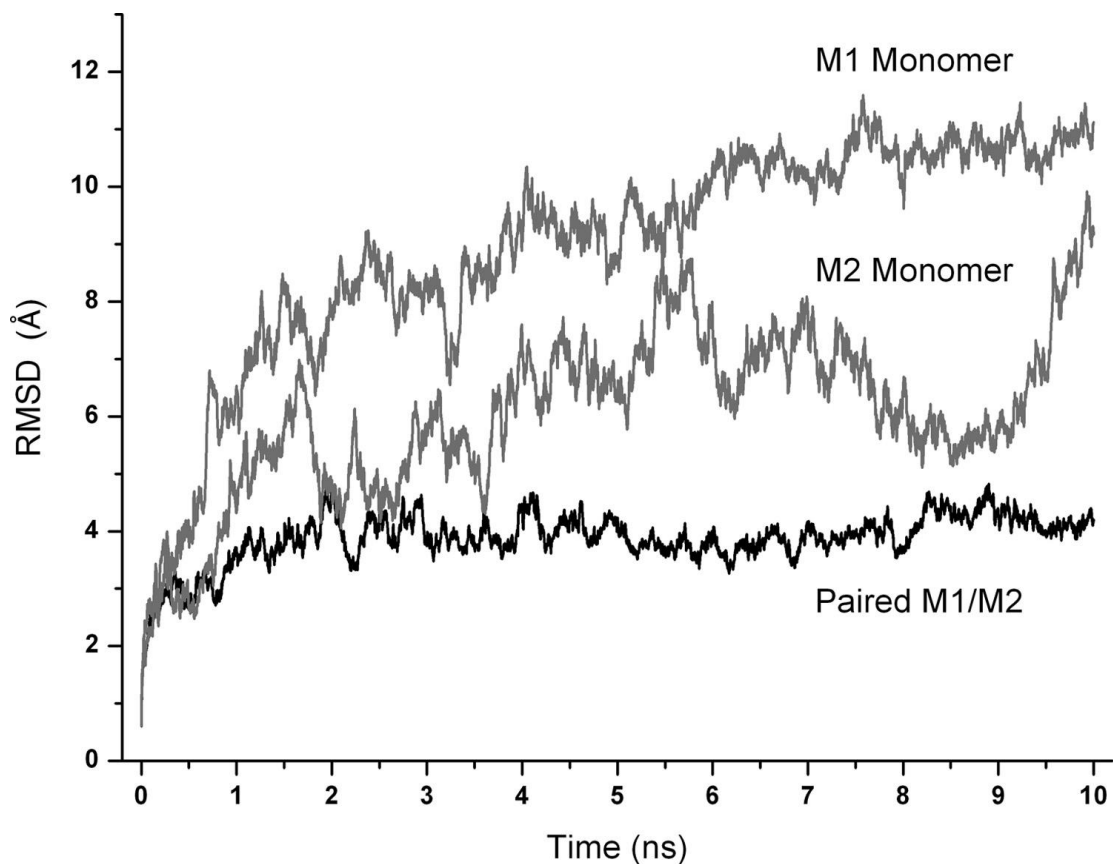


Figure 6. The RMSD values of the trajectories from molecular dynamics simulations of the explicitly solvated M1/M2 pair (bottom tracing). Equilibrium conformations were reached after 2-3 ns simulation. M1 and M2 were separately solvated and simulated under the same conditions as monomers. Their RMSD values are much larger than the corresponding values for the M1/M2 pair. The solvated structure of M1 appears to reach equilibrium at about 6 ns. These results indicate that M1 and M2 stabilize each other in the paired form.

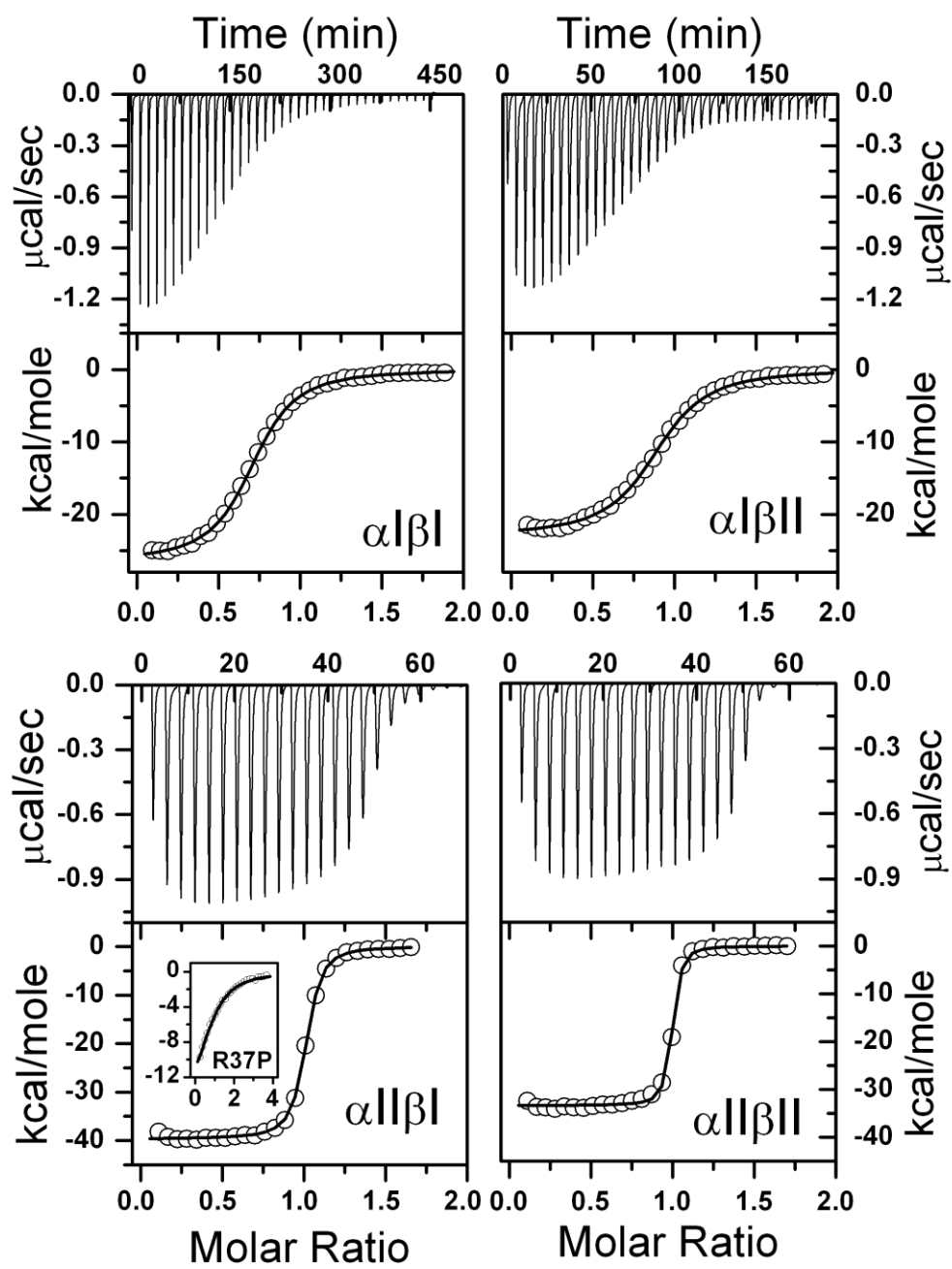


Figure 7. Isothermal titration calorimetry data at 25 °C for α I-N1/ β I-C1, α I-N1/ β II-C1, α II-N1/ β I-C1, and α II-N1/ β I-C1, as well as α II-N1-R37P/ β I-C1. All protein samples were dialyzed together in 5 mM phosphate buffer with 150 mM sodium chloride at pH 7.4 to ensure identical solution conditions of the titration pairs to avoid introducing heat of dilution in the titration experiments. Each α -spectrin protein (about 400 μ M α I-N1, or 60 μ M α II-N1) was titrated into the sample cell containing either β I-C1 or β II-C1 (about 40 μ M in α I, or 6 μ M in α II, titration). These results show that α -spectrin I and II do not contribute to the observed differences in dimer association to form tetramers; the differences are mostly due to differences in α -spectrin I and II. Our previously published K_d values are about 1 μ M for α I-N1 with β I-C1, and about 10 nM for α II-N1 with β I-C1. The K_d value for α II-N1-R37P is 10 μ M.

Table 3

Average values of results from ITC experiments where the ratios of $\Delta G\text{-sum}/\Delta G\text{-}K_d$ (see "Results") are within the range 1.0 ± 0.05

All measurements were at 25 °C. Protein titration pairs (α I-N1/ β I-C1, α II-N1/ β I-C1, and α II-N1-R37P/ β I-C1) were dialyzed together in 5 mM phosphate buffer with 150 mM sodium chloride at pH 7.4. Each α -spectrin protein (about 400 μ M α I-N1 or 60 μ M α II-N1) was titrated into a sample cell containing one of the β -spectrin proteins (about 40 μ M in the α I or 6 μ M in the α II titration).

Protein pair	K_d	ΔH	$T\Delta S$
	<i>nM</i>	<i>kcal/mol</i>	<i>kcal/mol</i>
α I- β I ^a	916 ± 91^b	-27.7 ± 5.1	-19.4 ± 5.1
α II- β I ^c	8.5 ± 2.2	-37.9 ± 7.2	-26.9 ± 7.3
α II-R37P- β I	10729.6	-16.2	-9.4

^a The α I- β I values are from an average of five different runs.

^b The standard deviation value is shown.

^c The α II- β I values are from an average of six different runs.

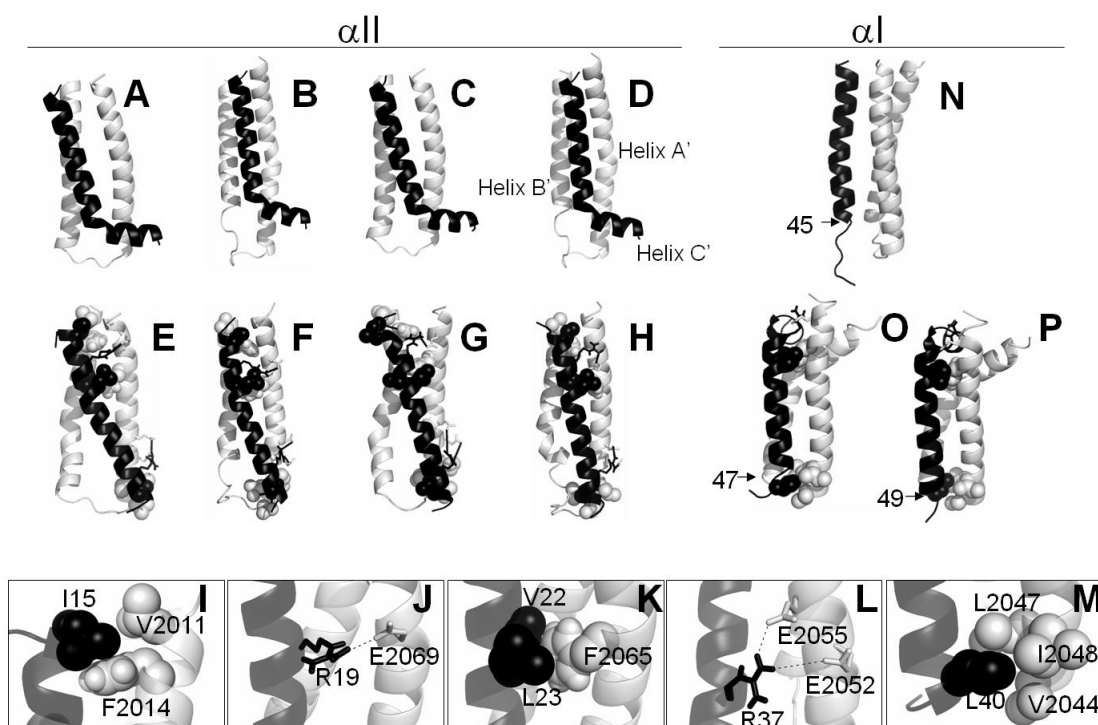


Figure 8. Homology models of $\alpha\text{II}\beta\text{I}$ (**A**) and $\alpha\text{II}\beta\text{II}$ (**B**). Note the bend at residue 33 in Helix C'. The boundaries of the helices are given in Table 4. These homology models were subjected to molecular dynamics simulations. The MD structures of $\alpha\text{II}\beta\text{I}$ (**C**) and of $\alpha\text{II}\beta\text{II}$ (**D**) show stable triple helical bundles of Helices A', B' and C' (A'B'C'). Helix C' in A'B'C' straightens at the bend and becomes a more regular helix. The other common features in these structures were inter-helix contacts for hydrophobic residues and ion pairs. The structural analyses were done with PDBsum. Details of $\alpha\text{II}\beta\text{I}$ hydrophobic clusters: L40 - V2044 - L2047 - I2048 hydrophobic cluster (**E**), I15 - V2011 - F2014 (**F**), and V22 - L23 - F2065 (**G**), and ion pairs: R37 - E2052, and E2055 (**H**), and R19 - E2069 (**I**). Also shown are the homology model $\alpha\text{I}\beta\text{I}$ (14) (**J**) and the MD structure after 30 ns simulation (**K**). The unstructured junction region around residues 46-52 in free Helix C' (**J**) becomes more helical, with residues 46-49 in helical form (**K**).

Table 4

The boundaries of helices, and the number of helical residues (number of amino acids (aa)), in the models of a triple helical bundle (A'B'C') of Helices A' and B' from β I- or β II-spectrin and Helix C' from α II-D1 or α II-D1 structural domain as a template (α I or α II, respectively) in homology modeling (HM)

The boundaries of these helices after MD simulations of these models for 10 ns (except the last entry was for 20 ns) are also given. A'B'C' of α I β I and α I β II are also given for comparison. The values of α I β I with α I have been published (14).

A'B'C'	Template	Helix A'				Helix B'				Helix C'			
		HM	aa	Residues	MD	HM	aa	Residues	MD	HM	aa	Residues	MD
α I β I	α I	2009–36 ^a	28	2010–38	29	2044–73	30	2044–72	29	12–43 ^a	32	14–41	28
	α II	2009–31	23	2010–32	23	2044–77	34	2044–76	33	12–43	32	14–42	29
α II β II	α I	2017–45 ^a	29	2018–45	28	2052–81	30	2052–79	28	12–43	32	14–41	28
	α II	2017–40	24	2018–40	23	2052–85	34	2052–84	33	12–43	32	15–41	27
α I β I	α I	2009–37	29	2012–36	25	2044–73	30	2044–69	26	21–45 ^a	25	22–47	26
	α I ^b	2009–37	29	2012–36	25	2044–73	30	2044–69	26	21–45	25	22–49	28

^a The numbering system for α I and β I differs from that of α II and β II. In the regions of interest, residue 12 in α I corresponds to residue 21 in α I. Residue 2017 in β II corresponds to residue 2009 in β I. Italic residue numbers are for α II or β II.

^b MD simulation for 20 ns is shown.

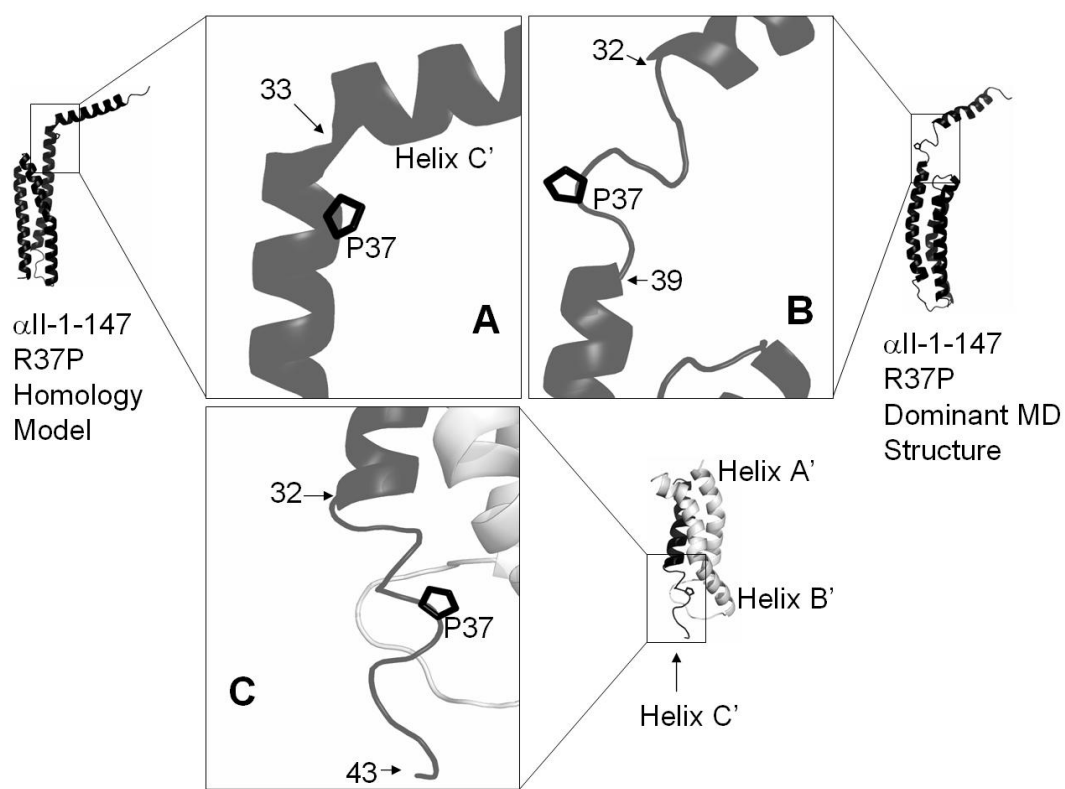


Figure 9. Homology model of free α II-R37P (**A**), with mutation R37P introduced to the crystal structure of α II-N1 (M2 in Fig 3.1). The MD structure of R37P in (**A**) shows 3 α turns for residues 32-39 (**B**). The mutation is also introduced to the bound state (A'B'C' helical bundle), and the MD structure shows 4 α turns for residues 32-43 (**C**).

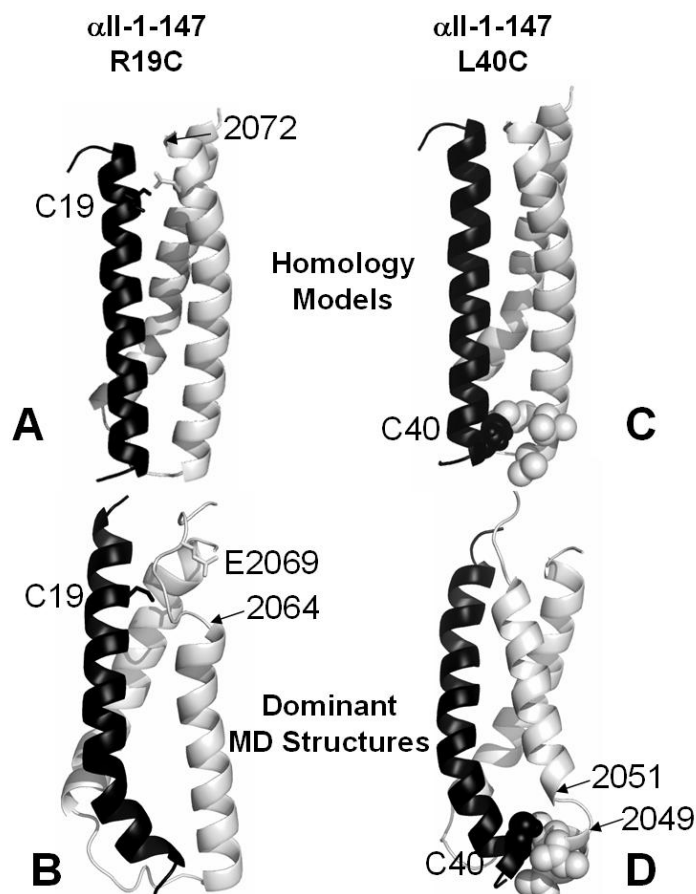


Figure 10. Mutation at residue 19 from R to C is introduced to the MD structure of α II β I (A), and the MD structure (B) shows a stable triple helical bundle with Helix C' curving slightly at the bottom. The R19 - K2070 and R19 - E2069 interactions at the top of the helical bundle in the WT are no longer possible in 19C (B), and Helix B' consequently terminates at residue 2064, as compared to residue 2072 in WT. A similar mutation at residue 40 from L to C was introduced (C), and the MD structure (D) again shows a stable triple helical bundle with Helix C' curving slightly at the bottom. The hydrophobic cluster at the bottom only includes V2044, L2047 and I2048.

REFERENCE

1. Bennett V., and Healy J. (2008) *Trends in Mol. Med.* **14**, 28-36
2. Grum, V. L., Li, D., MacDonalds, R. I., and Mondragon, A. (1999) *Cell* **98**, 523-535
3. Bignone, P. A., King, M. D., Pinder, J. C., and Baines, A. J. (2007) *J. Biol. Chem.* **282**, 888-896
4. Voas, M. G., Lyons, D. A., Naylor, S. G., Arana, N., Rasband, M. N., and Talbot, W. S. (2007) *Curr. Biol.* **17**, 562-568
5. Benz, P. M., Blume, C., Moebius, J., Oschatz, C., Schuh, K., Sickmann, A., Walter, U., Feller, S. M., and Renne, T. (2008) *J. Cell Biol.* **180**, 205-219
6. Speicher, D. W., DeSilva, T. M., Speicher, K. D., Ursitti, J. A., Hembach, P., and Weglarz, L. (1993) *J. Biol. Chem.* **268**, 4227-4235
7. Mehboob, S., Jacob, J., May, M., Kotula, L., Thiyagarajan, P., Johnson, M. E. and Fung, L. W.-M. (2003) *Biochemistry* **42**, 14702-14710
8. Li, Q., and Fung, L. W.-M. (2009) *Biochemistry* **48**, 206-215
9. Begg, G. E., Morris, M. B., and Ralston, G. B. (1997) *Biochemistry* **36**, 6977-6985
10. Bignone, P. A., and Baines, A. J. (2003) *Biochem. J.* **374**, 613-624
11. Long, F., Mcelheny, D., Jiang, S., Park, S., Caffrey M. S., and Fung, L. W.-M. (2007) *Protein Sci.* **16**, 2519-2530
12. Susuki K., and Rasband M. N. (2008) *Exp. Biol. Med.* **233**, 394-400
13. Antoniou, C, Lam, V. Q., and Fung, L. W.-M. (2008) *Biochemistry* **47**, 10765-10772
14. Park, S., Caffrey, M. S., Johnson, M. E., and Fung, L. W.-M. (2003) *J. Biol. Chem.* **278**, 21837-21844
15. Park, S., Johnson, M. E., and Fung, L. W.-M. (2002) *Blood* **100**, 283-288
16. An, X., Zhang, X., Salomao, M., Guo, X., Yang, Y., Wu, Y., Gratzer, W., Baines, A. J.,

- and Mohandas, N. (2006) *Biochemistry* **45**, 13670-13676
17. Song, Y., Pipalia, N., and Fung, L. W.-M. (2009) *Protein Sci.* **18**, 1916-1925
 18. Greenfield, N. J., and Fasman, G. D. (1969) *Biochemistry* **8**, 4108-4116
 19. Kabsch, W. (1993) *J. Appl. Cryst.* **26**, 795-800
 20. Otwinowski, Z., and Minor, W. (1997) *Methods in Enzymology* **276**, 307-326
 21. Adams, P. D., Grosse-Kunstleve, R. W., Hung, L.-W., Loerger, T.R., McCoy, A. J., Moriarty, N. W., Read, J. C., Sacchettini, J. C., Sauter, N. K., and Terwilliger, T.C. (2002) *Acta Cryst.* **D58**, 1948-1954
 22. Emsley, P., and Cowtan, K. (2004) *Acta Cryst.* **D60**, 2126-2132
 23. Lovell, S. C., Davis, I. W., Arendall III, W. B., deBakker, P. I. W., Word, J. M., Prisant, M. G., Richardson, J. S., and Richardson, D. C. (2003) *Proteins* **50**, 437-450
 24. Kabsch, W., and Sander, C. (1983) *Biopolymers* **22**, 2577-2637
 25. Laskowski, R. (2009) *Nucleic Acids Res.* **37**, D355-D459
 26. Xu, D., Tsai, C.-J., and Nussinov, R. (1997) *Protein Eng.* **9**, 999-1012
 27. Wallace, A. C., Laskowski, R. A., and Thornton, J. M. (1995) *Protein Eng.* **8**, 127-134
 28. Kumar, S., and Nussinov, R. (1999) *J. Mol. Biol.* **293**, 1241-1255
 29. Silva, P. J. (2008) *Proteins* **70**, 1588-1594
 30. Lusitani, D., Menhart, N., Keiderling, T. A., and Fung, L. W.-M., (1998) *Biochemistry* **37**, 16546-16554
 31. Van der Spoel, D., Lindahl, E., Hess, B., Groenhof, G., Mark, A. E., and Berendsen, H. J. C. (2005) *J. Comput. Chem.* **26**, 1701-1718
 32. van Gunsteren W. F., Berendsen H. J. C. (1987) GROMOS (GRoningen Molecular Simulation package) (Biomos BV, The Netherlands)
 33. Darden, T., York, D., and Pedersen, L. (1993) *J. Chem. Phys.* **98**, 10089-10092

34. Mehboob, S., Luo, B.-H., Patel, B. M., and Fung, L. W.-M. (2001) *Biochemistry* **40**, 12457-12464
35. An, X., Guo, X., Zhang, X., Baines, A. J., Debnath, G., Moyo, D., Salomao, M., Bhasin, N., Johnson, C., Discher, D., Gratzer, W. B., and Mohandas, N. (2006) *J. Biol. Chem.* **281**, 10527-10532
36. Li, A., and Daggett V. (1995) *Protein Eng.* **8**, 1117-1128
37. Lam, V. Q., Antoniou, A., Rolius, R., and Fung, L. W.-M. (2009) *Br. J. Haematol.* **147**, 392-395
38. Sumandea, C. A. and Fung, L. W.-M. (2005) *Molecular Brain Research* **136**, 81-90
39. Davis, L., Abdi, K., Machius, M., Brautigan, C., Tomchick, D., R., Bennett, V., and Michaely, P. (2009) *J. Biol. Chem* **284**, 6982-6987
40. Yan, Y., Winograd, E., Viel, A., Cronin, T., Harrison, S. C., and Branton, D. (1993) *Science* **262**, 2027-2030
41. Kusunoki, H., MacDonald, R. I., and Mondragon, A. (2004) *Structure* **12**, 645-656
42. Stabach, P. R., Simonovic, I., Ranieri, M. A., Aboodi, M. S., Steitz, T. A., Simonovic, M., and Morrow, J. S. (2009) *Blood* **113**, 5377-5384
43. Ipsaro, J. J., Huang, L., and Mondragon, A. (2009) *Blood* **113**, 5385-5393
44. Kusunoki, H., Minasov, G., MacDonald, R. I., and Mondragon, A. (2004) *J. Mol. Biol.* **344**, 495-511
45. Pascual, J., Pfuhl, M., Walther, D., Saraste, M., and Nilges, M. (1997) *J. Mol. Biol.* **273**, 740-751
46. Park, S. Y., Mehboob, S., Luo, B.-H., Hurtuk, M., Johnson, M. E. and Fung, L. W.-M. (2001) *Cell Mol Biol Letters* **6**, 571-585
47. Brown, J. H., Cohen, C., and Parry, D. A. (1996) *Proteins* **26**, 134-145

48. Gruber, M., and Lupas, A. N. (2003) *Trends Biochem. Sci.* **28**, 679-685
49. Kaminska, A., Strelkov, S. V., Goudeau, B., Olive, M., Daqvadorj, A., Fidzianska, A., Simon-Casteras, M., Shatunov, A., Dalakas, M. C., Ferrer, I., Kwiecinski, H., Vicart, P., and Goldfarb, L. G. (2003) *Hum. Genet.* **114**, 306-313
50. Tatulian, S. A. (2008) *Comput. Biol. Chem.* **32**, 370-374
51. Oh, Y., and Fung, L. W.-M. (2007) *Cell. Mol. Biol. Lett.* **12**, 604-620
52. Mooers, B. H. M., Baase, W. A., Wray, J. W., and Matthews, B. W. (2009) *Protein Sci.* **18**, 871-880
53. Hawwa R., Aikens, J., Turner, R. J., Santarsiero, B.D., and Mesecar, A.D. (2009) *Arch. Biochem. Biophys.* **488**, 109-120
54. Langosch, D., and Arkin, I. T. (2009) *Protein Sci.* **18**, 1343-1358
55. Karplus, M., and Kushick J. N. (1981) *Macromolecules* **14**, 325-332
56. Gilson, M. K., and Zhou, H.-X. (2007) *Annu. Rev. Biophys. Biomol. Struct.* **36**, 21-42
57. Del Sol, A., Tsai, C.-J., Ma, B., and Nussinov, R. (2009) *Structure* **17**, 1042-1050

APPENDIX B

Yeast Two-Hybrid and ITC Studies of Alpha and Beta Spectrin interaction at the
Tetramerization Site.

Akin Sevinc, Marta A. Witek, and Leslie W.-M. Fung. *Cell. Mol. Biol. Lett.* 2011, 16: 452-461.

ABSTRACT

Yeast two-hybrid (Y2H) and isothermal titration calorimetry (ITC) methods were used to further study the mutational effect of non-erythroid alpha spectrin (α II) at position 22 in tetramer formation with beta spectrin (β I). Four mutants, α II-V22D, V22F, V22M and V22W, were studied. For the Y2H system, we used plasmids pGBKT7, consisting of the cDNA of the first 359 residues at the N-terminal region of α II, and pGADT7, consisting of the cDNA of residues 1697 - 2145 at the C-terminal region of β I. Strain AH109 yeast cells were used for colony growth assays and strain Y187 was used for β -galactosidase activity assays. Y2H results showed that the C-terminal region of β I interacts with the N-terminal region of α II, either the wild type, or those with V22F, V22M or V22W mutations. The V22D mutant did not interact with β I. For ITC studies, we used recombinant proteins of the α II N-terminal fragment and of the erythroid beta spectrin (β I) C-terminal fragment; results showed that the K_d values for V22F were similar to those for the wild-type (about 7 nM), whereas the K_d values were about 35 nM for V22M and about 90 nM for V22W. We were not able to detect any binding for V22D with ITC methods. This study clearly demonstrates that the single mutation at position 22 of α II, a region critical to the function of non-erythroid spectrin, may lead to a reduced level of spectrin tetramers and abnormal spectrin-based membrane skeleton. These abnormalities could cause abnormal neural activities in cells.

Key Words: Spectrin tetramerization subunit interactions, Yeast two-hybrid, Isothermal titration calorimetry

List of the abbreviations: α II - non-erythroid alpha spectrin; α II-N - a recombinant protein consisting of the first 359 residues at the N-terminal region of α II; II-N-V22 Δ - a recombinant protein with a single residue replacement at position 22 of II-N; β I - erythroid beta spectrin; β I-C - a recombinant protein consisting of residues 1898-2083 at the C-terminal region of β I; β II - non-erythroid beta spectrin; β II-C - a recombinant protein consisting of residues 1697-2145 at the C-terminal region of β II; CD - circular dichroism; ITC - isothermal titration calorimetry; K_d - equilibrium dissociation constant; pAD - yeast plasmid pGADT7; pBD - yeast plasmid pGBKT7; Y2H - yeast two-hybrid.

INTRODUCTION

Spectrin, a prominent cytoskeletal protein, exerts its fundamental role in cells by forming a sub-membrane filamentous network. An essential aspect of the spectrin network formation is the tetramerization of spectrin heterodimers. We have previously used the yeast two-hybrid system and random mutagenesis to investigate the effects of amino acid mutations on the tetramerization of non-erythroid (brain) spectrin (fodrin) [1]. The Y2H techniques have been developed as convenient and useful methods to screen for protein interactors [2-4], particularly when libraries of vectors containing protein cDNAs are commercially available. We have used such methods to identify some interactors of non-erythroid alpha spectrin (II) [5]. These studies are often qualitative in nature - a protein either interacts or does not interact with another protein. However, several studies report quantitative results from Y2H studies. For example, colonies of Y2H system with common polymorphisms of *BRCA1* from cancer predisposing mutations were considerably smaller than controls [6], colony growth rates (cell viability) correlate with the strengths of interactions [7, 8], the levels of transcription activation correlate with the strength of the binding interaction in a “small colony phenotype”, a growth phenotype discovered serendipitously [9], and β -galactosidase activities correlate with protein-protein interaction affinities [10, 11]. Yet, some authors indicate that, “our results emphasize the difficulty of attempting to quantitate differences in affinity from two-hybrid experiments alone” [7]. Others show that Y2H results do not correlate with protein affinities [12-14]. Since protein expression, structures and nature of interaction may vary from system to system in Y2H systems, many studies have focused on studying single mutation effects on protein-protein interactions [e.g., 9].

In our study, we used both the Y2H system and ITC methods to further study the mutational effect of α II at position 22 on tetramer formation. Previously we have used ITC methods to determine K_d values of α II heterodimer association to form tetramers in model systems [e.g., 15-19]. Recently, we found that mutation of α II at position 37 increases the K_d value from about 9 nM for α II with beta I spectrin (β I) to 10 μ M for the R37P mutation [15]. Residue 22 in α II corresponds to a “d” position in the heptad repeat and is in the interface of the triple helical bundle in α II tetramers [15]. In this study, we found that the mutation effect was most severe for V22D, followed by V22W and V22M, whereas little effect was observed for V22F.

METHODS

Yeast two-hybrid assays

The Y2H system with colony growth and β -galactosidase detection methods were used to determine the interaction between α II and β II, wild-type or its mutants, at the tetramerization region. The Matchmaker GAL4 Two-Hybrid System 3 (Clontech, Mountain View, CA) was used. The yeast strain Y187, which is auxotrophic for leucine and tryptophan with Gal4-inducible *lacZ* gene, or strain AH109, which is auxotrophic for adenine, histidine, leucine, lysine, tryptophan and uracil and with Gal4-inducible *lacZ* genes was used. Plasmids pGBKT7 (pBD) with the cDNA of the non-erythroid alpha spectrin (α II) consisting of the first 359 residues at the N-terminal region (α II-N) (pBD- α II-N) and pGADT7 (pAD) with the cDNA of beta-spectrin consisting of residues 1697-2145 at the C-terminal region (β II-C) (pAD- β II-C) were previously prepared [1]. Plasmids of two mutations at position 22 of α II-N, V22W and V22M, prepared by standard methods [20] as well as two previously prepared mutants (V22D and V22F) [1] (pBD- α II-N-V22 Δ) were also used.

For the colony growth assay, AH109 cells with pAD- β II-C and pBD- α II-N, or pBD- α II-N-V22 Δ , were grown at 30 °C on agar plates with a growth medium containing all essential amino acids but tryptophan, leucine and histidine, and lacking adenine (SD/-W/-L/-H/-A with SD Minimal Agar Base and -Leu/-Trp/-His/-adenine DO Supplement, both from Clontech) for three days before photography. Under this high-stringency growth condition, cells with strongly interacting protein pairs grow and form colonies, whereas colonies with proteins with low-affinity interactions may be missed (Clontech user manual). We also prepared pAD- I-C, with I-C consisting of residues 1898-2083 of I and performed colony growth assay with pBD- α II-N or pBD- α II-N-V22D. For -Galactosidase assay via colony lift method, strain Y187 cells with pAD- β II-C and pBD- α II-N, or pBD- α II-N-V22 Δ , were grown at 30 °C on agar plates with a growth medium containing all essential amino acids but leucine and tryptophan (SD/-Leu/-Trp with SD Minimal Agar Base and -Leu/-Trp DO Supplement; both from Clontech) for three days before colony lifting steps, as described in the manufacturer user manual. Cells with interacting protein pairs produce -galactosidase to give a blue color on filter papers when soaked with a solution consisting of its substrate, 5-bromo-4-chloro-3-indolyl- β -D-galactopyranoside (X-gal soaking solution, see Clontech user manual).

Isothermal titration calorimetry

Recombinant proteins α II-N, α II-N-V22 (V22D, V22F, V22M and V22W) and I-C were prepared, following standard laboratory techniques [15]. Briefly, protein expression vector pGEX-2T was used to express glutathione S-transferase fusion protein, and purified with affinity column chromatography, with thrombin cleavage of fusion protein. DNA sequence analysis and protein mass spectrometry analysis results were obtained (Research Resources

Center, University of Illinois at Chicago). Protein purity was checked with gel electrophoresis, using 16% polyacrylamide gel with 0.1% SDS. Helical contents of the proteins were determined using circular dichroism spectra [20]. We have found that I-C and II-C proteins exhibit similar affinities for α II-N [15]. However, II-C recombinant protein is more difficult to prepare than I-C protein due to its low expression level. Thus, I-C was used for ITC experiments.

ITC measurements were performed at 25 °C using an isothermal titration calorimeter (VP ITC, MicroCal, LLC, Northampton, MA) [15]. Protein pairs (β I-C with α II-N, or α II-N-V22 Δ) were dialyzed overnight in 5 mM phosphate buffer with 150 mM sodium chloride at pH 7.4 (PBS) to ensure identical solution conditions in titrating protein pairs. In addition, all samples were thoroughly degassed prior to calorimetry titration. Each α II-N or α II-N-V22 sample (30 μ M) was titrated into the sample cell containing β I-C protein (3 μ M). Titrations of β I-C (30 - 100 μ M) into α II-N or α II-N-V22 (3 μ M) were also performed. Titration isotherms were analyzed with a single binding site assumption, as before [15], to obtain dissociation constants, K_d .

RESULTS

Yeast two-hybrid assays

For colony growth assay, cells with either I-C or II-C and with α II-N or α II-N-V22F, -V22M, or -V22W formed well separated colonies with diameters of 2 - 5 mm after 3 days, with no specific colony size associated with cells of a particular mutant (Fig. 1). However, cells with α II-N-V22D, with either I-C (data not shown) or II-C (Fig. 1) did not show any growth after 3 days.

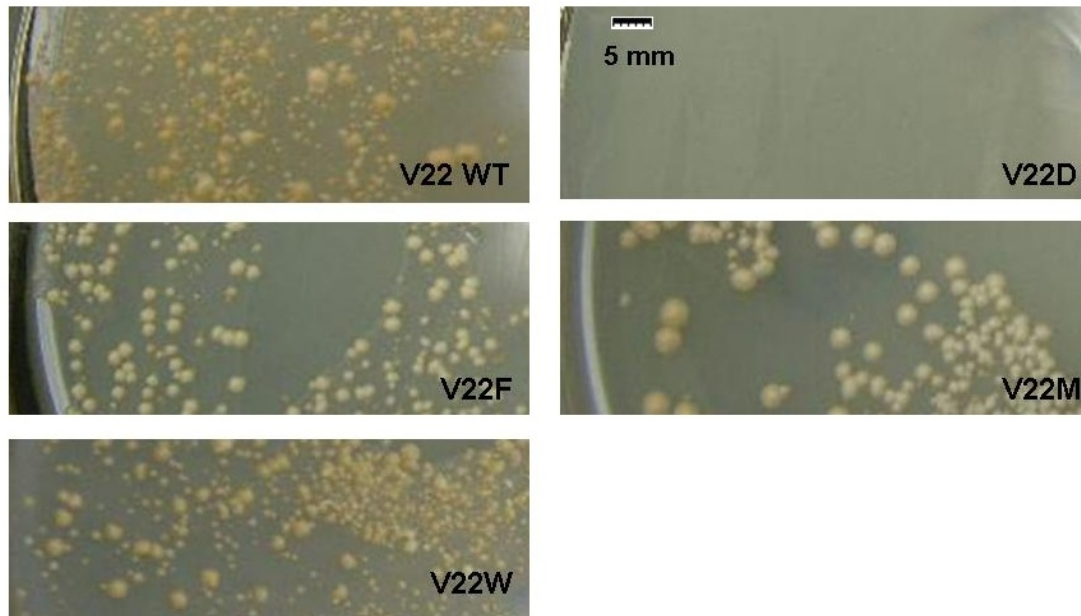


Fig. 1. Colony Growth Assay. AH109 cells co-transformed with pAD- β II-C and pBD- α II-N, or pBD- α II-N-V22D, -V22F, -V22M, or -V22W, were grown for 3 days at 30 °C, following procedures from the manufacturer (Clontech). Colonies, 2 - 5 mm in diameter, were found for cells expressing α II-N (marked as V22 WT above), α II-N-V22F (V22F), α II-N-V22M (V22M), or α II-N-V22W (V22W), whereas cells expressing α II-N-V22D (V22D) did not show any growth. The scale bar is shown in top right panel.

For the β -galactosidase activity (colony-lift) assay, Y187 cells with α II-N or α II-N-V22F, -V22M, or -V22W showed a distinct blue color, but without a consistent color variation associated with cells with a particular mutation (Fig. 2).

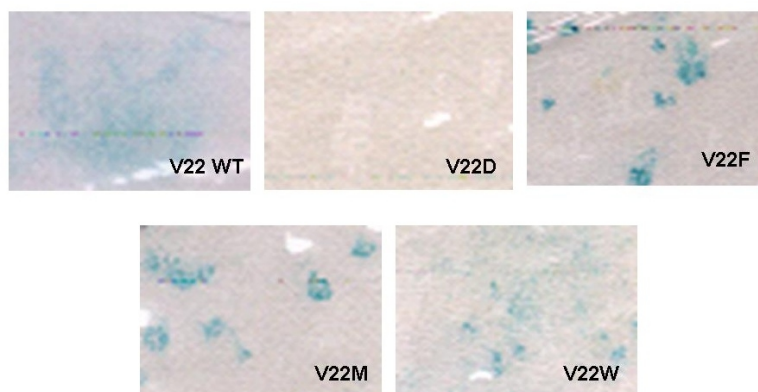


Fig. 2. β -Galactosidase Activity Assay via Colony Lift Method. Y187 cells co-transformed with pAD- β II-C and pBD- α II-N, - α II-N-V22D, - α II-N-V22F, - α II-N-V22M, or - α II-N-V22W were grown for 3 days at 30 °C following procedures from the manufacturer (Clontech). Colonies were transferred onto filter papers, subjected to freeze-thaw cycles, and incubated on a second set of filter papers pre-soaked with β -galactosidase substrate (X-gal) for 30 min. Filter papers for colonies with α II-N, α II-N-V22F, α II-N-V22M and α II-N-V22W all showed blue color, but those with α II-N-V22D did not show blue color.

Isothermal Titration Calorimetry Assay

Recombinant protein analysis

The SDS gel electrophoresis data showed that all α II-N (wild type and mutants) and β I-C proteins were ~90% pure. Electrophoretic masses were ~42 kDa for α II-N proteins and ~22 kDa for β I-C. Mass spectrometric results showed 42,241.0 Da for α II-N (expected mass is 42,242.5 Da), 42,258.6 Da for α II-N-V22D (expected mass is 42,258.5 Da), 42,289.0 Da for α II-N-V22F (expected mass is 42,290.6 Da), 42,274.8 Da for α II-N-V22M (expected mass is 42,274.6 Da), 42,329.8 Da for α II-N-V22W (expected mass is 42,329.6 Da) and 22,036.9 Da for β I-C (expected mass is 22,036.9 Da). The CD spectra of α II-N, α II-N-V22 Δ and β I-C exhibited characteristic features of similar spectrin recombinant proteins [21], with minima at

222 and 208 nm. Helical contents were ~75%, in good agreement with published results [21].

ITC results

The ITC isotherm of β I-C/ α II-N system at 25 °C showed that sufficient heat (-0.45 μ cal/sec) was released during titration of α II-N into β I-C (Fig. 3), with an average K_d value of 6.9 ± 0.5 nM ($n = 3$), in good agreement with previous findings of a similar system (with β I-C) [19], and the values are similar to that with β II-C [18]. The K_d value was 6.7 ± 0.3 nM for β I-C/ α II-N-V22F, 35 ± 4 nM for β I-C/ α II-N-V22M and 93 ± 28 nM for β I-C/ α II-N-V22W. However, for β I-C/ α II-N-V22D system, there was insufficient heat released either when α II-N-V22D (30 μ M) was titrated with β I-C (3 μ M) (Fig. 3, Tab. 1), or when β I (30 - 100 μ M) was titrated with α II-N-V22D (3 μ M), indicating that the K_d value for this system is larger than 100 μ M.

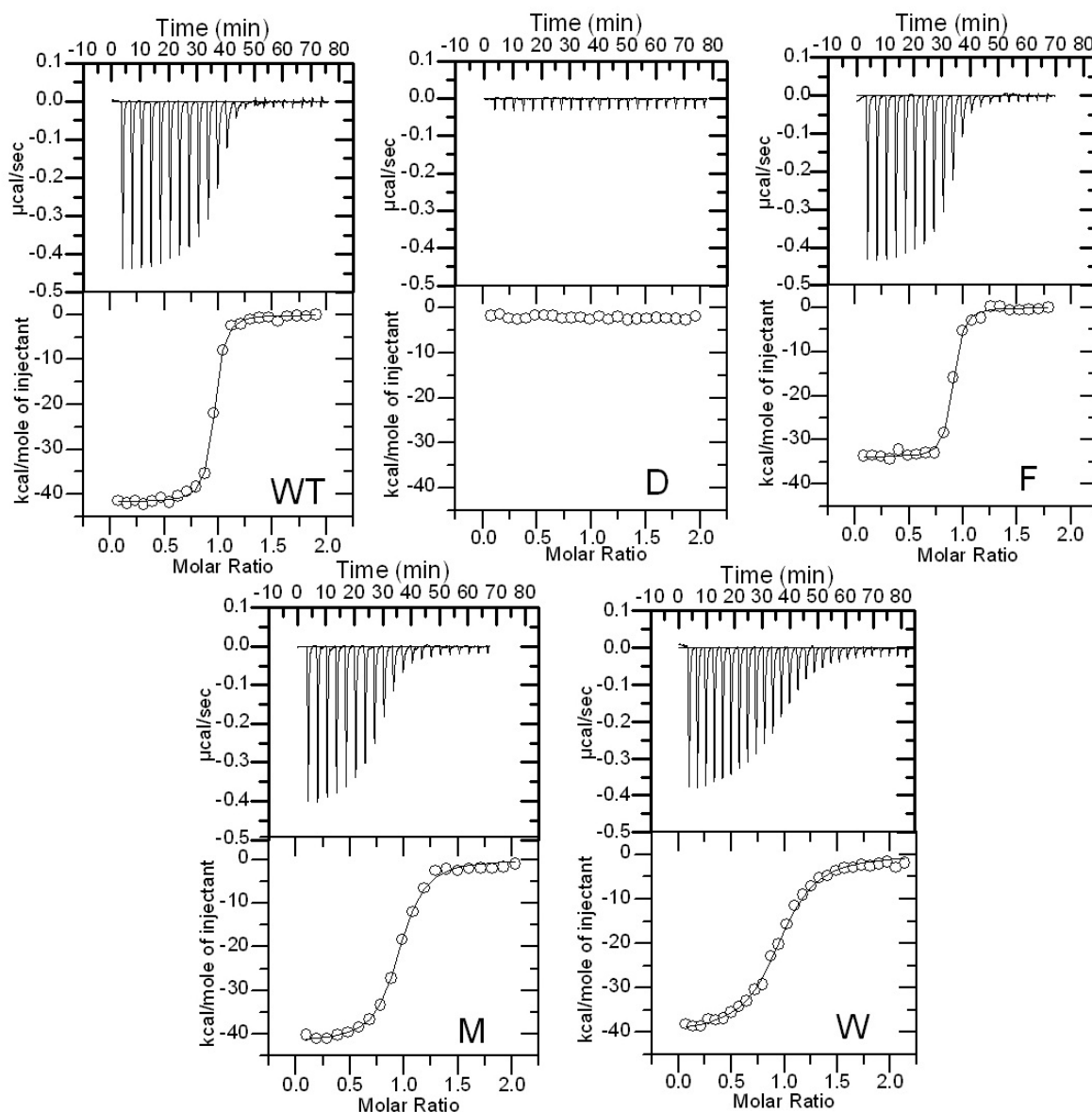


Fig. 3. ITC Measurements. Recombinant protein samples of β I-C, α II-N (marked as WT above), α II-N-V22D (D), α II-N-V22F (F), α II-N-V22M (M) and α II-N-V22W (W) were dialyzed together in 5 mM phosphate buffer with 150 mM sodium chloride at pH 7.4 and degassed thoroughly prior to ITC measurements. α II-N proteins (29 - 35 μ M) were each individually titrated into the sample cell containing β I-C protein (3 μ M). Typical ITC titration isotherms and fitted curves are shown. The average K_d values ($n = 3$), determined from the fitted curves using a single-binding site model of the manufacturer (MicroCal) software, were 6.9 nM for β I-C/ α II-N and 6.7 nM for β I-C/ α II-N-V22F, 35

nM for β I-C/ α II-N-V22M and 93 nM for β I-C/ α II-N-V22W. Little heat was released for β I-C/ α II-N-V22D titration and no K_d was obtained.

Tab. 1 Y2H and ITC results of alpha and beta spectrin model proteins interaction.

<u>pBD Plasmid^a</u>	<u>Colony Growth^b</u>	<u>-Galactosidase Activity^c</u>	<u>K_d (nM)^d</u>
α II-N	Yes	Blue color	6.9
II-N-V22D	No	No color	not detectable
α II-N-V22F	Yes	Blue color	6.7
α II-N-V22M	Yes	Blue color	35
α II-N-V22W	Yes	Blue color	93

^apAD- β II-C with different pBD- α II-N plasmids in the Y2H experiment; we also used or pAD- I-C with pBD- α II-N or pBD- α II-N-V22D, and the results were the same as those with pAD- β II-C ; ^byeast AH109 cells were grown in a medium containing all essential amino acids but tryptophan, leucine and histidine, and lacking adenine; ^cyeast Y187 cells were grown in medium containing all essential amino acids but leucine and tryptophan for the colony lift assay; ^dITC experiments using recombinant proteins of II-N and mutants listed and of I-C were carried out at 25 °C in 5 mM phosphate buffer with 150 mM sodium chloride at pH 7.4.

DISCUSSION

The Y2H systems have been widely used to study protein-protein interactions. In this study, both colony growth and -galactosidase activity detection results showed that II spectrin with mutations V22F, V22M or V22W interacted with II spectrin at the tetramerization site (N-terminal region of II and C-terminal region of II). However, II-N-V22D did not interact with either I-C or II-C. With those II mutants that interacted with II-C, we were not able to detect any differences in interactions between V22F, V22M or V22W with II-C. Both colony growth rate and colony size, as well as the blue color indication for -galactosidase activity did not show detectable differences

between V22, V22F, V22M and V22W.

The ITC methods require not only the preparation of recombinant proteins but also the characterization of these proteins for proper functional analysis. In our systems, we characterized the protein systems with high resolution mass spectrometry analysis as well as by circular dichroism analysis. We have found that, for both α and β spectrin recombinant proteins used for tetramerization studies, it is important to obtain their CD results to demonstrate that the proteins are folded properly before ITC experiments. The ITC results show that the K_d values for V22F and the wild type with I-C were about the same, with a K_d of about 7 nM. However, V22M and V22W both exhibited lower affinity than the wild type, with K_d values of 35 nM and 93 nM, respectively. The ITC results of V22D titration with I-C showed little interaction, with K_d values larger than 100 M. As indicated in METHODS, we have found that I-C and II-C proteins exhibit similar affinities for II-N [15], and in this study we showed that results similar to those of II-C were obtained when I-C was used with II-N wild type or with V22D.

Spectrin tetramer formation involves the bundling of three helices, one from α (Helix C') and two from β (Helix A' and Helix B'), forming a triple helical bundle [15, 21]. Mutations that affect the triple helical bundling lead to lower affinity. Previous studies reveal that the V22 position of II is critical for its tetramerization with β II [1]. Sequence alignment shows that II V22 corresponds to V31 in erythroid spectrin (I). I V31 has been identified as a hot spot that leads to severe clinical symptoms [22]. In triple helical bundling of II and II helices, an N-terminal hydrophobic cluster [18] involves three residues in the II Helix C' (I15, V22, and L23) and two residues in the II Helix A' (V2019 and F2022), and one residue in the II Helix B' (F2073) [15]. Thus, it is not surprising that mutations at the V22 position may affect non-

erythroid spectrin tetramer formation. Since V22 is involved in a hydrophobic cluster during helical bundling to form tetramers, a mutation from V to a charged residue D clearly weakens the hydrophobic cluster and thus severely reduces the ability of V22D to interact with Helices A' and B' in β II-C. Mutation of V22 to other hydrophobic residues such as V22F did not affect its interaction with β II-C. The mutations of V22M and V22W lowered the affinity by about 5 times and 10 times, respectively. Hydrophobicity of individual side chains, and the properties of the interacting clusters also affected the triple helical bundling. The K_d values determined by ITC represented a ΔG value of about -46.6 kJ/mol (-11.1 kcal/mol) for β II-C with either α II-N or α II-N-V22F, -42.6 kJ/mol (-10.1 kcal/mol) with α II-N-V22M, and -40.1 kJ/mol (-9.6 kcal/mol) with α II-N-V22W. Thus, the tetramers of these β II mutants and spectrin exhibit slightly differing stabilities from each other. As discussed previously [18], β II spectrin has recently been reported to be essential for stabilizing nascent sodium channel clusters [23], assembling the mature node of Ranvier [23], and regulating endothelial cell-cell contacts [24]. The tetramer formation of β II- β II spectrin is also essential in the regulatory step for neuritogenesis [25]. Tetramerization is clearly important for spectrin function. At present, no clinical mutations in β II spectrin, including the tetramerization region, have been identified. A reduced level of spectrin tetramers and abnormal spectrin-based membrane skeleton could cause abnormal neural activities in cells.

Acknowledgments

This work was supported by a grant from NIH to LWMF (GM68621). MW was supported by a fellowship from NIH (1T32DE018381-Multidisciplinary Oral Science Training Program).

REFERENCES

1. Sumandea, C. A. and Fung, L. W.-M. Mutational effects at the tetramerization site of nonerythroid alpha spectrin. **Mol. Brain Res.** 136 (2005) 81-90.
2. Fields, S. and Song, O. A novel genetic system to detect protein-protein interactions. **Nature** 340 (1989) 245-246.
3. Fields, S. Interactive learning: Lessons from two hybrids over two decades. **Proteomics** 9 (2009) 5209-5213.
4. Hu, X., Kang, S., Chen, X., Shoemaker, C. B. and Jin, M. M. Yeast surface two-hybrid for quantitative in vivo detection of protein-protein interactions via the secretory pathway. **J. Biol. Chem.** 284 (2009) 16369-16376.
5. Oh, Y., and Fung, L. W.-M. Brain proteins interacting with the tetramerization region of non-erythroid alpha spectrin. **Cell. Mol. Biol. Lett.** 12 (2007) 604-620.
6. Humphrey, J. S., Salim, A., Erdos, M. R., Collins, F. S., Brody, L. C., and Klausner, R. D. Human *BRCA1* inhibits growth in yeast: Potential use in diagnostic testing. **Proc. Natl. Acad. Sci. U. S. A** 94 (1997) 5820-5825.
7. Estojak, J., Brent, R. and Golemis, E. A. Correlation of two-hybrid affinity data with in vitro measurements. **Mol. Cell. Biol.** 15 (1995) 5820-5829.
8. Jabbour, A. M., Puryer, M. A., Yu, J. Y., Lithgow, T., Riffkin, C. D., Ashley, D. M., Vaux, D. L., Ekert, P. G., and Hawkins, C. J. Human Bcl-2 cannot directly inhibit the *Caenorhabditis elegans* Apaf-1homologue CED-4, but can interact with EGL-1. **J. Cell Sci.** 119 (2006) 2572-2582.
9. Coyne, R. S., McDonald, H. B., Edgemon, K., and Brody, L. C. Functional characterization of BRCA1 sequence variants using a yeast small colony phenotype

- assay. **Cancer Biol. Ther.** 3 (2004) 453-457.
10. Stavolone, L., Herzog, E., Leclerc, D. and Hohn, T. Tetramerization is a conserved feature of the virion-associated protein in plant pararetroviruses. **J. Virol.** 75 (2001) 7739-7743.
 11. Ma, L.-Y., King, G., and Rothfield, L. Mapping the MinE site involved in interaction with the MinD division site selection protein of *Escherichia coli*. **J. Bacteriol.** 185 (2003) 4948-4955.
 12. Larin, D., Mekios, C., Das, K., Ross, B., Yang, A.-S., and Gilliam, T. C. Characterization of the interaction between the Wilson and Menkes disease proteins and the cytoplasmic copper chaperone, HAH1p. **J. Biol. Chem.** 274 (1999) 28497-28504.
 13. Grootjans, J. J., Reekmans, G., Ceulemans, H. and David, G. Syntenin-Syndecan binding requires syndecan-syntenin and the co-operation of both PDZ domain of syntenin. **J. Biol. Chem.** 275 (2000) 19933-19941.
 14. Crowther, L. J., Yamagata, A., Craig, L., Tainer, J. A., and Donnenberg, M. S. The ATPase activity of BfpD is greatly enhanced by zinc and allosteric interactions with other Bfp proteins. **J. Biol. Chem.** 280 (2005) 24839-24848.
 15. Mehboob, S., Song, Y., Witek, M., Long, F., Santarsiero, B.D., Johnson, M. E. and Fung, L. W.-M. Crystal structure of the nonerythroid α -spectrin tetramerization site reveals differences between erythroid and nonerythroid spectrin tetramer formation. **J. Biol. Chem.** 285 (2010) 14572-14587.
 16. Kang, J., Song, Y., Sevinc, A., Fung, L.W.-M. Important residue (G46) in erythroid spectrin tetramer formation. **Cell Mol. Biol. Lett.** 15 (2010) 46-54.
 17. Lam, V.Q., Antoniou, C., Rolius, R., Fung, L.W. Association studies of erythroid alpha-

- spectrin at the tetramerization site. **Br. J. Haematol.** 147 (2009) 392-395.
18. Li, Q. and Fung, L. W.-M. Structural and dynamic study of the tetramerization region of non-erythroid α -spectrin: a frayed helix revealed by site-directed spin labeling electron paramagnetic resonance. **Biochemistry** 48 (2009) 206-215.
 19. Mehboob, S., Jacob, J., May, M., Kotula, L., Thiagarajan, P., Johnson, M. E. and Fung, L. W.-M. Structural analysis of the α N-terminal region of erythroid and nonerythroid spectrins by small-angle X-ray scattering. **Biochemistry** 42 (2003) 14702-14710.
 20. Mehboob, S., Luo, B.-H., Fu, W., Johnson, M. E. and Fung, L. W.-M. Conformational studies of the tetramerization site of human erythroid spectrin by cysteine-scanning spin-labeling EPR methods. **Biochemistry** 44 (2005) 15898-15905.
 21. Mehboob, S., Luo, B.-H., Patel, B. M. and Fung, L. W.-M. $\alpha\beta$ spectrin coiled coil association at the tetramerization site. **Biochemistry** 40 (2001) 12457-12464.
 22. Lecomte, M.C., Garbarz, M., Gautero, H., Bournier, O., Galand, C., Boivin, P., Dhermy, D. Molecular basis of clinical and morphological heterogeneity in hereditary elliptocytosis (HE) with spectrin alpha I variant. **Br. J. Haematol.** 85 (1993) 584-595.
 23. Voas, M.G., Lyons, D.A., Naylor, S.G., Arana, N., Rasband, M.N., and Talbot, W.S. α II-Spectrin is essential for assembly of the nodes of Ranvier in myelinated axons. **Curr. Biol.** 17 (2007) 562-568.
 24. Benz, P.M., Blume, C., Moebius, J., Oschatz, C., Schuh, K., Sickmann, A., Walter, U., Feller, S.M., and Renne, T. Cytoskeleton assembly at endothelial cell-cell contacts is regulated by α II-spectrin-VASP complexes. **J. Cell Biol.** 180 (2008) 205-219.
 25. Bignone, P.A., King, M.D., Pinder, J.C., and Baines, A.J. Phosphorylation of a threonine unique to the short C-terminal isoform of β II-spectrin links regulation of α - β -spectrin

interaction to neuritogenesis. **J. Biol. Chem.** 282 (2007) 888-896.

APPENDIX C

*copyright permissions for using previously published figures in this thesis

**NATURE PUBLISHING GROUP LICENSE
TERMS AND CONDITIONS**

Feb 12, 2013

This is a License Agreement between Marta Witek ("You") and Nature Publishing Group ("Nature Publishing Group") provided by Copyright Clearance Center ("CCC"). The license consists of your order details, the terms and conditions provided by Nature Publishing Group, and the payment terms and conditions.

All payments must be made in full to CCC. For payment instructions, please see information listed at the bottom of this form.

License Number	3086780256626
License date	Feb 12, 2013
Licensed content publisher	Nature Publishing Group
Licensed content publication	Nature Reviews Neuroscience
Licensed content title	The mechanobiology of brain function
Licensed content author	William J. Tyler
Licensed content date	Nov 20, 2012
Volume number	13
Issue number	12
Type of Use	reuse in a thesis/dissertation
Requestor type	academic/educational
Format	print
Portion	figures/tables/illustrations
Number of figures/tables/illustrations	1
High-res required	no
Figures	Fig 1b (The cell body of a neuron)
Author of this NPG article	no
Your reference number	
Title of your thesis / dissertation	Biophysical and Biochemical Studies of Alpha II Spectrin and Its Break-Down Products by Caspase-3
Expected completion date	Feb 2013
Estimated size (number of pages)	100
Total	0.00 USD
Terms and Conditions	

Terms and Conditions for Permissions

Nature Publishing Group hereby grants you a non-exclusive license to reproduce this

material for this purpose, and for no other use, subject to the conditions below:

1. NPG warrants that it has, to the best of its knowledge, the rights to license reuse of this material. However, you should ensure that the material you are requesting is original to Nature Publishing Group and does not carry the copyright of another entity (as credited in the published version). If the credit line on any part of the material you have requested indicates that it was reprinted or adapted by NPG with permission from another source, then you should also seek permission from that source to reuse the material.
2. Permission granted free of charge for material in print is also usually granted for any electronic version of that work, provided that the material is incidental to the work as a whole and that the electronic version is essentially equivalent to, or substitutes for, the print version. Where print permission has been granted for a fee, separate permission must be obtained for any additional, electronic re-use (unless, as in the case of a full paper, this has already been accounted for during your initial request in the calculation of a print run). NB: In all cases, web-based use of full-text articles must be authorized separately through the 'Use on a Web Site' option when requesting permission.
3. Permission granted for a first edition does not apply to second and subsequent editions and for editions in other languages (except for signatories to the STM Permissions Guidelines, or where the first edition permission was granted for free).
4. Nature Publishing Group's permission must be acknowledged next to the figure, table or abstract in print. In electronic form, this acknowledgement must be visible at the same time as the figure/table/abstract, and must be hyperlinked to the journal's homepage.
5. The credit line should read:
Reprinted by permission from Macmillan Publishers Ltd: [JOURNAL NAME]
(reference citation), copyright (year of publication)
For AOP papers, the credit line should read:
Reprinted by permission from Macmillan Publishers Ltd: [JOURNAL NAME],
advance online publication, day month year (doi: 10.1038/sj.[JOURNAL
ACRONYM].XXXXX)

Note: For republication from the *British Journal of Cancer*, the following credit lines apply.

Reprinted by permission from Macmillan Publishers Ltd on behalf of Cancer Research UK: [JOURNAL NAME] (reference citation), copyright (year of publication) For AOP papers, the credit line should read:
Reprinted by permission from Macmillan Publishers Ltd on behalf of Cancer Research UK: [JOURNAL NAME], advance online publication, day month year (doi: 10.1038/sj.[JOURNAL ACRONYM].XXXXX)

6. Adaptations of single figures do not require NPG approval. However, the adaptation should be credited as follows:

Adapted by permission from Macmillan Publishers Ltd: [JOURNAL NAME]
(reference citation), copyright (year of publication)

Note: For adaptation from the *British Journal of Cancer*, the following credit line applies.

Adapted by permission from Macmillan Publishers Ltd on behalf of Cancer Research UK: [JOURNAL NAME] (reference citation), copyright (year of publication)

7. Translations of 401 words up to a whole article require NPG approval. Please visit <http://www.macmillanmedicalcommunications.com> for more information. Translations of up to a 400 words do not require NPG approval. The translation should be credited as follows:

Translated by permission from Macmillan Publishers Ltd: [JOURNAL NAME]
(reference citation), copyright (year of publication).

Note: For translation from the *British Journal of Cancer*, the following credit line applies.

Translated by permission from Macmillan Publishers Ltd on behalf of Cancer Research UK: [JOURNAL NAME] (reference citation), copyright (year of publication)

We are certain that all parties will benefit from this agreement and wish you the best in the use of this material. Thank you.

Special Terms:

v1.1

If you would like to pay for this license now, please remit this license along with your payment made payable to "COPYRIGHT CLEARANCE CENTER" otherwise you will be invoiced within 48 hours of the license date. Payment should be in the form of a check or money order referencing your account number and this invoice number RLNK500955566.

Once you receive your invoice for this order, you may pay your invoice by credit card. Please follow instructions provided at that time.

**Make Payment To:
Copyright Clearance Center
Dept 001
P.O. Box 843006
Boston, MA 02284-3006**

For suggestions or comments regarding this order, contact RightsLink Customer Support: customercare@copyright.com or +1-877-622-5543 (toll free in the US) or +1-978-646-2777.

Gratis licenses (referencing \$0 in the Total field) are free. Please retain this printable license for your reference. No payment is required.

**THE AMERICAN ASSOCIATION FOR THE ADVANCEMENT OF SCIENCE LICENSE
TERMS AND CONDITIONS**

Feb 12, 2013

This is a License Agreement between Marta Witek ("You") and The American Association for the Advancement of Science ("The American Association for the Advancement of Science") provided by Copyright Clearance Center ("CCC"). The license consists of your order details, the terms and conditions provided by The American Association for the Advancement of Science, and the payment terms and conditions.

All payments must be made in full to CCC. For payment instructions, please see information listed at the bottom of this form.

License Number	3086771265067
License date	Feb 12, 2013
Licensed content publisher	The American Association for the Advancement of Science
Licensed content publication	Science
Licensed content title	Actin, Spectrin, and Associated Proteins Form a Periodic Cytoskeletal Structure in Axons
Licensed content author	Ke Xu, Guisheng Zhong, Xiaowei Zhuang
Licensed content date	Jan 25, 2013
Volume number	339
Issue number	6118
Type of Use	Thesis / Dissertation
Requestor type	Scientist/individual at a research institution
Format	Print
Portion	Text Excerpt
Number of pages requested	1
Order reference number	
Title of your thesis / dissertation	Biophysical and Biochemical Studies of Alpha II Spectrin and Its Break-Down Products by Caspase-3
Expected completion date	Feb 2013
Estimated size(pages)	100
Total	0.00 USD

Terms and Conditions**American Association for the Advancement of Science TERMS AND CONDITIONS**

Regarding your request, we are pleased to grant you non-exclusive, non-transferable permission, to republish the AAAS material identified above in your work identified above, subject to the terms and conditions herein. We must be contacted for permission for any uses other than those specifically identified in your request above.



1
PAYMENT

2
REVIEW

3
CONFIRMATION

Step 3: Order Confirmation

Thank you for your order! A confirmation for your order will be sent to your account email address. If you have questions about your order, you can call us at 978-646-2600, M-F between 8:00 AM and 6:00 PM (Eastern), or write to us at info@copyright.com.

Confirmation Number: 11069427
Order Date: 02/12/2013

If you pay by credit card, your order will be finalized and your card will be charged within 24 hours. If you pay by invoice, you can change or cancel your order until the invoice is generated.

Payment Information

Marta Witek
mwitek2@uic.edu
+1 (630)6738858
Payment Method: n/a

Order Details

Annual review of biochemistry

Order detail ID: 63439285
Order License Id: 3086781450654
ISSN: 0066-4154
Publication Type: Journal
Volume:
Issue:
Start page:
Publisher: ANNUAL REVIEWS

Permission Status: **Granted**

Permission type: Republish or display content
Type of use: Republish in a thesis/dissertation

Requestor type	Academic institution
Format	Print
Portion	chart/graph/table/figure
Number of charts/graphs/tables/figures	1
Title or numeric reference of the portion(s)	Figure 3
Editor of portion(s)	N/A
Author of portion(s)	N/A
Volume of serial or monograph	N/A
Page range of portion	1059
Publication date of portion	2011
Rights for	Main product

Duration of use	Life of current edition
Creation of copies for the disabled	no
With minor editing privileges	no
For distribution to	United States
In the following language(s)	Original language of publication
With incidental promotional use	no
Lifetime unit quantity of new product	0 to 499
Made available in the following markets	education
The requesting person/organization	Marta Witek
Order reference number	
Author/Editor	Marta Witek
The standard identifier	12345
Title	Biophysical and Biochemical Studies of Alpha II Spectrin and Its Break-Down Products by Caspase-3
Publisher	UIC
Expected publication date	Feb 2013
Estimated size (pages)	100

Note: This item will be invoiced or charged separately through CCC's **RightsLink** service. [More info](#) **\$ 0.00**

Total order items: 1

Order Total: \$ 0.00

Confirmation Number: 11069427

Special Rightsholder Terms & Conditions

The following terms & conditions apply to the specific publication under which they are listed

Annual review of biochemistry

Permission type: Republish or display content

Type of use: Republish in a thesis/dissertation

**NATURE PUBLISHING GROUP LICENSE
TERMS AND CONDITIONS**

Feb 12, 2013

This is a License Agreement between Marta Witek ("You") and Nature Publishing Group ("Nature Publishing Group") provided by Copyright Clearance Center ("CCC"). The license consists of your order details, the terms and conditions provided by Nature Publishing Group, and the payment terms and conditions.

All payments must be made in full to CCC. For payment instructions, please see information listed at the bottom of this form.

License Number	3086791410325
License date	Feb 12, 2013
Licensed content publisher	Nature Publishing Group
Licensed content publication	Nature Structural and Molecular Biology
Licensed content title	Structural and kinetic determinants of protease substrates
Licensed content author	John C Timmer ,Wenhong Zhu ,Cristina Pop ,Tim Regan ,Scott J Snipas et al.
Licensed content date	Oct 1, 2009
Volume number	16
Issue number	10
Type of Use	reuse in a thesis/dissertation
Requestor type	academic/educational
Format	print
Portion	figures/tables/illustrations
Number of figures/tables/illustrations	1
High-res required	no
Figures	Fig. 4A (specificity of caspase-3 and GluC)
Author of this NPG article	no
Your reference number	
Title of your thesis / dissertation	Biophysical and Biochemical Studies of Alpha II Spectrin and Its Break-Down Products by Caspase-3
Expected completion date	Feb 2013
Estimated size (number of pages)	100
Total	0.00 USD
Terms and Conditions	

Terms and Conditions for Permissions

Nature Publishing Group hereby grants you a non-exclusive license to reproduce this

**ELSEVIER LICENSE
TERMS AND CONDITIONS**

Feb 12, 2013

This is a License Agreement between Marta Witek ("You") and Elsevier ("Elsevier") provided by Copyright Clearance Center ("CCC"). The license consists of your order details, the terms and conditions provided by Elsevier, and the payment terms and conditions.

All payments must be made in full to CCC. For payment instructions, please see information listed at the bottom of this form.

Supplier	Elsevier Limited The Boulevard, Langford Lane Kidlington, Oxford, OX5 1GB, UK
Registered Company Number	1982084
Customer name	Marta Witek
Customer address	845 W. Taylor St. M/C111 Chicago, IL 60607
License number	3086800404107
License date	Feb 12, 2013
Licensed content publisher	Elsevier
Licensed content publication	Biophysical Journal
Licensed content title	Slow, Reversible, Coupled Folding and Binding of the Spectrin Tetramerization Domain
Licensed content author	S.L. Shammash, J.M. Rogers, S.A. Hill, J. Clarke
Licensed content date	21 November 2012
Licensed content volume number	103
Licensed content issue number	10
Number of pages	12
Start Page	2203
End Page	2214
Type of Use	reuse in a thesis/dissertation
Portion	figures/tables/illustrations
Number of figures/tables/illustrations	1
Format	print
Are you the author of this Elsevier article?	No
Will you be translating?	No

Order reference number

Title of your thesis/dissertation	Biophysical and Biochemical Studies of Alpha II Spectrin and Its Break-Down Products by Caspase-3
Expected completion date	Feb 2013
Estimated size (number of pages)	100
Elsevier VAT number	GB 494 6272 12
Permissions price	0.00 USD
VAT/Local Sales Tax	0.0 USD / 0.0 GBP
Total	0.00 USD

Terms and Conditions

INTRODUCTION

1. The publisher for this copyrighted material is Elsevier. By clicking "accept" in connection with completing this licensing transaction, you agree that the following terms and conditions apply to this transaction (along with the Billing and Payment terms and conditions established by Copyright Clearance Center, Inc. ("CCC"), at the time that you opened your Rightslink account and that are available at any time at <http://myaccount.copyright.com>).

GENERAL TERMS

2. Elsevier hereby grants you permission to reproduce the aforementioned material subject to the terms and conditions indicated.

3. Acknowledgement: If any part of the material to be used (for example, figures) has appeared in our publication with credit or acknowledgement to another source, permission must also be sought from that source. If such permission is not obtained then that material may not be included in your publication/copies. Suitable acknowledgement to the source must be made, either as a footnote or in a reference list at the end of your publication, as follows:

“Reprinted from Publication title, Vol /edition number, Author(s), Title of article / title of chapter, Pages No., Copyright (Year), with permission from Elsevier [OR APPLICABLE SOCIETY COPYRIGHT OWNER].” Also Lancet special credit - “Reprinted from The Lancet, Vol. number, Author(s), Title of article, Pages No., Copyright (Year), with permission from Elsevier.”

4. Reproduction of this material is confined to the purpose and/or media for which permission is hereby given.

5. Altering/Modifying Material: Not Permitted. However figures and illustrations may be altered/adapted minimally to serve your work. Any other abbreviations, additions, deletions and/or any other alterations shall be made only with prior written authorization of Elsevier Ltd. (Please contact Elsevier at permissions@elsevier.com)

6. If the permission fee for the requested use of our material is waived in this instance,

THE END